THE INVESTIGATION OF POTENTIAL CORROSION RESISTANT PHOSPHORUS CONTAINING AND POLYMER FILMS USING X- RAY PHOTOELECTRON SPECTROSCOPY

by

AMY LOUISE ASUNSKIS

B.S., Truman State University, 1995

AN ABSTRACT OF A DISSERTATION

submitted in partial fulfillment of the requirements for the degree

DOCTOR OF PHILOSOPHY

Department of Chemistry
College of Arts and Sciences

KANSAS STATE UNIVERSITY
Manhattan, Kansas

2006

Abstract

This dissertation will examine the fabrication of different phosphorus containing films and their use as corrosion preventative films and adhesion materials between polymers and metal and metal alloys. Orthophosphate films are used in several metals and metal alloys to prevent corrosion and promote adhesion between paints or polymers and metal substrates. One key component is to examine the use of different phosphorus containing acids that might lead to phosphorus containing films which would compliment the mainly orthophosphate films currently in use.

The objectives of this study are to see if it is possible to fabricate different phosphorus containing films, use them to adhere polymers to metal and metal alloys, and test the phosphorus containing films' and polymer films' corrosion protection properties. The thermoplastic resin, Poly(ether ketone ketone), or PEKK was found to adhere well to different phosphorus containing films and protect the underlying layers from oxidation in 4-D water.

The phosphorus containing films were created by electrochemical deposition in different 5 M phosphorus containing acids. The metal or metal alloy was abraded to remove the native oxide and treated in the electrochemical cell. The second, separate polymer films were created by dip coating the metal or metal alloy in a polymer solution. The film thickness in both cases was controlled to be less than 100Å to ensure that the underlying metal or metal alloy could be detected.

The surface chemical analysis was collected using X-ray photoelectron spectroscopy, or XPS. Core level and valence band XPS were used to distinguish the differences in the chemistry at the surfaces. The valence band XPS spectra were interpreted using spectra generated by multiple scattered wave calculations and band structure calculations. In the cases were more than one film was present subtraction and addition spectrum were used to interpret the chemistry in the interface region of the films.

THE INVESTIGATION OF POTENTIAL CORROSION RESISTANT PHOSPHORUS CONTAINING AND POLYMER FILMS USING X- RAY PHOTOELECTRON SPECTROSCOPY

by

AMY LOUISE ASUNSKIS

B.S., Truman State University, 1995

A DISSERTATION

submitted in partial fulfillment of the requirements for the degree

DOCTOR OF PHILOSOPHY

Department of Chemistry
College of Arts and Sciences

KANSAS STATE UNIVERSITY
Manhattan, Kansas

2006

Approved by:

Major Professor
Peter M.A. Sherwood

Abstract

This dissertation will examine the fabrication of different phosphorus containing films and their use as corrosion preventative films and adhesion materials between polymers and metal and metal alloys. Orthophosphate films are used in several metals and metal alloys to prevent corrosion and promote adhesion between paints or polymers and metal substrates. One key component is to examine the use of different phosphorus containing acids that might lead to phosphorus containing films which would compliment the mainly orthophosphate films currently in use.

The objectives of this study are to see if it is possible to fabricate different phosphorus containing films, use them to adhere polymers to metal and metal alloys, and test the phosphorus containing films' and polymer films' corrosion protection properties. The thermoplastic resin, Poly(ether ketone ketone), or PEKK was found to adhere well to different phosphorus containing films and protect the underlying layers from oxidation in 4-D water.

The phosphorus containing films were created by electrochemical deposition in different 5 M phosphorus containing acids. The metal or metal alloy was abraded to remove the native oxide and treated in the electrochemical cell. The second, separate polymer films were created by dip coating the metal or metal alloy in a polymer solution. The film thickness in both cases was controlled to be less than 100Å to ensure that the underlying metal or metal alloy could be detected.

The surface chemical analysis was collected using X-ray photoelectron spectroscopy, or XPS. Core level and valence band XPS were used to distinguish the differences in the chemistry at the surfaces. The valence band XPS spectra were interpreted using spectra generated by multiple scattered wave calculations and band structure calculations. In the cases were more than one film was present subtraction and addition spectrum were used to interpret the chemistry in the interface region of the films.

Table of Contents

List of Figures

List of Tables

Acknowledgements

Thanks to my major professor, Dean Peter Sherwood, whose vast knowledge and enthusiasm in the field of surface science has encouraged and inspired me. The dedication and care he gives to all tasks he undertakes are qualities that I hope to be able to carry with me in my career.

Thanks to the ESCA group for sharing their knowledge and friendship, John Rotole, Ahmad Audi, Greg Claycomb, Karen Gaskell, and Stephanie Rasinski; with special thanks to Dr. Yuqing Wang, who was always kind and willing to help out, and his family for being welcoming and smiling all the time.

Thanks to my committee for their support: Dr Eric Maatta, Dr. Christopher Levy, Dr. Michael O'Shea, and Dr. Naiqian Zhang.

Thanks to my family for their love and support, especially Dr. Daniel Asunskis, my husband, who is an exceptional young scientist and loyal friend that I am forever grateful to have in my life. And thanks and love to my parents, David and Debbie Ruggeri, for always encouraging me in all my endeavors and allowing me to see my potential, I will always be thankful for the opportunities that you gave me.

Thanks to the National Science Foundation for the funding of this project and the department of the chemistry for their support of me as a graduate teaching assistant.

Dedication

To Daniel Asunskis,

my husband and friend

CHAPTER 1 - X-ray Photoelectron Spectroscopy

1.1. INTRODUCTION

X-ray photoelectron spectroscopy, XPS, has its roots in early experiments done by scientists in atomic physics and the discovery of the wave-particle duality. The first experiment was conducted by Hertz in 1887 and the first detection system was used in 1907 and employed magnets to bend the path of the emitted electrons depending on velocity and a positively charged photographic plate for detection.[1] In the 1950s Kai Siegbahn, developed an electron spectrometer containing an X-ray emission source and with an electromagnetic energy analyser.[1] The first X-ray photoelectron spectrum was collected on sodium chloride in 1954 by Seigbahn's group. Many other advances in the field of XPS were attributed to Seigbahn who also coined the alternate name of XPS, electron spectroscopy for chemical analysis, or ESCA.[2]

XPS is a valuable surface sensitive technique that uses soft X-rays with small line widths, < 1.0 eV and high line energy, > 1000 eV. Mg or Al Kα and in rare cases Ti or Si Kα, radiation have been used to probe approximately the top 100 nanometers of the surface. The incident radiation of 1486.6 eV for Al or 1253.6 eV for Mg, has sufficient energy to overcome the binding energy of the electron residing in their respective shells and excite them to the vacuum level. This is known as the photoelectron effect and is explained by the three step model shown in Figure 1.1.[3,4] The X-ray emission line from the soft x-ray source penetrates into the sample and excites a photoelectron from the atom in step 1. The excited photoelectron then journeys through the surface to the vacuum level in step 2. The photoelectron has a chance of experiencing collisions, known as the inelastic scattering process, from atoms or other electrons in the surface. The inelastic scattering process is complex and still being explored. A review of the elastic and inelastic processes involved can be found in a publication by A. Jablonski and C. J. Powell.[5]

The depth of the atom that the photoelectron is emitted from has an effect on the probability of the photoelectron reaching the surface without suffering energy loss, there is a higher probability of the photoelectron reaching the vacuum from an atom that is closer to the surface, 67% of the signal coming from a depth that is known as the surface's escape depth. A

majority of the signal, 95%, comes from photoelectrons that originate from ≤ 3 times the escape depth.[6] The photoelectrons that have collisions or other effects and still reach the vacuum are at lower kinetic energy and contribute to the background signal and the asymmetric tails on the lower kinetic energy side of the peaks in the XPS spectrum. This added intensity in the lower kinetic energy region is in the same region as the "shake-up" satellites, discussed below, are seen.

In step three, the photoelectron leaves the surface and enters the vacuum. It travels through the vacuum unimpeded and enters the electron energy analyzer. An appropriate electron energy analyzer then determines the kinetic energy of the photoelectron. An electrostatic hemispherical analyzer is often used, which acts as an energy filter, allowing a spectrum to be obtained by setting the potentials on the hemispheres such that particular kinetic energy of electrons can be selected. The number of ejected electrons at each energy is counted, using a detector, and recorded as a spectrum of photoelectron energy versus photoelectron intensity.

1.2. SPECTRAL FEATURES

In 1907 Einstein developed the equation that is used in XPS to determine the binding energy from the kinetic energy of the photoelectrons measured in the spectrum.[1] Einstein's explanation was one of the key components in the development of quantum theory. This equation takes the modern form:

$$KE = h\nu - BE \qquad (1)$$

Where ν is the frequency of the excitation radiation and h is Planck's constant. KE is the kinetic energy of the electron and BE is the binding energy of the electron with respect to the vacuum level.

In the case of solid samples it is important to consider the contact potential between the sample and the spectrometer. This contact potential is the difference in the work function of the sample, ϕ, and the work function for the instrument, ϕs. The work function for the instrument takes a specific value for a particular spectrometer and can be easily calculated, usually having a value of between 2 eV and 5 eV. Equation (1) can be modified by replacing the binding energy

with respect to the vacuum level, BE, with the binding energy with respect to the Fermi level, BE', where:

$$BE = BE' - \phi \quad (2)$$

$$\text{and thus } KE = h\nu - BE' + \phi \quad (3)$$

The contact potential is $(\phi - \phi s)$

so equation (3) becomes: $KE = h\nu - BE' + \phi + (\phi - \phi s)$

$$KE = h\nu - BE' - \phi s \quad (4)$$

In insulators this equation must be adjusted by sample charging, S, to give the final equation:

$$KE = h\nu - BE' - \phi s - S \quad (5)$$

1.2.1. Core level and valence band XPS. There are two different types of regions that can be recorded in XPS: the core level and the valence band. Core levels in XPS are far enough apart in energy to give separate regions that are representative of the shell that the photoelectron originates. Core electrons take no significant part in chemical bonding and have an energy which is determined by the electrostatic interactions between the core electron and the other electrons and the atomic core. Valence electrons take a significant part in chemical bonding and have an energy which is determined by the molecular orbital energy. The electrostatic interactions give core binding energies that depend upon the charge on the atom, the charge on surrounding atoms, and differences in extraatomic relaxation energy. This gives rise to chemical shifts in the core region. An example of chemical shifts can be seen in the N 1s XPS spectrum of NaN3 shown in Figure 1.2. The structure of the anion, azide, is N- = N+ = N-. The negative charge on the terminal nitrogens gives it a lower binding energy and the positive charge on the central nitrogen gives it a higher binding energy resulting in the shifting of the peaks in the XPS spectrum seen in Figure 1.2. The peak intensity ratio is 1:2. In cases where the chemical states are similar, the shifts may be too small to resolve leaving little information gained about the surface chemistry.

Valence band XPS is especially valuable because the origin of the shift is different from that of the core region, so in cases where the core shifts are too small the valence band region can show significant differences. This region is more sensitive to changes in the chemistry at the surface, which makes it useful in distinguishing between similar compounds and different crystal structures of the same compound. The valence band spectra are interpreted in this work by band structure calculations run on a program known as CYSTAL modified by Dean P. M. A. Sherwood.[7,8] The ability to accurately calculate the spectrum using a method that has effective predictive power can be useful in ruling out the possibility of decomposition of the sample due to exposure to X-rays, when using achromatic radiation, and the vacuum of the spectrometer.

1.2.2. Shake-up satellites and relaxation. Two important additional considerations need to be noted.

1.2.2.1. Relaxation: In the photoelectron process an electron is removed from the energy level of an atom and a hole is created. This removes one of the shielding electrons between the nucleus and the outer lying electrons. The molecule is now in a high-energy state and redistribution and relaxation of the electrons in the outer shells occurs in order to lower the overall molecular energy. This relaxation energy needs to be considered in both core and valence band XPS, and it can have a value as large as 10% of the binding energy. The calculation of this relaxation energy assists in the interpretation of both core and valence band XPS.

1.2.2.2. Shake-up satellites: Electronic energy levels should be represented by a number of electronic configurations of the molecule a situation described as configuration interaction. The primary peak in the photoelectron process involves a transition between the most prominent configuration in both the ground and the excited state, but other transitions are possible, especially those that involve different final state configurations. A common behavior resulting from configuration interaction is the *configuration interaction satellite*, often called a *shake-up satellite*. This process may cause the photoemission to occur simultaneously with the excitation of an electron to an unoccupied energy level leaving the ejected photoelectron with less kinetic energy. The peak in the spectrum for this excited electron shows up higher in binding energy than the principle peak and is hidden below the intensity due to the electron inelastic scattering process. In conjugated systems, such as aromatic rings, this feature is more intense and has a smaller shift at 5 eV to 6 eV from the primary peak so it is observed in the XPS spectrum. The π

→ π* transition is seen in the C 1s region for poly(ether ketone ketone), PEKK studied in chapter 5 and 6.

1.2.3. Coster-Kronig Process. One of the processes that can occur after photoemission is the Auger process. In an Auger process, the core-electron hole is filled by an electron in a higher shell and a second electron is ejected from the surface. The nomenclature used for the Auger process labels the energy level where the hole was created first, the initial energy level of the relaxed electron next, and the ejected Auger electron last, for example KL1L3. In this nomenclature K is the same as the quantum number n = 1 and L is n = 2. The 1 in L1, refers to the quantum number lj = 0, so L1 is the 2s and L3 2 p3/2.[6]

The Coster-Kroning process is a fast process that occurs when the relaxed or ejected electron comes from the shell that the initial hole was formed, for example L1L2M4 where L1, 2 s, and L2, 2 p1/2, are from the shell n = 2.[6] Dectection of these transitions is rare since the electrons are of low energy, but when detected they cause a broadening in the peaks in the XPS spectrum. This occurs more commonly in the 2s, 3s, and 2 p1/2 peaks.[6] An example of broadening in the Fe 2p1/2 peak is shown in chapter 6 in section 6.3.1.

1.3. INSTRUMENTATION

A typical instrumental setup for XPS is shown in Figure 1.3. The X-ray gun produces soft X-ray radiation that is directed toward the sample. The ejected photoelectrons from the sample enter the lens system through the source slit followed by the electrostatic hemispherical analyzer. If the photoelectron is traveling at the kinetic energy specified by the analyzer, it will enter the detector through the collector slit to be recorded. There are three instruments used in our laboratories, two of the instruments have a similar setup to Figure 1.1 and are shown in Figures 1.4 and 1.5.

1.3.1. ES200N. The AEI Kratos ES200N has a 120mm hemispherical analyzer that is usually operated in the fixed analyzer transmission mode and is equipped with a hemispherical analyzer pointed out in Figure 1.5. The hemisphere is housed in a protective case made of mu metal. The instrument is also equipped with a single channel detector and sample preparation pre-chamber. The achromatic Mg Kα (1253.6 eV) radiation at 240W provides a linewidth of 0.85 eV.[1] The base pressure of the instrument was kept at 10-9 Torr or better using diffusion pumps.

1.3.2. Sage 100. The SPECS Sage 100, Figure 1.4, has a 95 mm hemispherical analyzer inside the chamber is usually operated in the fixed analyzer transmission mode with a pass energy of 30 eV for the overall spectrum and 15 eV for the core level and valence band spectra. The x-ray gun, pointed out in Figure 1.4 (b), produces achromatic Mg Kα (1253.6 eV) radiation at 240W and is equipped with a water-cooled x-ray gun cap. The water-cooled cap is used to reduce the chance of sample decomposition and carbon contamination.[9] The achromatic Mg Kα radiation has a line width of 0.7 eV.1 The base pressure of the instrument is kept at 2 x 10-8 torr or better with a turbomolecular pump.

1.3.3. HA150. The other instrument, a VSW HA150, has a large hemispherical analyzer and an achromatic, monochromatic, and ultraviolet (UV) light source. The VSW HA150, Figure 1.6, has a 150mm hemispherical analyzer usually operated in the fixed analyzer transmission mode with a pass energy of 50eV for the overall and 20 eV for the core level and valence band spectra. The HA150 is also equipped with a 16-plate multi-channel detection system. The Al Kα X-radiation (240 Watts) generated from a monochromator with 35 quartz crystals provides a linewidth of better than 0.2 eV. The base pressure of the instrument is kept at 10-9 Torr or better with a diffusion pump.

1.3.4. Differences in instrumentation. An illustration of the instrument setup for the HA 150 is illustrated in Figure 1.7. Two changes have been introduced on this instrument to improve the spectral resolution. The first change was made by placing a monochromator (labeled crystal disperser) between the source and the sample. The monochomator allows only the most intense feature of the emission line, Kα1,2, to reach the sample and removes the less intense features Kα3,4 and Kβ lines along with the continuous background called Bremstrahlung radiation. Aluminum X-ray emission has a linewidth of 0.85 eV, which the monochromator can reduce to less than 0.2 eV.

In achromatic radiation, each spectrum has a feature that is separated by approximately 10 electron volts to lower binding energy from the main intense peak that is one-tenth its size. This feature is called a satellite and arises from the Kα3,4 x-ray lines. The satellites do not interfere as often in the interpretation of the core regions, because the binding energies of the core electrons are sufficiently separated. However, it is important to remove satellites from the valence band spectra because the energy spacing between the O 2s region in the valence band and the first peak seen for the phosphates is approximately 10 electron volts. The added

intensity from the satellite at this position gives the inaccurate perception that the first peak in the phosphate is more intense than the other peaks.

The second change illustrated in Figure 1.7 can be made by replacing the single channel (electron multiplier) detector, from Figure 1.1, with a multi-channel detector. The single channel detector has a shape similar to a French horn. When an electron hits the horn portion of the detector a flood of electrons is released. These electrons travel down the tube of the detector hitting the sides and releasing more electrons and amplifying the signal.

The multi-channel detector, in contrast, consists of two microchannel plates stacked one on top of the other that have a separate potential applied across each of them. The plates are porous and when a photoelectron enters one of the holes and hits the side, it is multiplied the same way as in the single-channel detector. Sixteen gold wires are positioned below the plates to count the electrons. The signal from the 16 gold wires is averaged and used as one point on the spectrum. These changes in instrumentation allows for better signal-to-noise for the spectrum.

1.4. DATA ANALYSIS

1.4.1. Calculations. Since valence band spectra represent bonding in the molecule quantitative and qualitative analysis are difficult to apply. A good model to use for interpretation is spectra generated by using calculations.[10,11] Two common calculations used for this purpose are band structure and Xα cluster calculation.

1.4.1.1. Band structure calculation. Band structure calculations look at a solid as an infinite structure of repeating crystal unit cells. The crystal structure for the compound is entered into the program Crystal[7,8] along with atomic positions. The calculations are kept similar to one another by employing STO-3G basis sets for each calculation. Crystal performs ab initio calculations of the ground state energy and electronic wave function. One electron eigenfunctions of the Fock Hamiltonian are represented by linear combinations of Bloch functions, which are also a linear combination of atomic orbitals. A Mulliken analysis is used to obtain orbital, atomic and total densities of states. The separate densities of states for each type of orbital for each atom in the compound were evaluated and adjusted by their atomic photoelectron cross sections using values as determined by Scofield[12]. These cross-section-adjusted total densities of states were then convoluted with a Gaussian/ Lorentzian product

function of 0.5. Two output styles are used in our analysis; one is energy band calculations and one is the XPS spectrum that is generated using a modification of the Crystal program written by Dr. Sherwood.

The energy band calculations are used in our group to determine whether the energy bands are flat or not. The energy band calculations for three different phosphates is shown in Figure 1.8.[13] The bands for each of the phosphates are flat showing that there is not much dispersion of the energy due to the localization of the electrons around the phosphorus-oxygen bonds. From this, it can be inferred that the valence band spectra of the phosphate ion will appear similar to the valence band spectra for that same phosphate ion with a different cation. The effect of using different cations on sulfate, SO_4^{2-} and bisulfate, HSO^{4-} ions have been previously studied by our group.[14] The valence band region spectra were shown to remain unchanged, except in cases where the metal cation used has a core metal peak in the valence band spectra near the phosphate bonding region in the spectra as is the case in metals such as iron and indium. The ionic nature of the phosphates also shows that other calculations that only take the ion into consideration can be used without losing valuable valence band information.

1.4.1.2. Xα cluster calculations. Xα cluster calculations start with the ion of interest and apply results to the solid. Several properties of the ion such as bond lengths and angles are input into the calculation program. A charged sphere, known as a Watson sphere, is placed around the single ion to equilibrate the charge by counteracting the charge of the ion with an opposite charge surrounding the cluster. An Xα cluster calculation of the PO_4^{3-} ion is shown in Figure 1.9. The number of allowed molecular orbitals is determined by the number of atomic orbitals in the PO_4^{3-} ion and is grouped into singlets (of A symmetry), doublets (of E symmetry), and triplets (of T symmetry) according to the symmetry of the Td group. In the lower symmetry phosphorus containing compounds, the triplets and doublets are often replaced by singlets covering a significant energy range leading to a broader spectrum.

1.4.2. Addition and difference spectra. The buried interface between a metal substrate and a thin film coating can be studied by using valence band XPS. A diagram of the thin film, orthophosphate, on a metal substrate is shown in Figure 1.10. The buried interface can be studied by using three spectra: (1) the spectrum of the orthophosphate alone, labeled O, (2) the spectrum of the metal substrate alone, labeled M, and (3) the spectrum of the metal substrate

with a thin film, which in this example is orthophosphate, labeled A. The film must be sufficiently thin to see the underlying substrate so that the buried interface is being studied.

The addition spectrum is obtained by adding the spectrum of the orthophosphate alone to the spectrum of the metal substrate alone. The resultant spectrum is compared to the spectrum of the metal substrate with the orthophosphate film.

If there is no interaction in the orthophosphate/metal interface

$A = M + O$

If there is chemical interaction in the orthophosphate/metal interface

$A \neq M + O$

The interface spectrum can be obtained by creating a difference spectrum from the subtraction of the addition spectrum from the spectra of orthophosphate film on the metal substrate. If the difference spectrum is a flat line there was no interaction in the buried interface. The difference spectrum, if not a flat line, represents the shifts of the peaks between the addition spectrum and the spectrum of the orthophosphate film on the metal substrate. This process was published previously on PVA coated on orthophosphate on aluminum metal and is reprinted here in Figure 1.11.[15] The addition spectrum of the spectra of PVA and orthophosphate film on aluminum metal is shown in Figure 1.11 (c) and compared to the spectrum of PVA coated on an orthophosphate film on aluminum metal, Figure 1.11 (d). The difference spectrum is shown in Figure 1.11 (e) and each peak shows a shift in the peaks between the addition spectrum and the PVA coated on orthophosphate film on aluminum metal showing that there is a chemical change in the interface caused by bonding in the interface region.

When creating addition and difference spectrum there are few factors to consider in insure the best results. The first concern is lining up the spectrum so that the addition and difference spectra accurately display the difference in chemistry at the interface. The three experimental spectra of the orthophosphate film on aluminum, the PVA film, and PVA coated on the orthophosphate film on aluminum, were initially height normalizing by setting the highest point in each spectrum to 10,000 counts. The spectra were then lined up using the correction factor determined by setting the hydrocarbon peak in the C 1s to 284.6 eV.

The addition spectrum where obtained by varying the percent representation of each spectra in the addition spectra. From the example spectra shown in Figure 1.11 above, the percent mixing from PVA spectrum is varied in 5% increments from 100% PVA to 0% PVA while the orthophosphate spectra percent mixing is varied from 0% PO43- to 100% PO43-. This results in 20 different addition spectra of which each is used to create 20 different difference spectra.

The chi squared value is then obtained for each difference spectra and graphed versus % mixing. The lowest value on the graph shows the smallest changes between the experimental and addition spectra. This % mixing value is then used to create the addition and difference spectra. An example graph is shown in Figure 1.12 for PVA coated on pyrophosphate, the addition and difference spectra are shown later in Figure 4.10.

1.5. ACKNOWLEDGEMENTS

Special thanks to Dr. Sherwood, D. Briggs, M. P. Seah and VSW for the Figures below that were reprinted from their work.

1.6. REFERENCES (see Reference chapter)

1.7. FIGURES

Figure 1-1 The three step model showing the excitation (1), transport through the surface to the vacuum (2), and the escape of the photoelectron into the vacuum (3). Reprinted from Dr Sherwood's class notes.

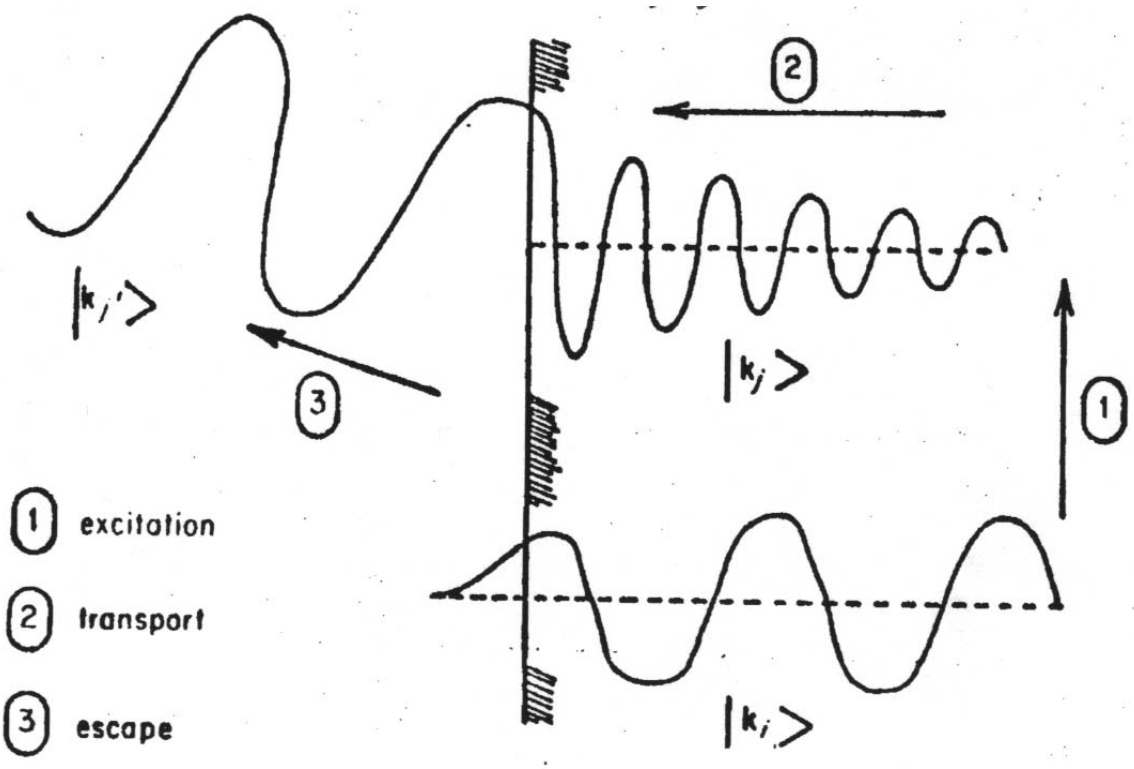

Figure 1-2 The N 1s XPS spectrum of NaN_3. Reprinted from a publication by K. Siegbahn.[16]

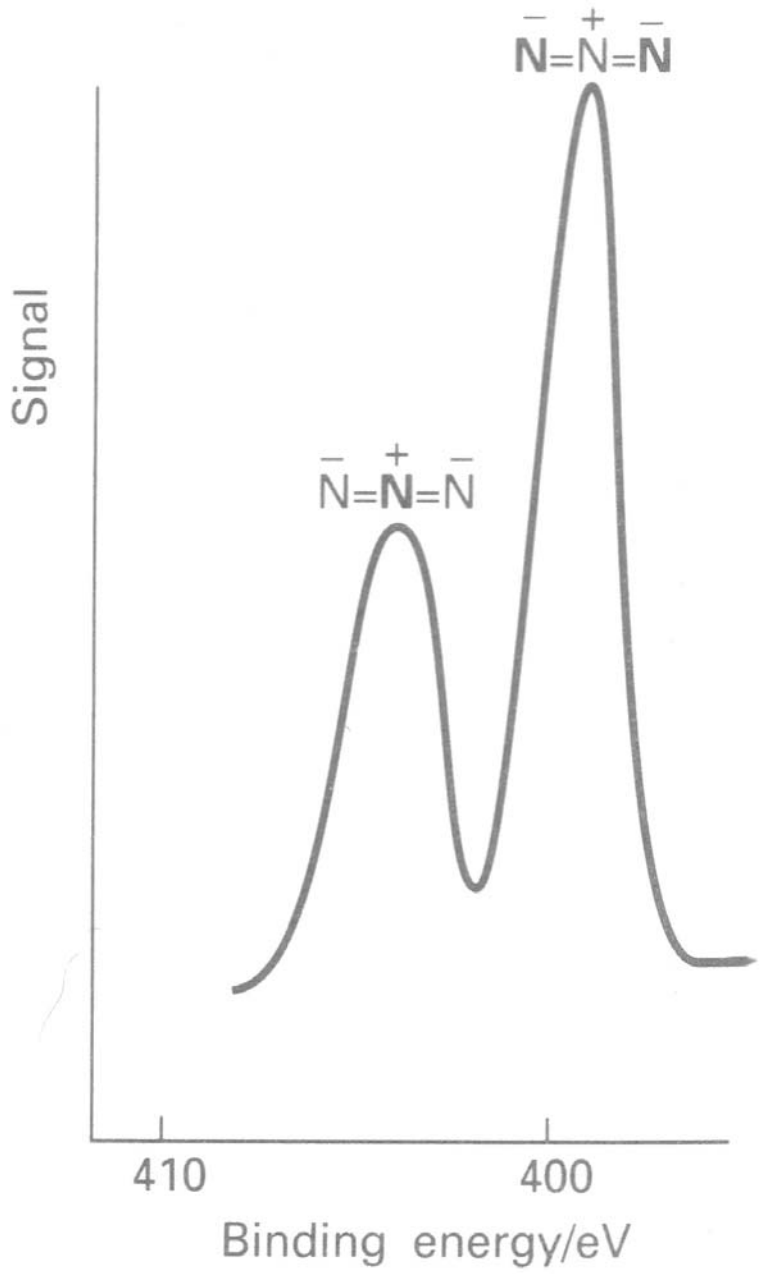

Figure 1-3 Instrumental setup for XPS. Reprinted from a manual on AEI VSW ES200N from Vacuum Science Workshop, VSW.

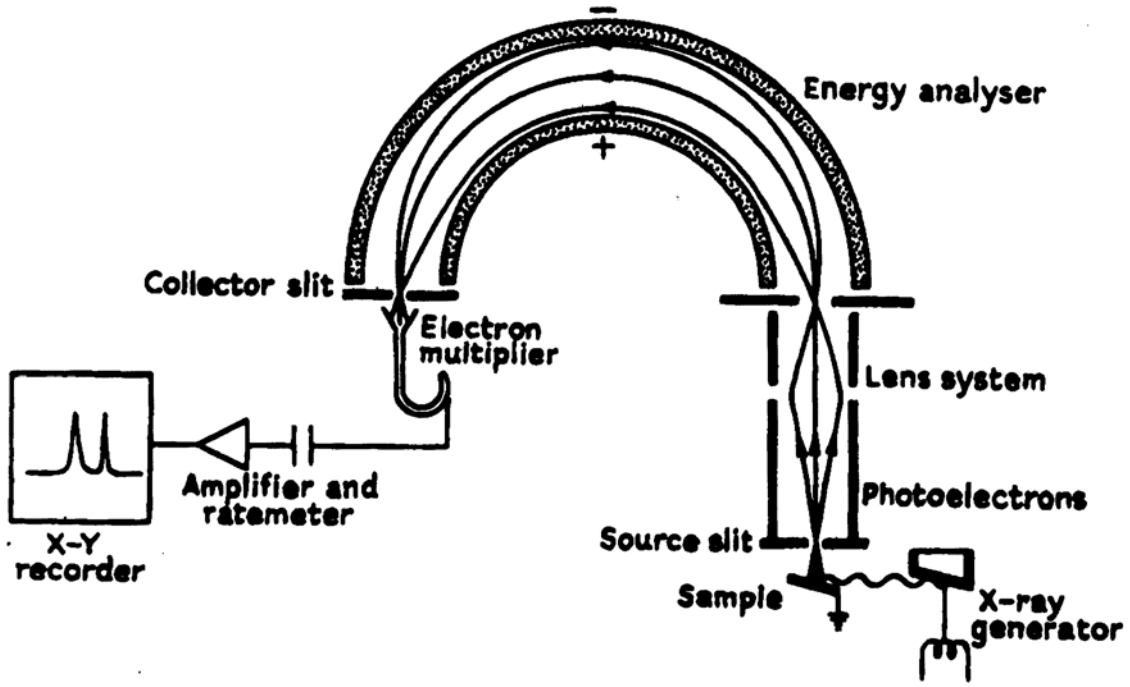

Figure 1-4 The SPECS Sage 100 instrument (a) the full view including the electronics and (b) a closer view of the chamber and X-ray gun. Pictures taken in Dr. Sherwood's former laboratory at Kansas State University.

(a) Left (b) below

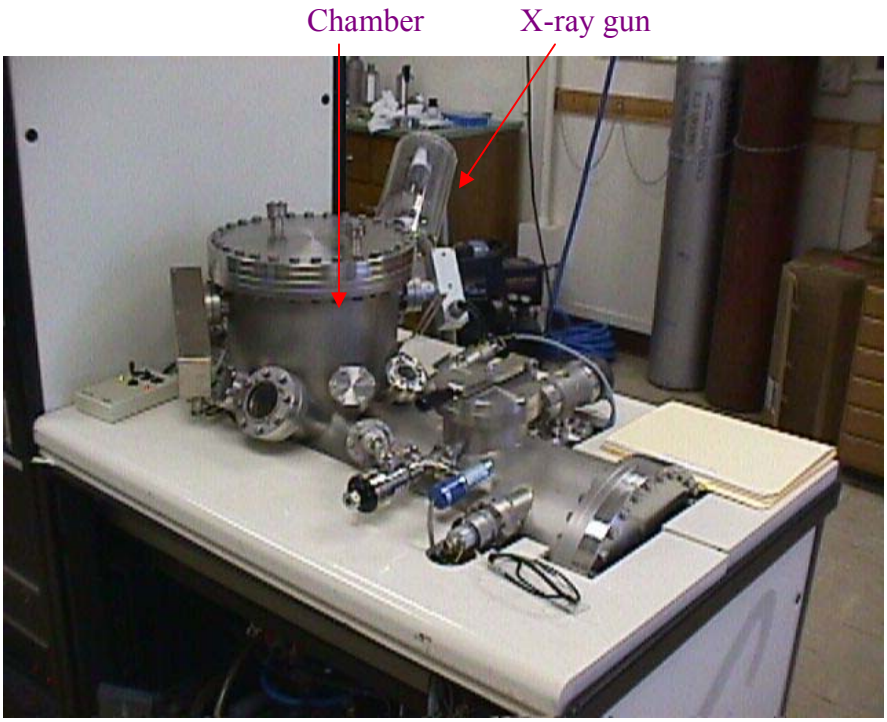

Figure 1-5 The AEI Kratos ES200N instrument showing an achromatic X-ray source and hemispherical analyzer. Picture taken in Dr. Sherwood's former laboratory at Kansas State University.

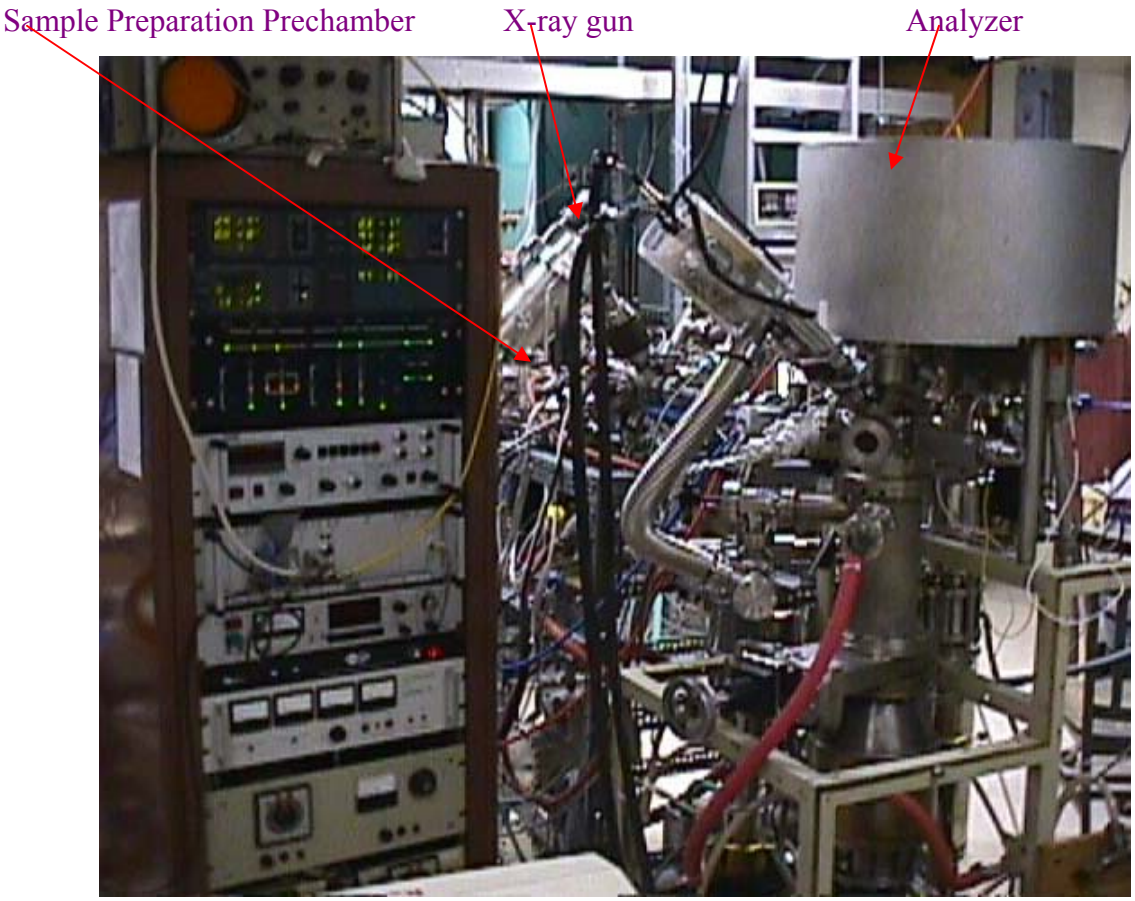

Figure 1-6 The VSW HA 150 instrument showing the monochrometor and 16- channel detector. Picture taken in Dr. Sherwood's new laboratory at Oklahoma State University. Figure 1.6.

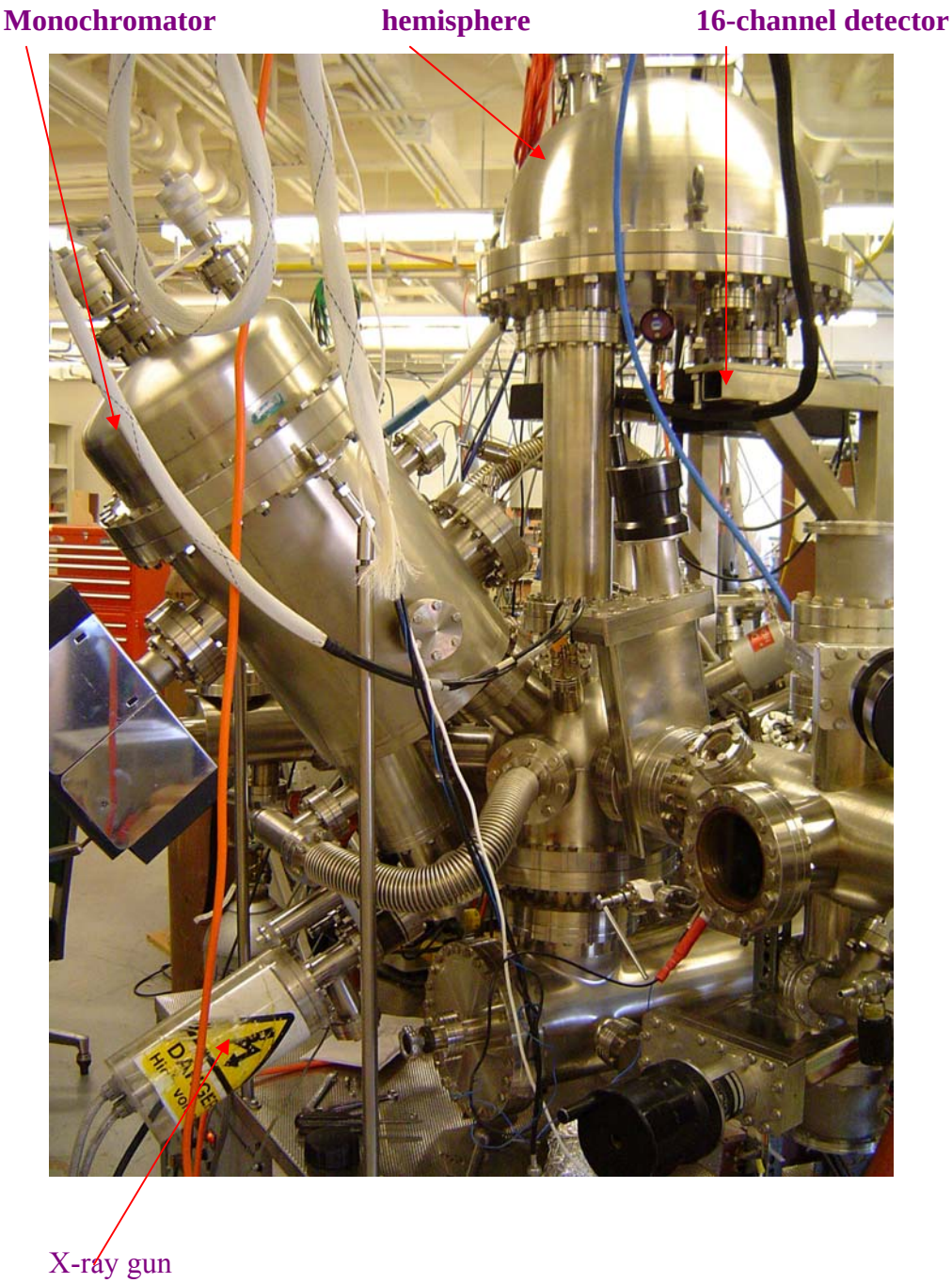

Figure 1-7 Instrumental setup for XPS with a monochromator (with 35 quartz crystals). Reprinted from Briggs and Seah.[1]

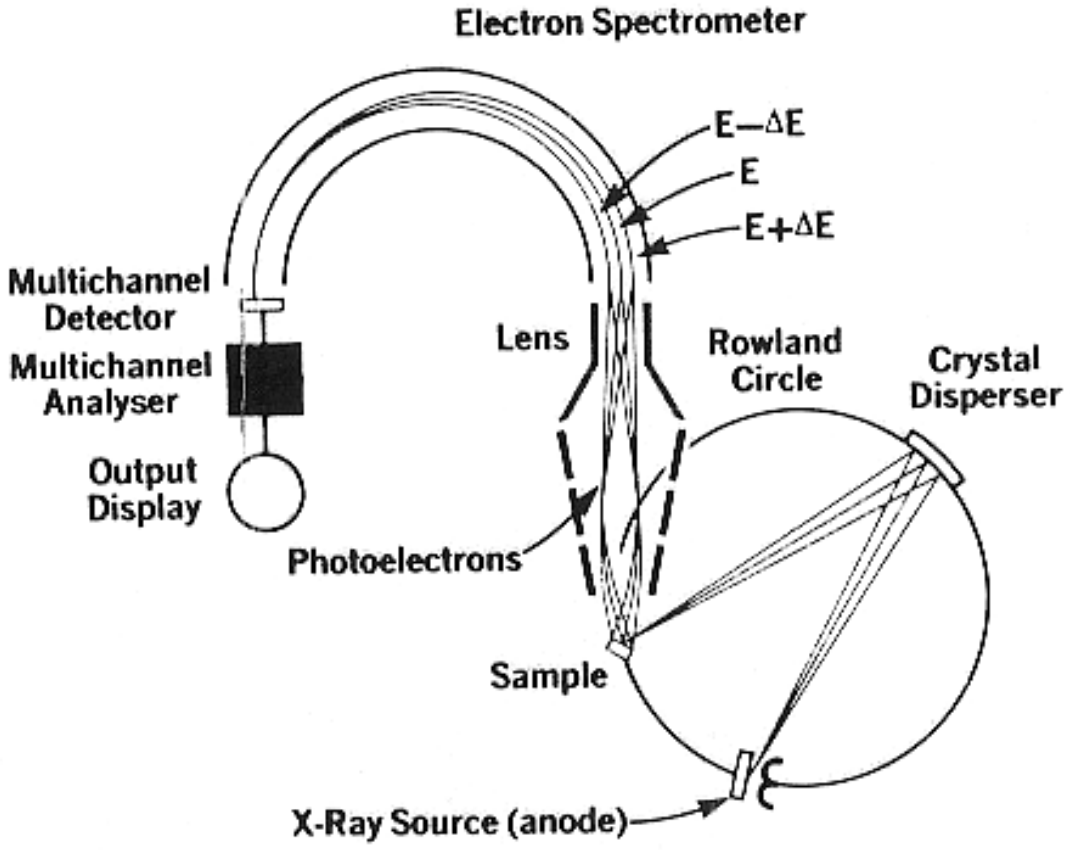

Figure 1-8 Calculation of the energy bands for (a) $Al_4(P_4O_{12})$ (b) $AlPO_4$ and (C) $FePO_4 \cdot 2H_2O$. Reprinted from Dr. Sherwood's publication.

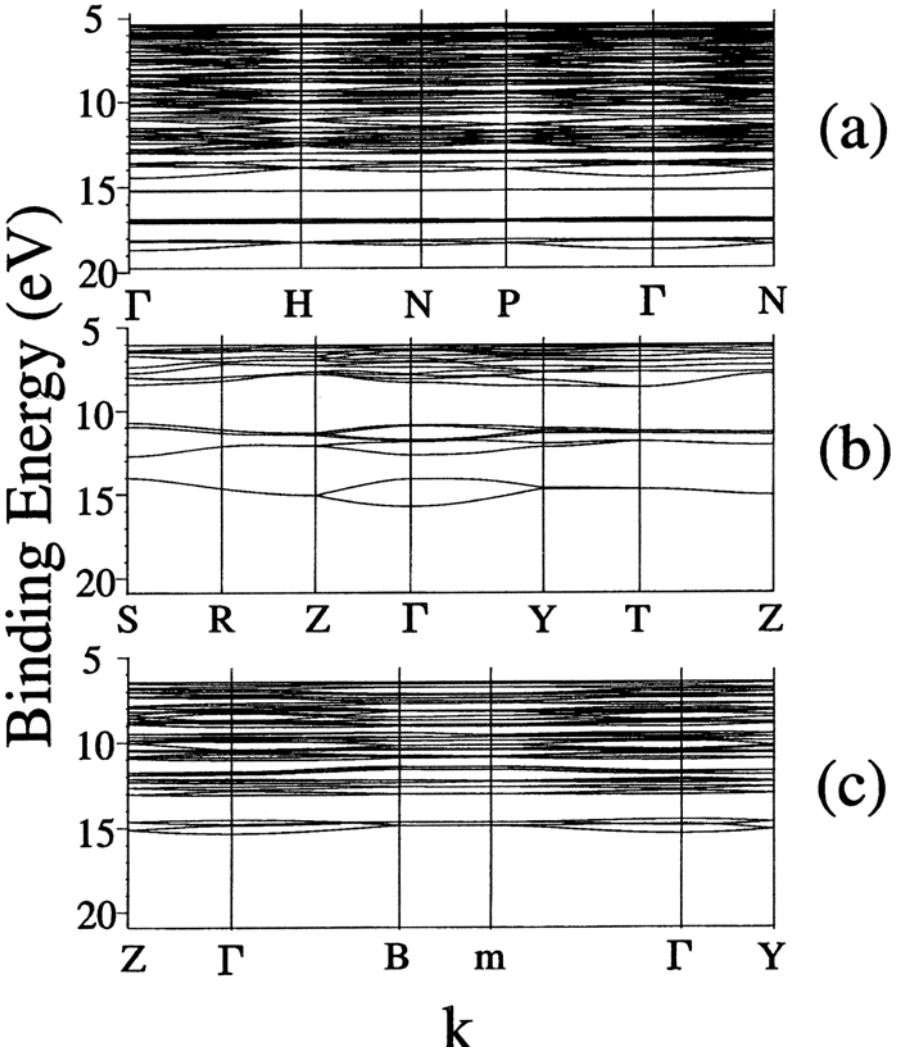

Figure 1-9 Xα Cluster calculation of the PO_3^{4-} ion showing the percentage of the atomic orbital that mixes to form the molecular orbital. The Reprinted from Dr. Sherwood's publication.

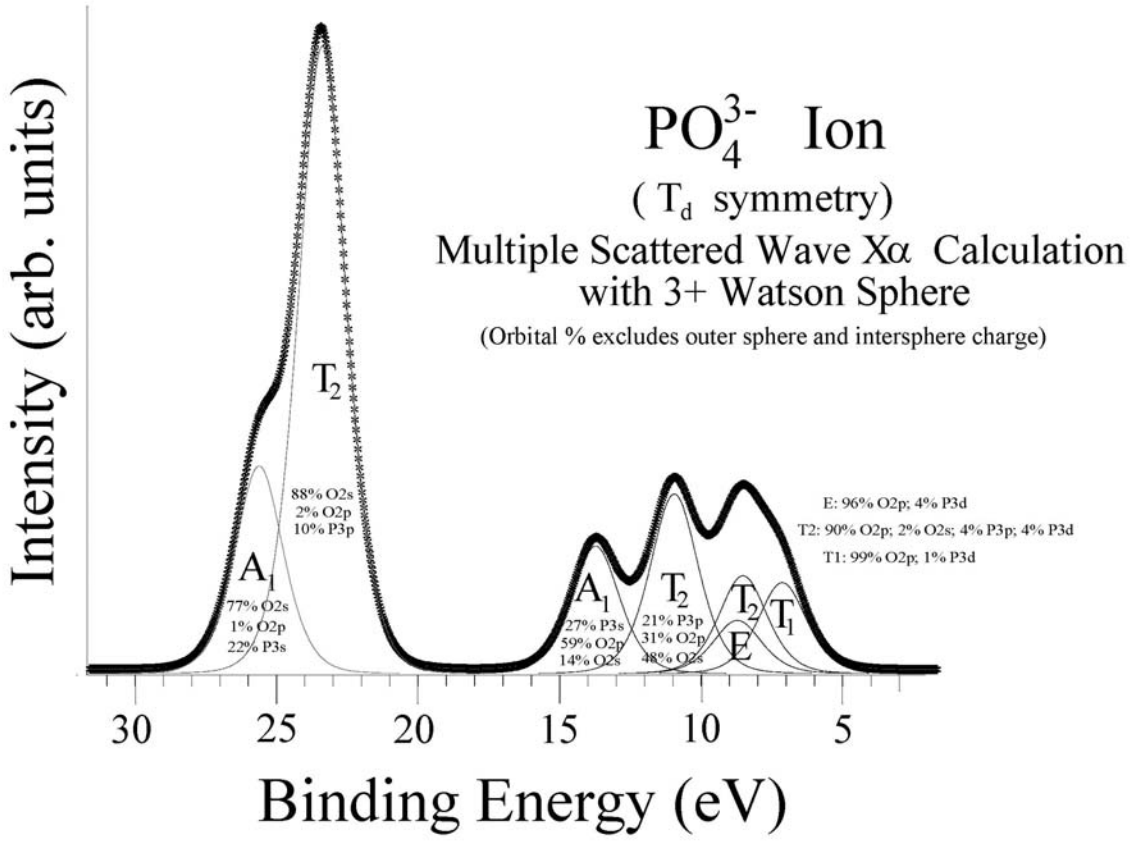

Figure 1-10 Diagram of the buried interface between a thin orthophosphate film and a metal substrate.

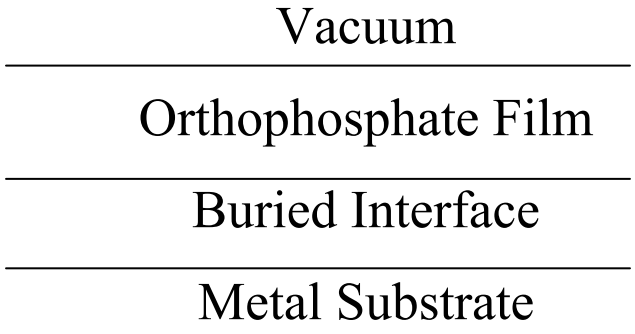

Figure 1-11 Valence band spectra of orthophosphate (a), polyvinyl alcohol, PVA, (b), the addition of (a) and (b) [= (a) + (b)] (c), PVA coated on an orthophosphate film on aluminum metal (d), and the difference of (c) and (d) [= (d) – (c)]. Reprinted from reference 15.

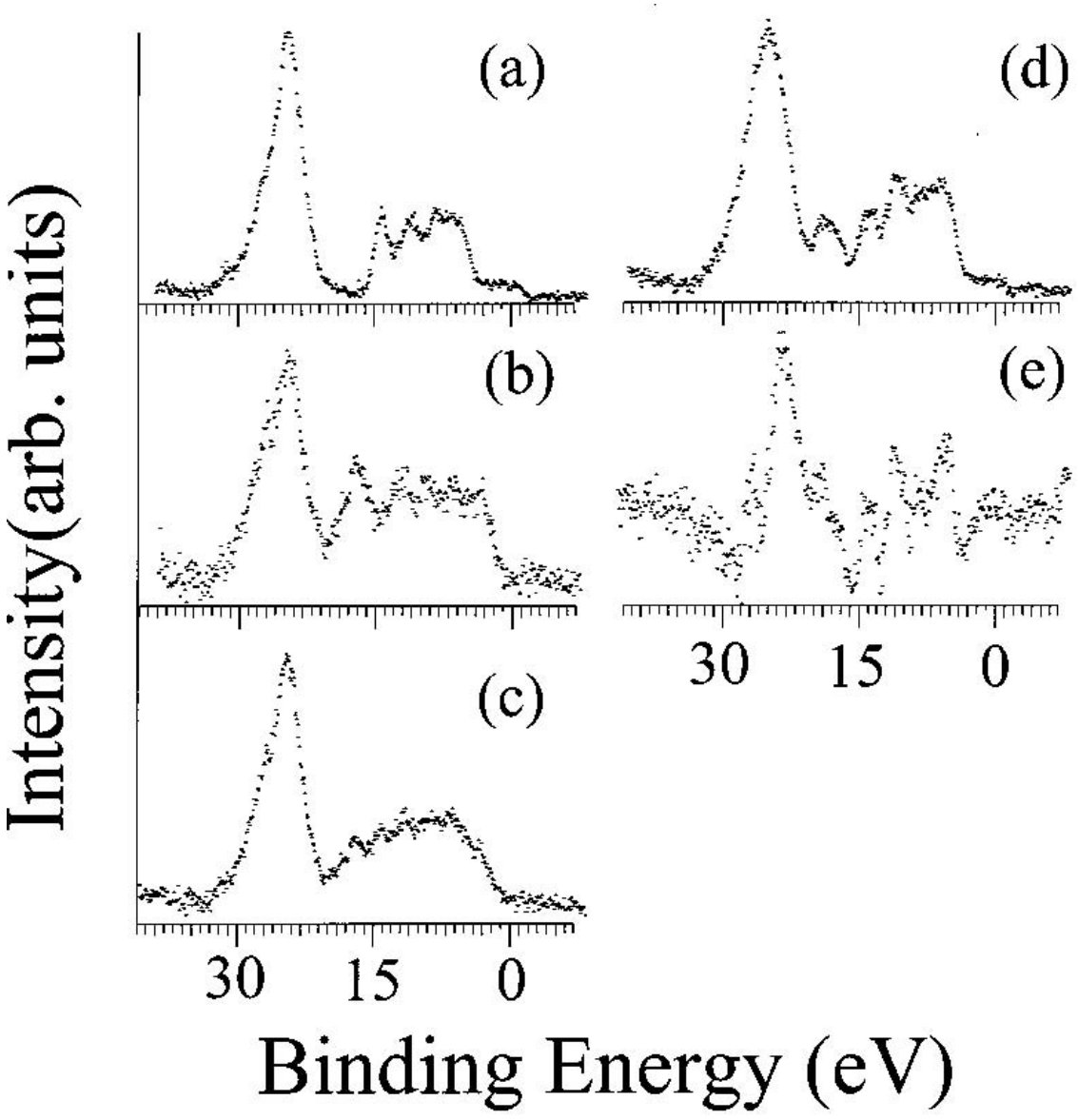

Figure 1-12 Chi squared versus % contribution of PVA for the PVA coated on pyrophosphate film on aluminum metal. The lowest point on the graph at 30% PVA is the value used for creating the addition and difference spectra in Figure 4.10.

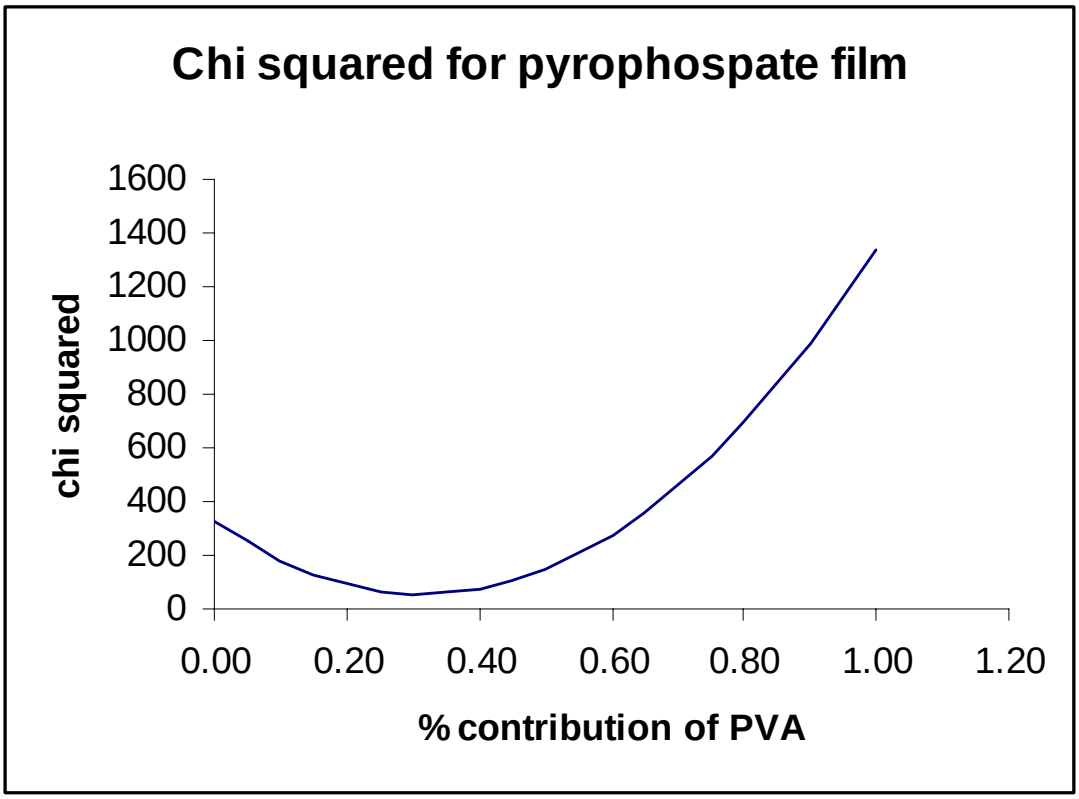

CHAPTER 2 - Phosphorus-Containing Compounds and Polymers

2.1 PHOSPHORUS CONTAINING COMPOUNDS

This section will review a basic history of phosphates, the different structures of phosphates and the formation of phosphorus containing compounds, followed by a summary of previous work on distinguishing phosphates using XPS.

2.1.1. History and Structure. Phosphates were discovered as early as 1816, but were not fully studied and categorized until the late 1940s when analytical techniques and the development of quantum mechanics (1925) made it possible to distinguish between them.[1] Potassium and sodium phosphates are produced in bulk for commercial use as drying agents, water softeners, and as ingredients in detergents and fertilizers. Calcium phosphates are currently being used as coatings for titanium implant devices.

The separation of phosphates into categories begins with the simplest building block, the orthophosphate ion, PO_4^{3-}, (sometimes referred to as simply the phosphate ion). The orthophosphate ion has three negative charges and a tetrahedral arrangement in which any one of the oxygen atoms can be shared with neighboring orthophosphate ions in P-O-P bridges to form a multitude of condensed phosphates. Orthophosphate salts are prepared by the reaction of orthophosphoric acid with metal carbonates to produce mono-metal, di-metal, and/or tri-metal orthophosphates:[2]

$$2H_3PO_4 + K_2CO_3 \rightarrow CO_2 + H_2O + 2KH_2PO_4 \qquad (3)$$

$$H_3PO_4 + Rb_2CO_3 \rightarrow CO_2 + H_2O + Rb_2HPO_4 \qquad (4)$$

$$2H_3PO_4 + 3Cs_2CO_3 \rightarrow 3CO_2 + 3H_2O + 2Cs_3PO_4 \qquad (5)$$

The orthophosphate ion that shares only one oxygen atom is known as an end group, shown in Figure 2.1.[1] Combining two end groups forms the pyrophosphate ion, $P_2O_7^{4-}$. Pyrophosphate salts are prepared by thermal condensation of the orthophosphate salts:[3]

$$2MH_2PO_4 \rightarrow M_2H_2P_2O_7 + H_2O \qquad (6)$$

$$2M_2HPO_4 \rightarrow M_4P_2O_7 + H_2O \quad (7)$$

Monosodium pyrophosphate can also be prepared by reacting disodium dihydrogen pyrophosphate with pyrophosphoric acid, but it is unstable in water and methanol, and returns to disodium dihydrogen metaphosphate.[2]

$$Na_2H_2P_2O_7 + H_4P_2O_7 \rightarrow 2NaH_3P_2O_7 \quad (8)$$

Two oxygen atoms on the orthophosphate ion can be shared so that more than two orthophosphate ions can be connected. This connector is called a middle group and is shown in Figure 2.1. The middle groups can be used to form chain or cyclic phosphates that contain varying numbers of phosphorus atoms. The chains contain two end groups and enough middle groups to equal the total number of phosphorus atoms present minus two, for example, $P_3O_{10}^{5-}$ has three phosphorus atoms and the structure has two end groups and one middle group. The cyclic phosphates contain all middle groups connected in a ring. The simplest chain phosphate is the tripolyphosphate ion, $P_3O_{10}^{5-}$, and the simplest cyclic phosphate is the trimetaphosphate ion, $P_3O_9^{3-}$. Increasing to three shared oxygen atoms known as the branching group, shown in Figure 2.1, can create another type of condensed phosphate called an ultraphosphate.

2.1.2. Other phosphorus containing compounds

The ions, HPO_3^{2-} and $H_2PO_2^-$ along with $P_2O_7^{4-}$, are studied in chapter 4 as films on aluminum metal. The structures HPO_3^{2-} and $H_2PO_2^-$ are created by replacing the oxygen in PO_4^{3-} with hydrogen. For the HPO_3^{2-}, one of the oxygen atoms is replaced with hydrogen and in $H_2PO_2^-$ two of the oxygen atoms are replaced.

2.1.3. Previous work on phosphorus containing compounds.

Only a few studies exist for phosphorus containing compounds using valence band XPS.[4,5,6,7] Two studies in particular stand out.[6,7] In one of the studies, G. Hollinger and E. Bergignat studied different indium phosphorus oxide films of the form InP_xO_y on the surface of indium phosphide (InP) semiconductors. They divided the phosphorus oxide films into three groups depending on the crystal structure that they most closely resembled. The groups are $In(OH)_3$, $InPO_4$, and $In(PO_3)_3$. The samples were made by starting with n-type doped InP and

performing either thermal (T), chemical(C), or anodic (A) oxidation.[6] Table 2.1 lists the sample number (which correspond to the preparation method) and atomic composition of the samples.

The outer valence band XPS spectra of the region near the Fermi edge of the samples studied are shown in Figure 2.2. After interpreting the valence band XPS spectra, the samples were placed into one of the three groups mentioned above: group I included A_1, C_2, and A_2, group II included T_1, C_3, and A_3, and group III included $C_1$and A_4. The group I compounds have a large amount of oxygen character with no phosphorus detected in A_1. The valence bands XPS spectra show this by only having two peaks in the outer valence band region, which is comparable to an indium oxide structure such as $In(OH)_3$• X H_2O. The group II compounds have considerably more phosphorus character and have an outer valence band region with three peaks, the two peaks at higher binding energy being the common identifiers for PO_4^{3-} ion. Group III have an O/P ratio close to 3, which is the ratio for the ring metaphosphates, $P_3O_9^{3-}$.

The valence band for indium containing compounds has a high intensity peak for In4d that is located at the same binding energy as the peak O 2s and approximately 10 eV higher in binding energy than the highest binding energy peak for the low binding energy region of the phosphates. This makes monochromatic radiation essential in order to avoid interference of satellites, which would give the impression that the highest binding energy peak of the phosphate had more intensity than predicted. The phosphorus and oxygen bonding region of the valence band for all of these compounds follow a trend of increasing width from the group I to the group III compounds. The group III compounds have phosphate regions that are so wide that the In4d peak interferes with the high binding energy peak for the metaphosphate ion making resolution of the peak difficult.

There is enough evidence in this study to show that there is a difference between even similar structured InP_xO_y compounds. The one disadvantage of this work is that they compare their XPS spectra to commercially supplied powders, but do not employ any external standard such as calculations for ruling out the possibility of vacuum degradation or decomposition of the samples. Other groups[4,5] have borrowed this data for their own studies and compared it to calculated spectra employing various calculation methods.

The second study was conducted by Dr. Sherwood's group wherein different sodium phosphorous containing powders were investigated using core level and valence band XPS.[7] The Valence band spectra of $Na_2H_2PO_2 \cdot 0.8H_2O$ (a), $Na_2H_2P_2O_7 \cdot 6H_2O$ (b), $Na_4P_2O_7$ (c),

$Na_5P_3O_{10}\cdot 6H_2O$ (d), and $Na(PO_3)_n$, corresponding to $Na_4P_4O_{12}$ (e) are shown in Figure 2.3. There are substantial chemical differences seen in these spectra especially in the three peaks in the outer valence band region between 0 eV and 20 eV. The spacing, intensity and structure of these three peaks are different in each spectrum, making it easy to distinguish between even the hydrate and anhydrous phosphates, $Na_2H_2P_2O_7\cdot 6H_2O$ (b) and $Na_4P_2O_7$ (c).

The paper interpreted the spectra by comparing the experimental spectra with spectra generated from band structure calculations and from spectra generated form multiple scattered wave X alpha calculations, an example of this approach is shown in Figure 2.4. The Na metal peak shown at 30 eV in the spectra in Figure 2.3 and the nonlinear background was removed. The final spectrum of the outer valence band region of $Na_4P_2O_7$ is shown in Figure 2.4 (c). This spectrum is compared to the spectra generated using multiple scattered wave Xα calculations on an ionic cluster, (a), and using a band structure calculation (b). The characteristics of the three peaks are predicted by both calculations along with the shoulder at 26 eV for the phosphorus – oxygen type bond contribution to the O 2s peak.

2.2 POLYMERS

2.2.1. Polyvinyl alcohol. Polyvinyl alcohol, or PVA, is not prepared by the use of monomers but from polyvinyl acetate. The first step was to successfully produce polyvinyl alcohol in bulk. F. Klatte first reported production of the polyvinyl esters in 1910.[8] The ester polymerization process proposed was exothermic and had to be done carefully and took up to a week to avoid explosions due to adding too much ester monomer at one time. In 1924, W. O. Herrman and W. Haehnel discovered a safer method for the production of polyvinyl acetate that could be reproduced in bulk using a mercury catalyst that was replaced by a non-mercury catalyst in 1927.[9,10]

The next step was to produce PVA in bulk. It was already known that the hydrolysis of vinyl acetate gave an oily resin of vinyl alcohol. This process was modified to produce PVA using polyvinyl acetate. The reaction mechanism for the hydrolysis of polyvinyl acetate to form PVA is shown in Figure 2.5 (a). In 1932, W. O. Herrman reported that varying the alcohol could be used to vary the characteristics of the ester byproduct, Figure 2.5 (b).[11] In bulk industrial production the esters can be recycled to reduce waste.

Solubility of PVA is a property determined by the amount of polymerization and hydrolysis, with hydrolysis taking the major role.[12] The more hydrolysis of the polyvinyl acetate the less soluble the PVA and less hydrolysis leaves residual acetate on the surface of the PVA that increases its solubility. To make an aqueous solution of PVA produced using increased hydrolysis, heated water is necessary but lower hydrolysis allows PVA to dissolve in cold water. There are several types of PVA produced by companies depending on the degree of solubility needed. PVA is used in the textile market for the adhesion of staple yarns and hydrophilic cotton fibers, which uses a highly hydrolyzed polyvinyl acetate and filament yarns and spun yarns, which use less hydrolyzed polyvinyl acetate. PVA is also used in paper manufacture as sizing agents, which are coated on the surface of paper.

PVA was recently used in our group[12] to test the adhesive properties of an orthophosphate film between the polymer and aluminum metal. The results are seen in Figure 1.11, where buried interface studies showed that PVA and the orthophosphate film had formed bonding in the interface.

2.2.2. Poly(ether ketone ketone). Poly(aryl ether ketone)s, or PAEK are a type of high temperature thermoplastics that are known for high strength, stiffness and chemical resistance. Poly(ether ketone ketone), or PEKK, and poly(ether ether ketone), or PEEK, are the most commonly used PAEKs. Their strength has been applied in aerospace, as coatings and as insulators. The difference between PEEK and PEKK as materials are reviewed in various publications and PEKK is stated as having a better thermal stability, mechanical properties, processibility, and environmental durability.[13-17] The PEKK repeat unit is shown in Figure 2.6 with the carbon and oxygen in different chemical environments numbered. For carbon, the C-C and C-H type bonds are labeled 1, the C-C=O type bonds are labeled 2, the C-O type bonds are labeled 3, and the C=O type bonds are labeled 4. For oxygen the C=O type bonds are labeled 5 and the C-O type bonds are labeled 6.

PEKK has been used previously in our laboratory[18] as a strengthener for carbon composite matrices. Figure 2.7 shows the XPS spectra for the PEKK coated on carbon fibers treated in nitric acid for 20 seconds and 120 seconds. A thick film of PEKK was formed on copper to collect an XPS spectrum representative of the PEKK repeat unit to compare to the PEKK films, Figure 2.7 (a). The C 1s, column II, and O 1s, column III, were curve fitted to shown the components of each peak. The C 1s has 4 component peaks in the curve-fit spectrum

labeled from right to left in the figure as type 1, 2, 3, and 4 and the O 1s has two component peaks labeled from right to left as type 5 and 6. The valence band XPS spectrum is representative of the PEKK valence band with a triplet peak structure at 20 eV, confirmed in earlier work, for aromatic rings.[19]

The untreated carbon fiber was coated in PEKK and the excess solution removed, Figure 2.7 (b) and not removed, Figure 2.7 (c). The C 1s, column II, shows a peak for the carbon adsorbed to the surface from air exposure and the diffusion pumps used to bring the instrument to UHV calibrated to 284.6. The C 1s spectrum also has a shoulder for oxide in the carbon fiber with the excess solution removed and the characteristics peaks of PEKK in the carbon fiber without the excess solution removed. The PEKK had dried on the surface, but no bonded with the surface is evident since the valence band XPS spectrum, column IV, is similar to the PEKK spectrum in (a) and there was no sign of shifting in the peaks characteristic to bonding.

The carbon fiber was then treated in nitric acid for 20 seconds and 120 seconds, Figure 2.7 (d) and (f), respectively, and then each treated carbon fiber was coated with PEKK with the excess PEKK solution removed, Figure (e) and (g). Bonding is shown here with the change in the peaks for the C 1s and O 1s before and after coating and the shifting of the peaks in the valence band. The thick PEKK film on copper metal and carbon fiber treated with nitric acid for 20 seconds and coated with PEKK were then submersed in a saline solution at 365 K to test their performance in atmospheric and aqueous conditions. The XPS spectra before and after the exposure of the films to the solution for 5 and 10 days are shown in Figure 2.8. In both tests, the C 1s, column II, and O 1s, column III, spectra show an increase in the oxide peak and decrease in the peaks representative of PEKK. The valence band spectra, column IV, show the degradation of the PEKK with longer exposure times as a peak that appears at a higher binding energy than the principal O 2s peak at 25 eV.

2.3. ACKNOWLEDGEMENTS

Special thanks to Dr. Sherwood, Y. Q. Wang, G. Hollinger, and E. Bergignat for the Figures below that were reprinted from their work.

2.4. REFERNCES (see Reference chapter)

2.5. TABLES

Table 2-1 Sample number and atomic composition of the oxide samples.

Sample number	Atomic Composition
A_4	$InP_{4.3}O_{13.8}$
C_1	$InP_{3.1}O_9$
C_3	$InP_{1.8}O_{6.8}$
A_3	$InPO_{5.4}$
T_1	$InP_{0.74}O_{3.8}$
A_2	$InP_{0.76}O_{5.9}$
C_2	$InP_{0.24}O_{4.9}$
A_1	$InO_{4.1}$

2.6. FIGURES

Figure 2-1 The different bonding that can occur in an orthophosphate ion. The end group has one covalently bonded oxygen atom, the middle group has two, and the branching has three.

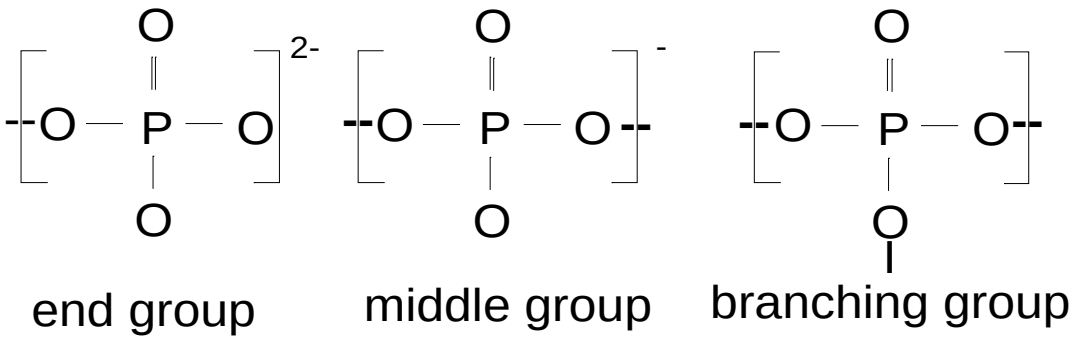

Figure 2-2 Valence band XPS spectra of InPxOy. The sample labels are shown in Table 2.1.

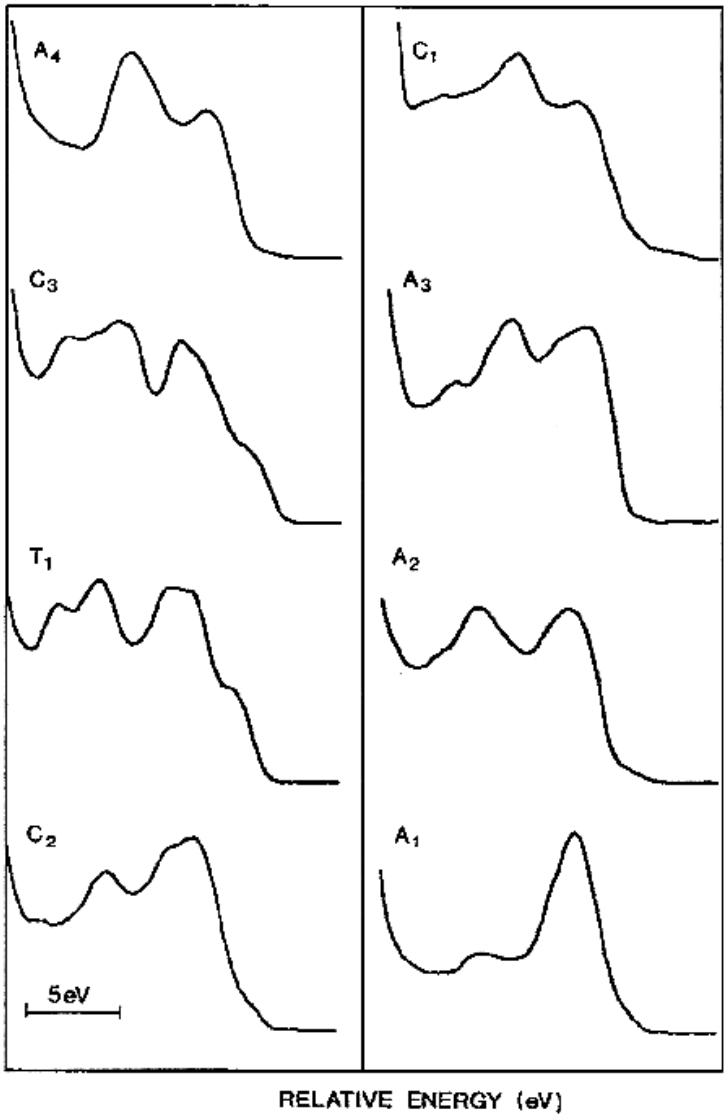

Figure 2-3 Valence band XPS spectra of different phosphate powders. $Na_2H_2PO_2 \cdot 0.8H_2O$ (a), $Na_2H_2P_2O_7 \cdot 6H_2O$ (b), $Na_4P_2O_7$ (c), $Na_5P_3O_{10} \cdot 6H_2O$ (d), and $Na(PO_3)_n$, corresponding to $Na_4P_4O_{12}$ (e).[7]

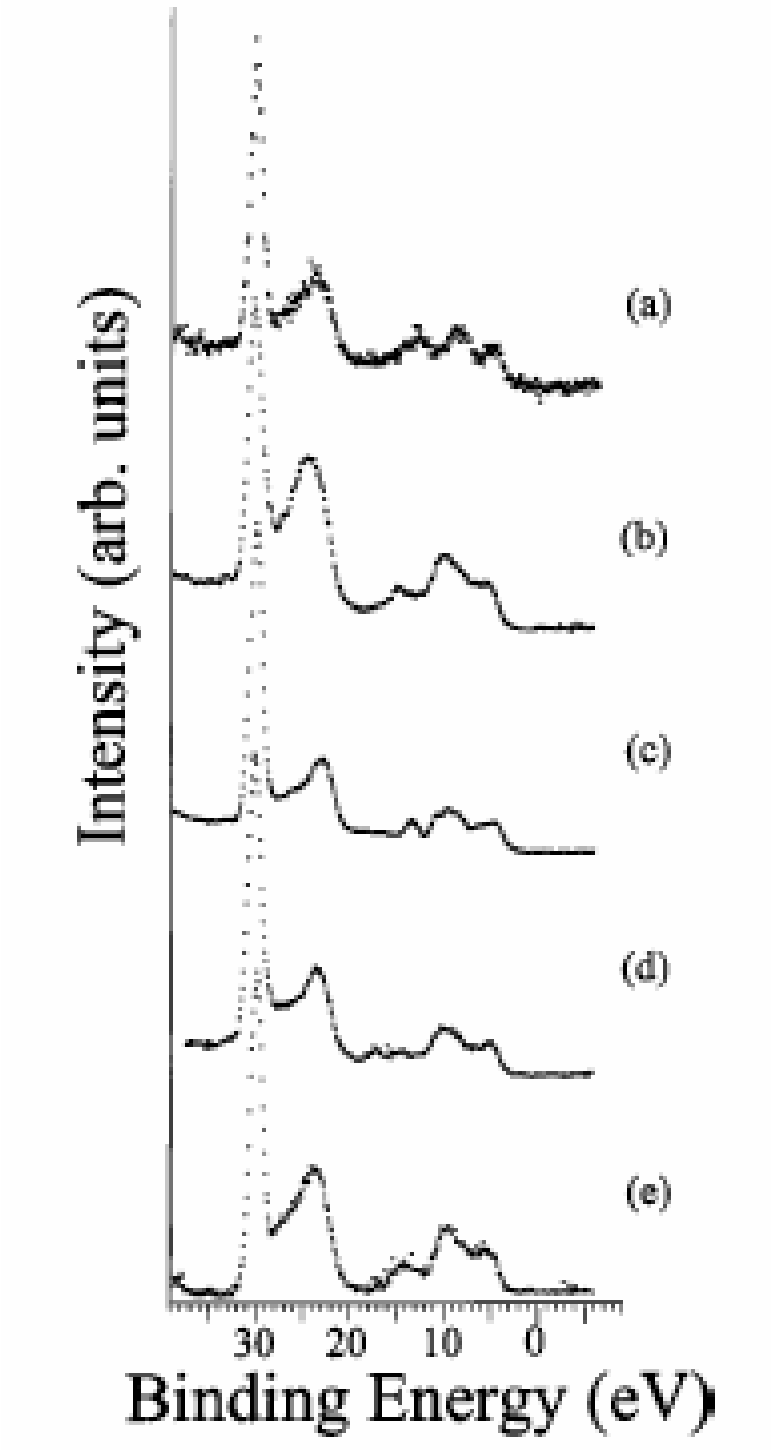

Figure 2-4 Outer valence band region of a powder sample of $Na_4P_2O_7$ (c) compared to spectra generated using Xα cluster (a) and band structure (b) calculations.[7]

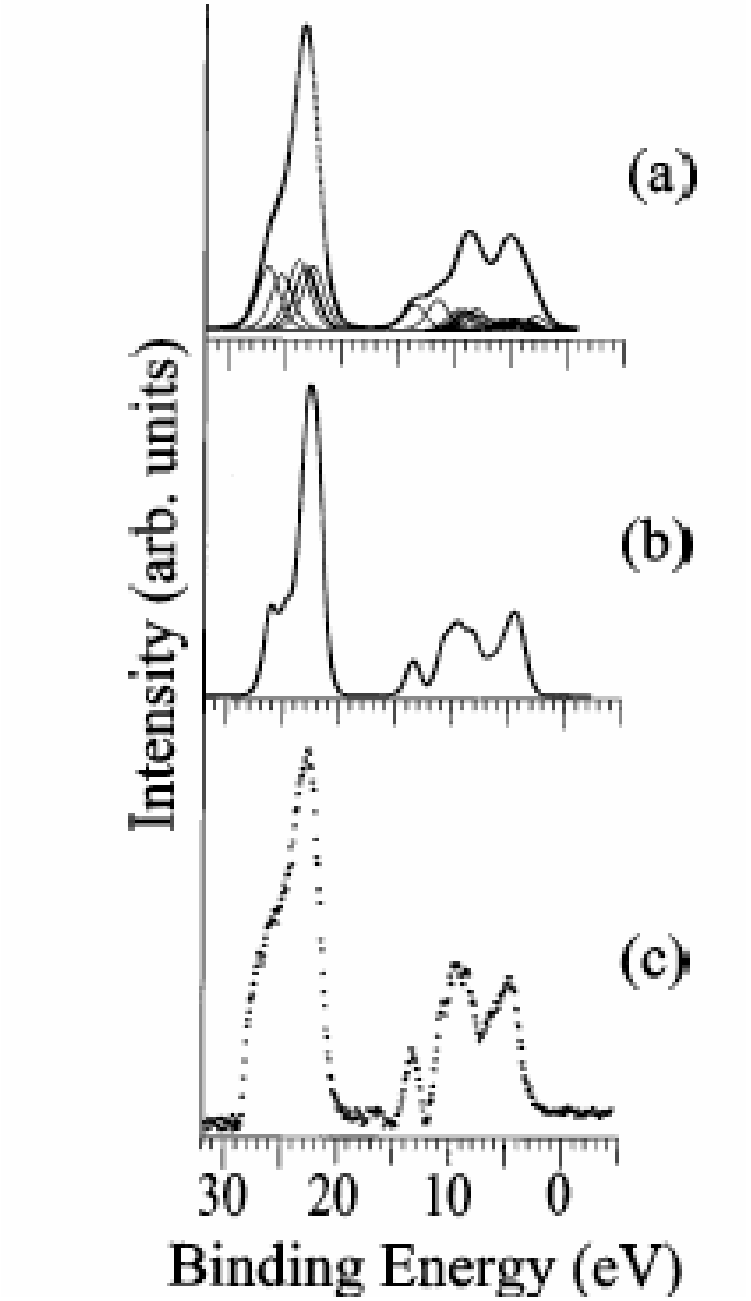

Figure 2-5 The reaction mechanism for the hydrolysis of polyvinyl acetate to form PVA (a), the reaction in (a) with varied alcohols to form different ester products.

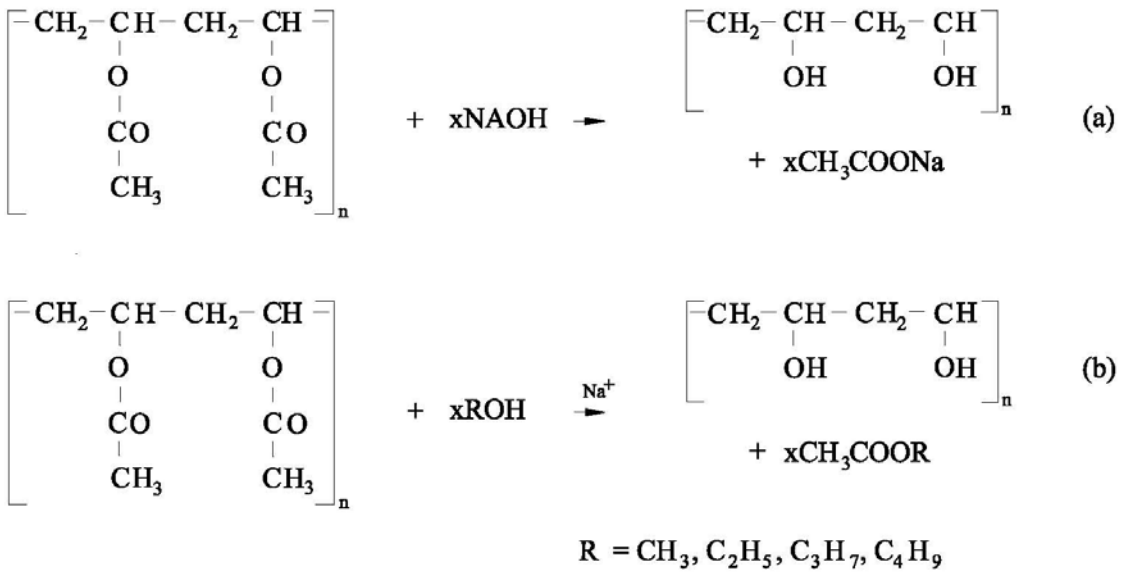

Figure 2-6 The PEKK repeat unit. The carbons and oxygen in different environments are numbered.

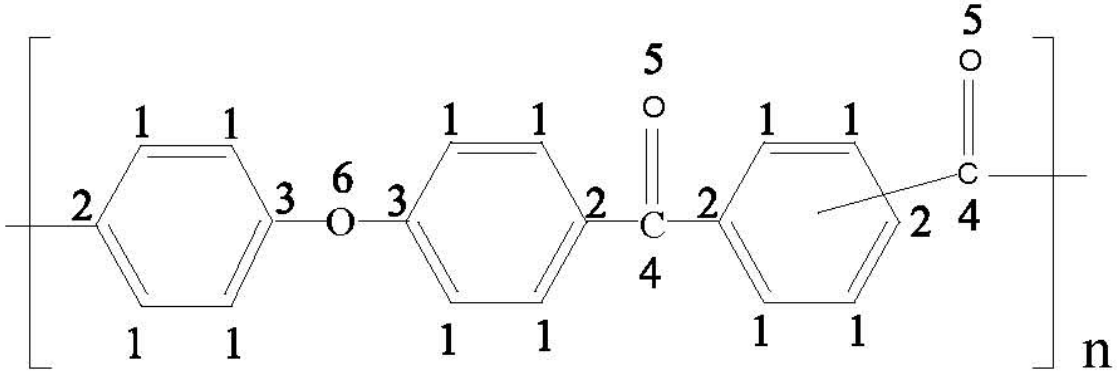

Figure 2-7 The overall, column I, C 1s, column II, O 1s, column III, and valence band XPS spectra of PEKK coated on copper metal (a), untreated carbon fiber with the excess PEKK solution removed (b), and not removed (c). A carbon fiber treated in nitric acid for 20 seconds (d), the carbon fiber in (d) coated with PEKK (e) and a carbon fiber treated in nitric acid for 120 seconds (f), the carbon fiber in (f) coated with PEKK (g), the treated carbon fibers coated with PEKK had the excess solution removed.[18]

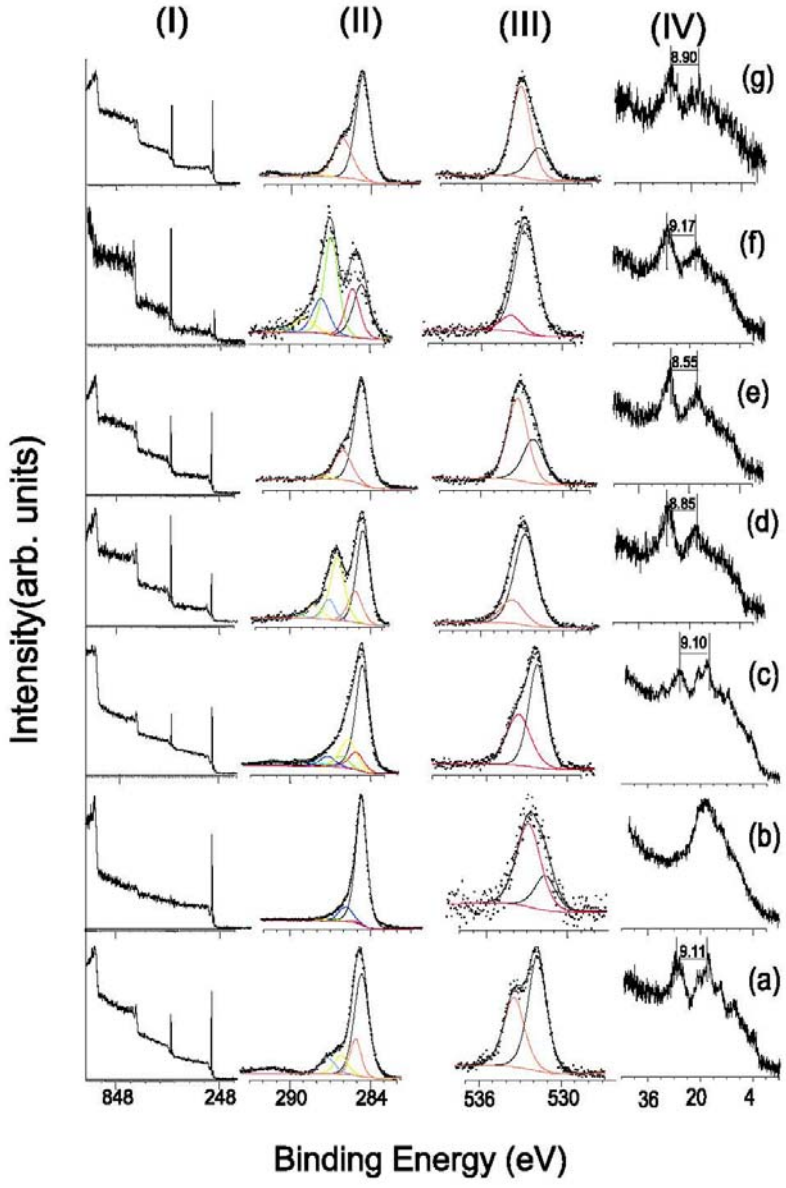

Figure 2-8 The overall, column I, C 1s, column II, O 1s, column III, and valence band, column IV, XPS spectra of a thick film of PEKK on copper (a) treated in 365 K saline solution for 5 days (b) and 10 days (c). The carbon fiber treated in nitric acid for 20 seconds (d) treated in 365 K saline solution for 5 days (e) and 10 days (f).[18]

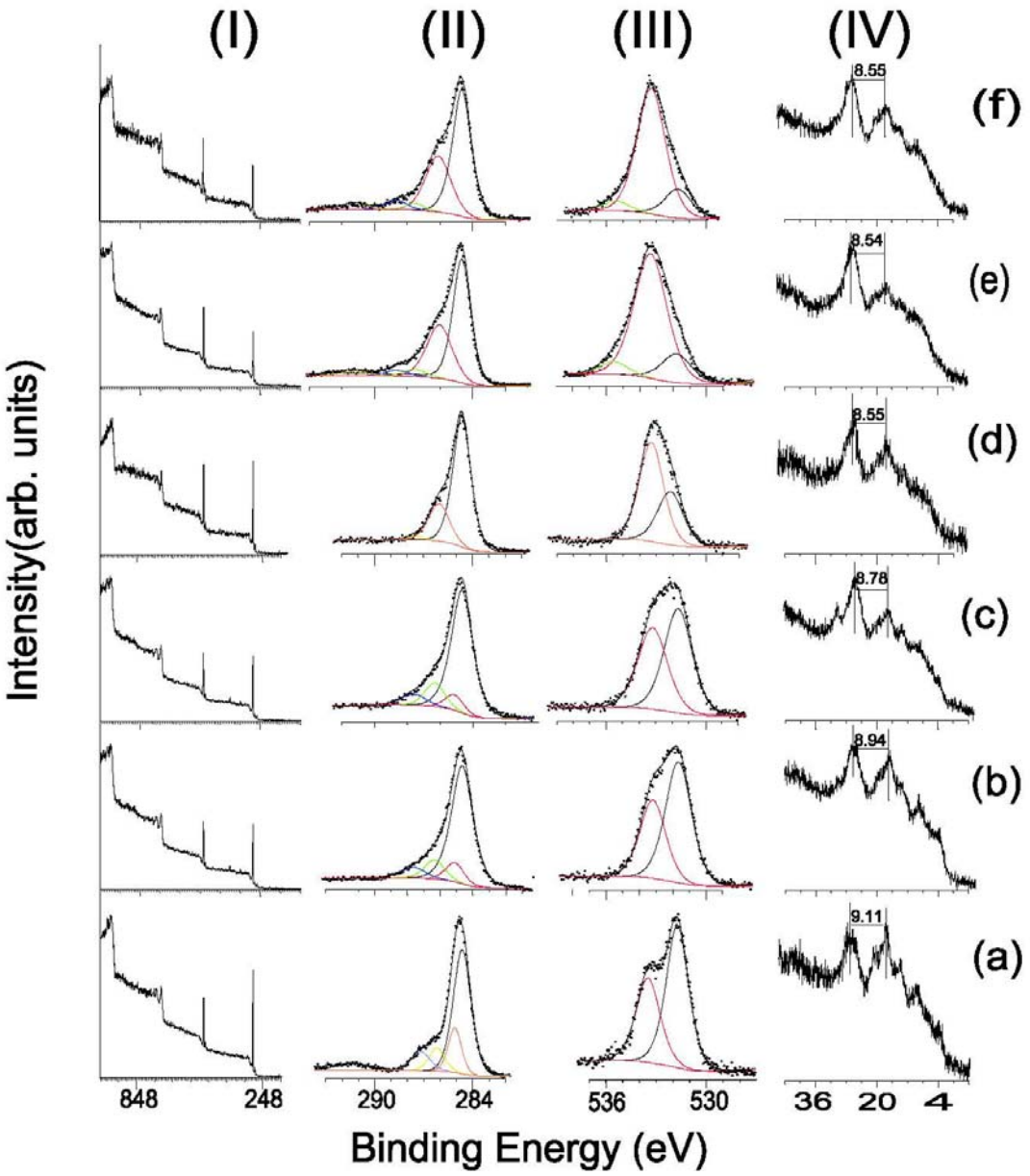

CHAPTER 3 - Corrosion and Corrosion Resistant films

3.1. CORROSION

One of the principal interests of our research group is a study of the surface chemistry of metal surfaces with the goal of developing methods for the protection of metals and other materials against corrosion. Corrosion has been seen as one of the industrial world's biggest expenses. There are several methods that have been used over the years to prevent the corrosion of metals in bridges, buildings, cars, etc.[1-8]

Before discussion of the prevention of corrosion, the definition of corrosion versus erosion should be made clear. Corrosion is the chemical or electrochemical reaction of metal with the moisture in the atmosphere and salt in water. Erosion is the physical wear of metals from mechanical wear or abrasion. Erosion can be seen in the degradation of moving parts over time and an example of corrosion can be seen in the rusting of metal frame cars. The fastest and most dangerous type of material breakdown is when both corrosion and erosion are occurring.[9]

3.2. PHOSPHATES AS COATINGS

The creation of a stable thin film on metals to prevent corrosion has been a focus of Dr. Sherwood's group for many years and several articles have been published on corrosion and its investigation by XPS.[1,7,10-16] This section will review the basic history and structure of phosphates as coatings and previous phosphate coatings formed and studied by our group.

3.2.1. History. Phosphates were first reliably reported as coatings in the treatment of metals in 1869 when a British patent was issued that described a method to prevent moisture from rusting corset stays.[17,18] In this procedure, the metal strips were heated until they were red hot and dipped into a phosphoric acid solution. The resulting coating was thin and not resistant to wear. In 1906, another British patent was issued that described the formation of a phosphatizing

solution made from dissolving iron filings in dilute phosphoric acid. Later, the iron filings where replaced with magnesium and zinc salt.

The phosphate coatings that are currently used in industry are illustrated in Figure 3.1.[19] The coating consists of an outer layer of porous aluminum phosphate on the surface and then an intermediate layer of metal oxide between the metal and the phosphate. The thickness of the coating is approximately 4000 angstroms (3000 and 1000 angstroms of aluminum phosphate and aluminum oxide, respectively) and its uses include protective coatings on nuts, bolts, and other small parts to prevent corrosion and improve adhesion. The coating is also absorbent so it can be easily lubricated and used on moving parts in engines. Phosphate coatings have been produced on aluminum metal for a number of years; for example, Boeing has used phosphate coatings on aluminum for adhering aluminum panels together for airplanes.

3.2.2. Previous work on phosphate coatings. Our group has discovered and examined the formation of a new type of phosphate film that is free of the intermediate oxide layer and bonded directly to the metal surface.[1] These phosphate films have a thickness that is less than 100 angstroms, which can vary depending on the potential applied during formation. These coatings have been shown to form on metals such as aluminum[1], iron[1], copper[12], titanium[13], and vanadium[14]. The aluminum and iron studies indicated that different phosphate coatings can be formed and that it is possible to distinguish between them using valence band XPS**.** The studies were conducted in an anaerobic cell that is in an adjacent chamber to the main chamber where XPS is collected.[13,20] This chamber allows a clean metal surface to be placed in an electrochemical cell where the phosphate coating is formed chemically in a 5M orthophosphoric acid solution at -.5 volt vs SCE. In these reducing conditions, phosphate formation is favored over oxide formation. The advantage of having the metal in the anaerobic cell is that XPS can be run on the sample before and after treatment with acid and problems with exposing the sample to air during transfer is avoided

Aluminum and iron metal with their native oxide intact have different reactions when exposed to atmospheric conditions. Aluminum metal is very reactive in air, but is protected from reaction by its native oxide layer. When the oxide layer is removed, aluminum reacts quickly in air to replace it, keeping the underlying aluminum metal protected. Iron metal is less reactive in the presence of air, but its native oxide layer is porous allowing for the attack of the underlying

metal. Iron metal reacts with moisture in the air to form iron oxide, or rust, which is flaky and falls off of the iron surface allowing the metal underneath to be exposed, repeating the process.

Aluminum metal was studied in the anaerobic cell. The oxide layer was removed from the metal surface by argon ion etching and a clean surface was detected using XPS. The clean metal surface was then placed in an electrochemical cell, and chemically reacted with phosphoric acid to form a phosphate film, which was detected using XPS. The procedure was then repeated with iron.

The aluminum phosphate film formed on aluminum metal was the most interesting of the metal phosphate films studied. Instead of forming the aluminum orthophosphate film that was expected, another form of phosphate was present. The coating was later determined to be aluminum tetrametaphosphate, $Al_4P_4O_{12}$, the surface reaction being crudely represented by the equation:[1]

$$4H_3PO_4 + 4Al \rightarrow Al_4P_4O_{12} + 4H_2O + 2H_2 \qquad (9)$$

Figure 3.2 shows the outer valence band region between 0 eV and 20 eV of the aluminum phosphate film formed on aluminum metal in the anaerobic cell compared to the experimental spectra of aluminum tetrametaphosphate. The aluminum tetrametaphosphate film was then exposed to atmospheric conditions for two weeks and the unstable aluminum tetrametaphosphate film had reacted in air and converted to an aluminum orthophosphate film:[1]

$$P_4O_{12}^{4-} + 4H_2O \rightarrow 4PO_4^{3-} + 8H^+ \qquad (10)$$

The spectrum of the experimental aluminum phosphate coating is shown in Figure 3.3 compared to the experimental spectrum of aluminum orthophosphate. The experimental spectra of aluminum tetrametaphosphate and the aluminum orthophosphate were also compared to spectra generated from band structure calculations in Figure 3.4. Alpha aluminum oxide (α-Al_2O_3) was included in Figure 3.4 to show that oxides can be excluded as a possibility in both films.

The differences are seen in Figure 3.4 by the peaks labeled 1 at 16 electron volts, 2 at 14 electron volts, and 3 at 3.4 electron volts, all energies are reported for the experimental spectra

since absolute binding energies in the calculations can be shifted according to the basis set used. The aluminum oxide shows no intense features at the position of 1 and 2, only 3, the aluminum orthophosphate shows intense features at 2 and 3, but not 1, and the aluminum tetrametaphosphate shows intense features at 1 and 3, and a less intense feature in the valley at 2.

When the experiment was repeated on iron metal, it formed an orthophosphate film directly in anaerobic cell through the reaction with the metal surface represented by the equation:[1]

$$6H_3PO_4 + 4Fe \rightarrow 2Fe_2(PO_4)_3 + 9H_2 \qquad (11)$$

This coating remained unchanged after exposure to air for two weeks and is shown in Figure 3.5 compared to the experimental spectrum of ferric orthophosphate. The characteristics peaks are seen for orthophosphate at 11 and 14 electron volts. Preliminary results show that the most stable phosphate film is the orthophosphate ion, but further studies with different metals may reveal a more or equally as stable film.

3.3. ACKNOWLEDGEMENTS

Special thanks to Dr. Sherwood, G. D. Davis, T. S. Sun, J. S. Ahearn, and J. D. Venables for the Figures below that were reprinted from their work.

3.4. REFERENCES (see Reference chapter)

3.5. FIGURES

Figure 3-1 Phosphoric acid anodized aluminum surface.[19]

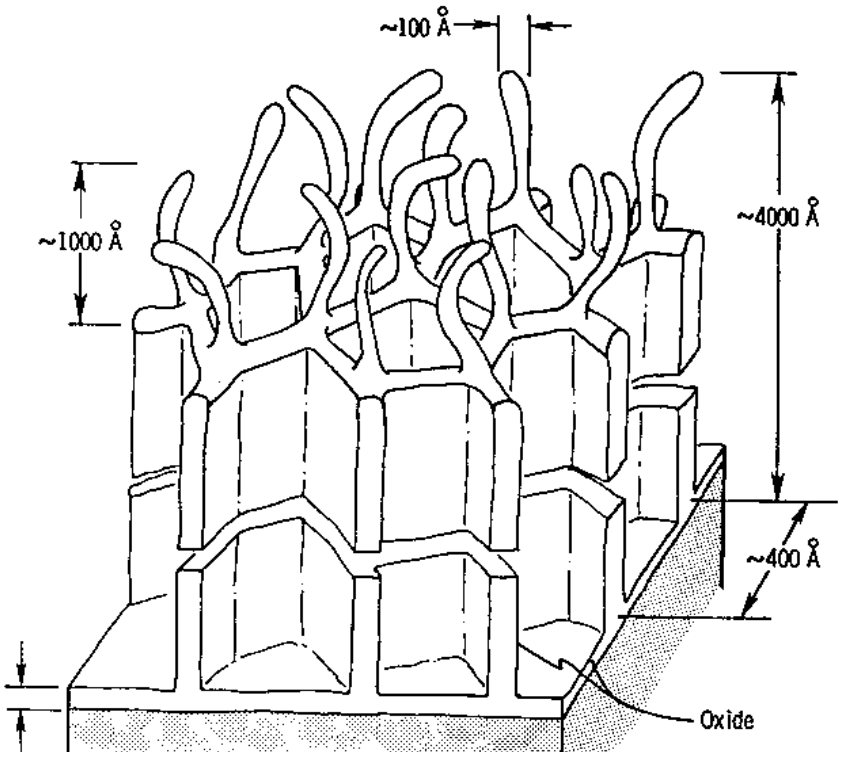

Figure 3-2 Valence band XPS spectra of the product of the reaction of aluminum metal with 5 M orthophosphoric acid before air exposure compared to an aluminum tetrametaphosphate powder.[1]

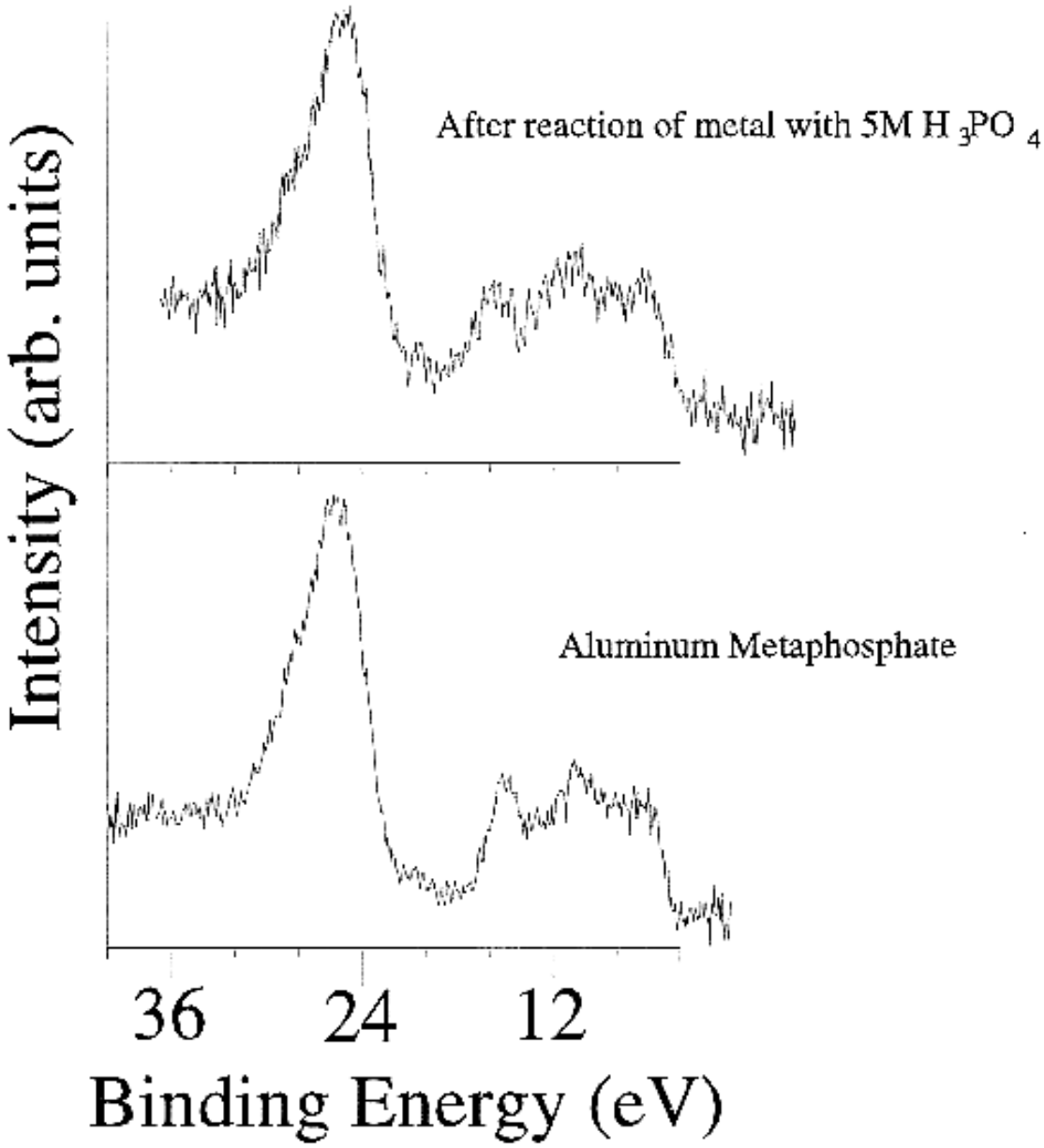

Figure 3-3 Valence band XPS spectra of the aluminum phosphate coated sample after exposure to the atmosphere for two weeks compared to an aluminum orthophosphate powder.[1]

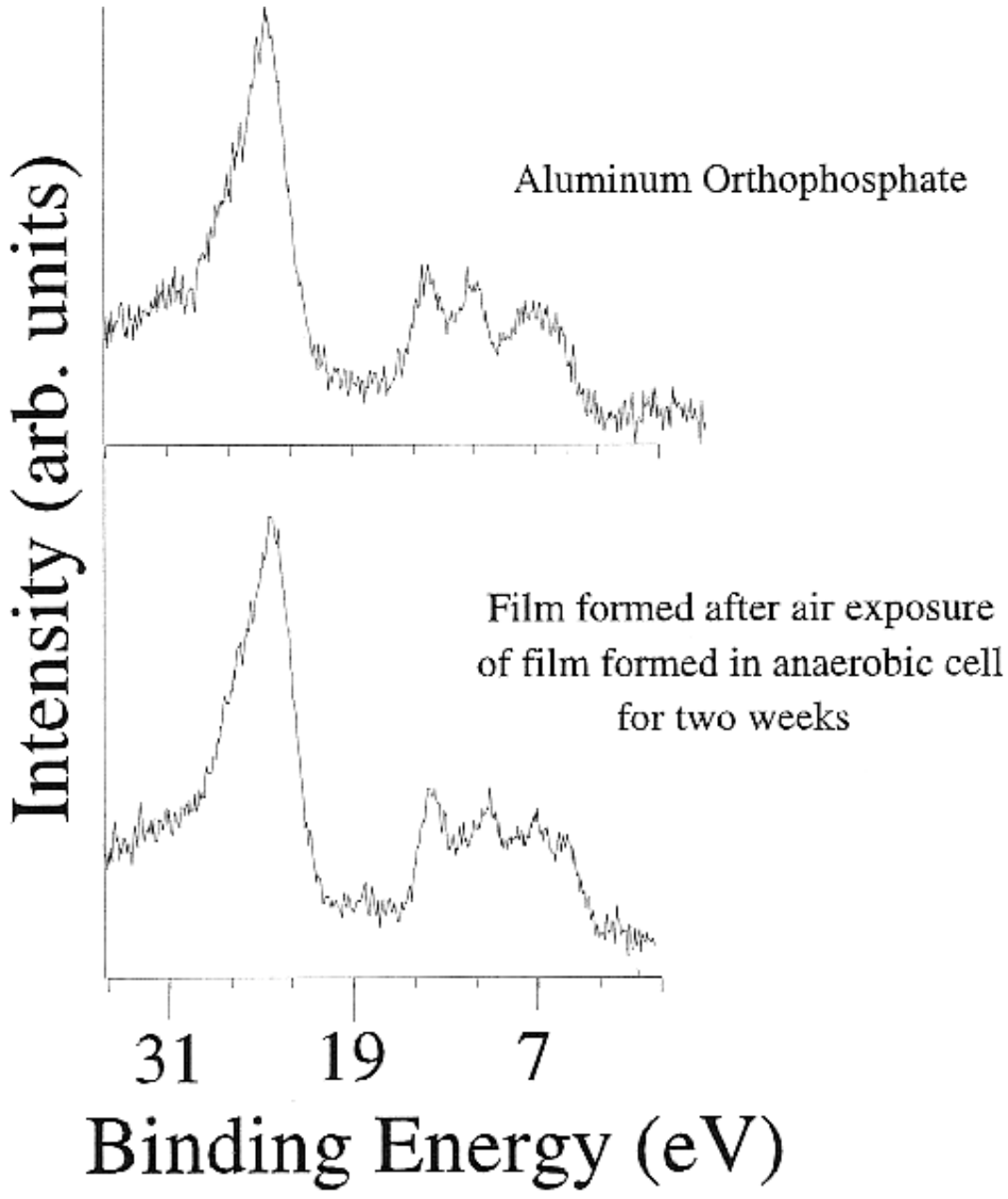

Figure 3-4 the Outer valence band region of experimental α-Al_2O_3 compared with $AlPO_4$ and $Al_4(P_4O_{12})_3$ and valence band spectra generated by band structure calculations.[1]

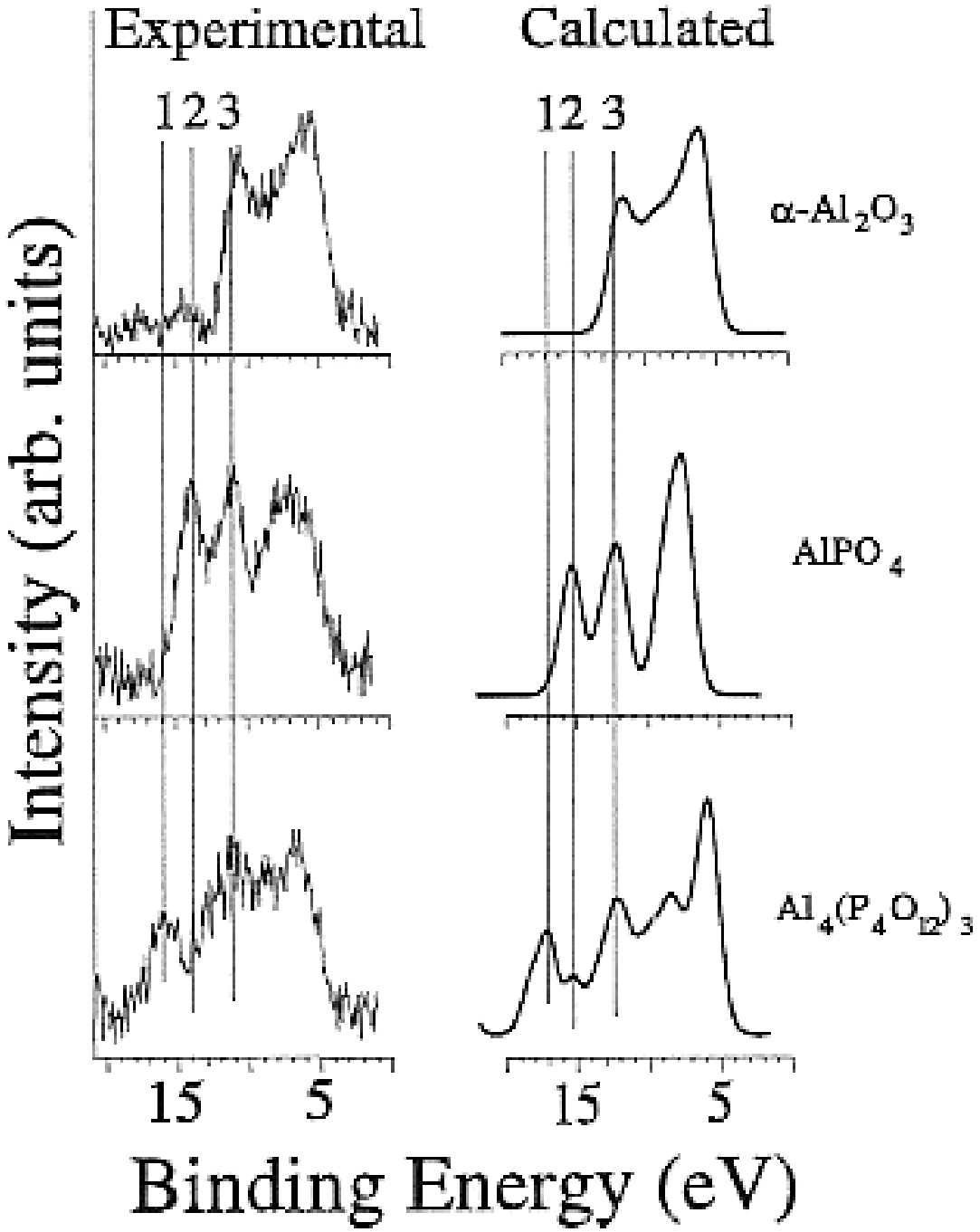

Figure 3-5 Valence band spectra of the iron sample after exposure to the atmosphere for two weeks.[1]

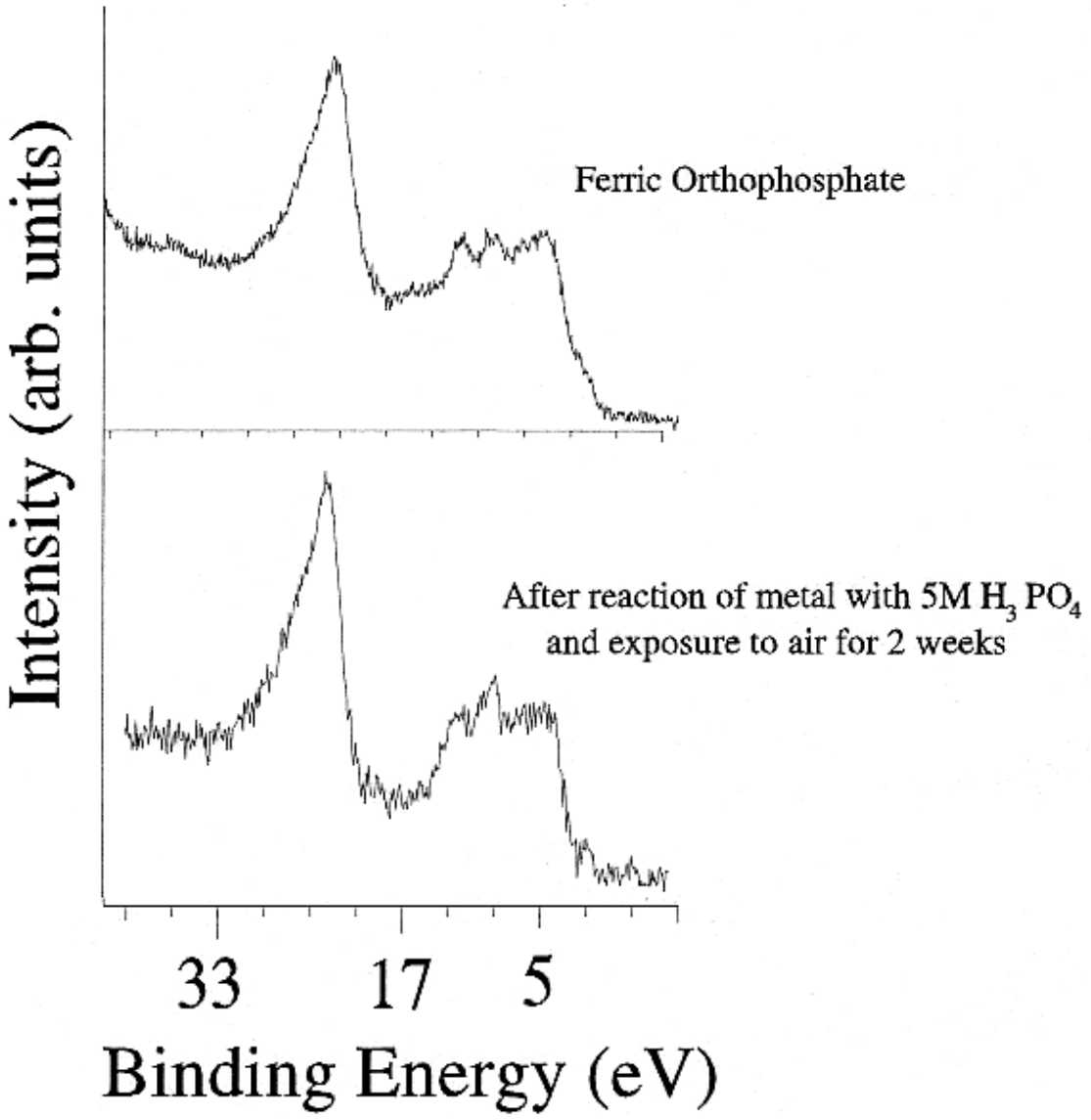

CHAPTER 4 - T The Study of the Formation of Films on Aluminum Metal using different Phosphorus Containing Acids and Polyvinyl Alcohol by Core Level and Valence Band X-ray Photoelectron Spectroscopy

4.1. INTRODUCTION

X-ray photoelectron spectroscopy (XPS) has been used by our group to study the formation of oxide free phosphate films on clean aluminum surfaces.[1-6] One such study indicated that different chemical compositions of phosphate films could be formed after transfer from ultra-high vacuum, UHV, conditions to atmospheric conditions. An ionic tetrametaphosphate, $P_4O_{12}^{4-}$, film was observed in UHV, but after two weeks exposure to atmospheric conditions in the laboratory an ionic orthophosphate, PO_4^{3-}, film was observed.[3] This finding lead to further studies of the different phosphorus containing compounds in an attempt to characterize them using primarily valence band, VB, XPS to distinguish the chemical differences in the surfaces. The first study was conducted on the sodium phosphate powders, $Na_4P_2O_7$, $Na_5P_3O_{10}$, $Na_4P_4O_{12}$, $Na_2H_2P_2O_7$, and NaH_2PO_2.[7] The VB- XPS spectra of the powders showed significant differences in the spectra which were interpreted by calculations. These differences showed that VB- XPS could be used to distinguish between phosphates with different chemical compositions.

A recent publication[6], showed that different oxide free phosphorus films containing the ions HPO_3^{2-} and $H_2PO_2^-$ can be formed on abraded aluminum metal by using their respective phosphorus containing acids. These films give VB- XPS spectra that had subtle chemicals differences similar to those observed in the phosphate powder research, showing that phosphorus containing films can also be characterized using VB- XPS. The difference between the first study of phosphate films mentioned and this particular study is that the oxide free films were formed in atmospheric conditions using a new technique developed in our laboratory.[2] All the VB- XPS spectra in these studies were compared to spectra generated from multiple scattered

wave Xα cluster and/or band structure calculations to aid in the characterization of the powders and films.

Films containing the orthophosphate ion, PO_4^{3-}, have recently been studied for their potential as an adhesion promoter between aluminum metal and the polymer polyvinyl alcohol, PVA.[2] PVA is a water soluble polymer that can be formed on the surface of orthophosphate. The phosphate is seen as an adhesion promoter between the aluminum metal to form a uniform thin coating of PVA on aluminum that would not have otherwise occurred.

This chapter covers the ongoing studies and characterization of new phosphorus containing films. The films containing the linear phosphate ion, $P_2O_7^{4-}$, cyclic phosphate ion, $P_4O_{12}^{4-}$, and tetradhedral phosphorous ions, HPO_3^{2-} and $H_2PO_2^{-}$, were formed on the abraded surface of aluminum metal and studied using core level and valence band XPS spectra compared to spectra generated using band structure and Xα cluster calculations. PVA was then coated on the existing phosphorus containing films and the buried interface between the layers was analyzed using VB- XPS.

4.2. EXPERIMENTAL

4.2.1. Materials and sample preparation.

4.2.1.1. Materials. Aluminum foil (99.999%) was purchased from Goodfellow Cambridge Limited, England (LS178013 B G) with a thickness of 0.125 mm and degreased with acetone prior to use. Silicon carbide 600 sandpaper was purchased from Carborundum Abrasives. 85% orthophosphoric acid was purchased from Fisher Scientific. Pyrophosphoric acid, 99.99% Metaphosphoric acid, and 99% phosphorous acid were purchased from Aldrich. 50% hypophosphorous acid was purchased from Sigma-Aldrich. The polyvinyl alcohol was purchased from Sigma and had a mean molecular weight of between 30 000 and 70 000.

4.2.1.2. Preparation of the phosphorus containing films on abraded aluminum metal. The phosphorous acids were diluted with quadruplely distilled (4-D) water to make 5 M solutions. The solutions were then deoxygenated for 2 hours using nitrogen. The aluminum metal was abraded by hand with fine sandpaper for 5 minutes while in solution and left to stand for an additional 10 minutes in solution. The films were then dried overnight in atmospheric conditions.

4.2.1.3. PVA film preparation. A 0.25 % solution of PVA in 4-D water was prepared using the previously described method.[2] PVA films were formed on the dried phosphorus containing films by dipping the metal in the 0.25 wt% PVA solution twice with a 12 second break between each successive dip.

4.2.2. Surface analysis. All spectra were collected with a VSW HA150 spectrometer (150 mm hemispherical analyzer) operated in the fixed analyzer transmission mode with a pass energy of 20 eV, also equipped with a 16-plate microchannel detection system. The Al Kα X radiation (240 Watts) generated from a 35 quartz crystal monochromator which provides a linewidth of better than 0.2 eV. The base pressure of the instrument was 10^{-9} Torr or better. All spectra were referenced against the C1s peak at 284.6 eV.

4.2.3. Calculations. Both band structure and Xα cluster calculations were used to generate the spectra used to interpret the experimental valence band XPS spectra.

4.2.3.1. Band structure calculations. The band structure calculations were carried out using an extended version of the program CRYSTAL.[8,9] This program performs *ab initio* calculations of the ground state energy, electronic wave function and properties of periodic systems. One electron eigenfunctions of the Fock Hamiltonian are represented by linear combinations of Bloch functions, which are also a linear combination of atomic orbitals. A Mulliken analysis is used to obtain orbital, atomic and total densities of states. The separate densities of states for each type of orbital for each atom in the compound were evaluated and adjusted by their atomic photoelectron cross sections using values as determined by Scofield[10]. These cross-section-adjusted total densities of states were then convoluted with a Gaussian/ Lorentzian product function. All of the calculations employed the STO-3G basis set. Calculations were performed for the $P3_22$ structure for (berlinite) of $AlPO_4$[11], the orthorhombic structure of $Na_4P_2O_7$[12] and the tetragonal structure of $Na_4P_4O_{12}$[13].

4.2.3.2. Xα cluster calculations. We find that for these systems the energies in the band structure calculations do not vary much for the different directions of the crystal, the bands are flat. This allows the spectra to be interpreted by both band structure and Xα cluster calculations. Xα cluster calculations[14] were carried out using multiple scattered-wave Xα calculations based on an ion representative of the crystal lattice symmetry. A "Watson sphere" with a charge opposite to the ionic charge is used to neutralize the charge of the ion. Calculations for the PO_4^{3-}

and $P_2O_7^{4-}$ ions are reported in this chapter. The parameters for the calculations are shown in Table 4.1.

4.3. RESULTS AND DISCUSSION

The chemical composition of the films formed on aluminum metals after exposure of the abraded metal to different phosphorus containing acid solutions were determined by core level and valence band XPS.

4.3.1. Core XPS for phosphorus containing films. Figure 4.1 shows the Al 2p, column I, P 2p, column II, and O 1s, column III, of the phosphorus containing acids H_3PO_4 (a), $H_4P_2O_7$ (b), $H(PO_3)_n$, which corresponds to $H_4P_4O_{12}$ (c) [7], H_3PO_3 (d), and H_3PO_2 (e). The spectra show the features expected for the respective region. Al 2p spectra show a more intense peak corresponding to the oxygen content at 75 eV and a less intense peak corresponding to the aluminum metal that shifts between 71 eV to 72 eV. P 2p spectra have a peak centered at 134 eV and O 1s spectra have a peak centered at 532.5 eV. The spectra were also run with a $^{+}$10 volt applied bias, not shown here, with no change noted in the peaks.

The Al 2p region, Figure 4.1 I, can also be used to compare the thickness of the films by observing the intensity of the peak centered between 71 eV and 72 eV. A thicker film would give less intense peaks from the underlying aluminum metal. Another observation that should be noted is the shift of the underlying aluminum metal peaks. The separation of the peaks in Figure 4.1 I (a) between the oxygen component peak and the metal peak is 3.94, for Figure 4.1 I (b) its 3.20, Figure 4.1 I (c) is 2.85, and Figure 4.1 I (e) is 3.85. The separation for Figure 4.1 I (d) is not reported since the film is sufficiently thick to not show the underlying aluminum metal peak. With the exception of the $P_2O_7^{4-}$ film, the separations can be compared by using the film thickness with thinner films showing a larger separation.

4.3.2. Valence band XPS for phosphorus containing films. Valence band XPS has been used in our laboratory to compliment the core level XPS and further distinguish the chemical difference between similar compounds. Valence band XPS becomes more valuable when the core level shifts are not significant enough to be used for characterization. The original valence band spectra for the phosphorus containing films are shown in Figure 4.2. The spectra show in the same order as Figure 4.1, H_3PO_4 (a), $H_4P_2O_7$ (b), $H_4P_4O_{12}$ (c), H_3PO_3 (d), and H_3PO_2 (e).

The spectra in Figure 4.2 have similar characteristic peaks; the most intense peak, O 2s, at 25 eV and three peaks in the lower binding energy region between 0 to 20 eV. Substantial differences can be seen in the spectra with the two peaks around 9 eV to 10 eV and 13 eV to14 eV showing the most change.

The film formed on aluminum metal using H_3PO_4 is shown in Figure 4.2 (a). PO_4^{3-} is the most stable of the phosphate ions, consisting of a single tetrahedral PO_4^{3-} with one P-O type bond, shown in Figure 4.3 (a). The film formed using $H_4P_2O_7$ is shown in Figure 4.2 (b). $P_2O_7^{4-}$ has two tetrahedral PO_4^{3-} units joined at the apex with an oxygen atom with two unique P-O type bonds from the P-O type bond and the P-O-P type bridging oxygen bond that have a 6:1 ratio, shown in Figure 4.3 (b). $H_4P_4O_{12}$, film formed shown in Figure 4.2 (c), is a cyclic phosphate with 4 tetrahedral PO_4^{3-} units connected in a ring by bridging oxygen atoms with two unique P-O type bonds from P-O type bond and P-O-P type bridging oxygen bond, with an 8:4 ratio, shown in Figure 4.3 (c). H_3PO_3 and H_3PO_2 are formed by replacing the P-O bond in the tetrahedral PO_4^{3-} ion with P-H type bonds. The structure and spectra for H_3PO_3 and H_3PO_2 are discussed in a previous publication[4] and are shown here for later comparison when the respective phosphorus containing films on aluminum metal are coated with PVA.

4.3.3. Outer valence band region for phosphorus containing films. The nonlinear background and valence band region from 20 eV to 40 eV was removed to show a closer view of the outer valence band region where the bonding between phosphorus and oxygen is shown. Figure 4.4 shows the resultant experimental spectra of the film formed on aluminum metal using H_3PO_4, Figure 4.4 I (a), and $H_4P_2O_7$, Figure 4.4 II (a), compared to the spectra generated from band structure calculations of $AlPO_4$ and $Na_4P_2O_7$, Figure 4.4 I (b) and II (b), respectively. The spectra generated using Xα cluster calculation for the ions PO_4^{3-}, Figure 4.4 I (c), and $P_2O_7^{4-}$, Figure 4.4 II (c), are also shown.

The two peaks of interest here are the highest binding energy peaks, for both films formed on the aluminum metal. These peaks are at 10 eV and 13 eV with a separation of 3 eV for the PO_4^{3-} film and 10 eV and 13.3 eV with a separation of 3.3 eV for the $P_2O_7^{4-}$ film. The peak shapes for the PO_4^{3-} and $P_2O_7^{4-}$ films also show substantial differences. The PO_4^{3-} film has two sharp peaks at 10 eV and 13 eV and the $P_2O_7^{4-}$ film has a rounded peak at 13.3 eV and a broader rounded peak at 10 eV. The peak shapes can be predicted using the Xα cluster calculations in Figure 4.4 (c). The high symmetry PO_4^{3-} ion has singlet, doublet, and triplet

peaks predicted by the calculation that are added to create the valence band spectrum. Figure 4.4 I (c) shows the Xα cluster calculation using a PO_4^{3-} ion. The higher binding energy peaks at 9 eV and 13 eV predict the peaks that are seen in the experimental spectrum Figure 4.4 I (a).

Figure 4.4 II (c) shows how the experimental spectrum for the $H_4P_2O_7$ treated sample compares with the spectrum generated using Xα cluster calculations. The agreement is good, with the three principle spectral features in the experimental spectrum identified by calculation. In the lower symmetry $P_2O_7^{4-}$, some of the triplets and doubles have been replaced with singlets that cover more energy range and cause the three spectral features to become broader. This broadening is confirmed in the experimental spectrum of the $P_2O_7^{4-}$ film by the loss of the valley at 8 eV that is seen in the experimental spectrum of the PO_4^{3-} film.

Figure 4.5 shows the experimental spectrum for the outer valence band region, between 0 and 20 eV, for the film formed on aluminum metal using $H_4P_4O_{12}$, Figure 4.5 (a), and the spectra generated from band structure calculations of $Na_4P_4O_{12}$, Figure 4.5 (b). The high binding energy peaks are at 10 eV and 14.5 eV with a separation of 4.5 eV. The peak at 14.5 is a sharp peak and at 10 eV the peak is still sharp but is broader than the 14.5 eV peak. The experimental XPS spectrum is predicted well by the band structure calculation.

When comparing the valence band XPS spectrum of the film formed using $H_4P_4O_{12}$ to the spectra of the films formed using $H_4P_2O_7$ and H_3PO_4 substantial differences exist. In the film formed using H_3PO_4, the two high binding energy peaks are separated completely from each other and the third peak is at 6 eV. The valley between the second peak and third peak decreases in the spectra for the films formed using $H_4P_2O_7$ and $H_4P_4O_{12}$ as a result of the lower symmetry of these species compared to the PO_4^{3-} ion, as predicted in the Xα cluster calculation of the $P_2O_7^{4-}$ ion in Figure 4.5 II (c). The differences between the spectra of $H_4P_2O_7$ and $H_4P_4O_{12}$ are significant and, in particular, the separation between the two high binding energy peaks is more than 1 eV different at 3.3 eV and 4.5 eV, respectively.

The adhesive abilities of the phosphorus containing films were then tested by using PVA to form a second film over the phosphorus films. This was studied using core and valence band XPS that is predicted using spectra generated using band structure and Xα cluster calculations. The chemistry at the interface between the phosphorus containing films and PVA will also be discussed.

4.3.4. Core XPS for PVA coated on phosphorus containing films formed on aluminum metal. The XPS spectra for the core level of the phosphorus containing films formed on aluminum metal further coated using PVA are shown in Figure 4.7. The O 1s region, shown in Figure 4.7 I, has one peak centered between 533 eV and 533.5 eV. The C 1s region, Figure 4.7 II, is shown here because of the differences observed in the PVA coating since the repeating unit of PVA, shown in Figure 4.6 (c), contains carbon. The O 1s XPS spectrum, Figure 4.6 (a), and valence band XPS spectrum, Figure 4.6 (b), were run and reported by Y. Wang and P. M. A. Sherwood and reprinted here for comparison.[2]

The C 1s region in Figure 4.7 II reflects the added carbon components and has three peaks shifted from the hydrocarbon peak calibrated at 284.6 eV. The C-C-O, type 1, bond is centered 285 eV and a less intense peak for the C-O, type 2, bond is at 289 eV. The C 1s region was previously curve fitted and discussed for PVA coated on abraded aluminum metal treated using H_3PO_4.[2] P 2p region Figure 4.7 (III) has one peak centered between 133 and 133.5 eV.

Al 2p region Figure 4.7 (IV) shows a more intense feature between 73.5 and 74.5 eV containing oxygen content. The thickness of the coating can be observed again by using the intensity of the peak between 70 eV and 71eV. The addition of the PVA coating has still provided a metal peak in this region for the $P_2O_7^{4-}$ (a) and HPO_3^{2-} (b) films. The metal peak in Al 2p for the $H_2PO_2^-$ film, Figure 4.7 (c), is not very intense, but the two films, HPO_3^{2-} and PVA, combined still have a thickness <100 Å. Closer examination shows that shifting in the metal peak occurs similar to the phosphorus containing films formed prior to PVA coating, shown in Figure 4.1. In the case of the PVA coated on abraded aluminum metal treated using H_3PO_3, Figure 4.7 IV (b), the metal peak at 71 eV is almost as intense as the oxygen component peak at 74 eV and has a separation of 3 eV. The PVA coated on abraded aluminum metal treated using $H_4P_2O_7$, Figure 4.7 IV (a), has a medium intensity metal peak at 70 eV compared to the oxygen component peak at 74 eV and a separation of 4 eV. As observed earlier, the less intense metal peak has a large shift from the oxygen component peak.

4.3.5. Valence band XPS for PVA coated on phosphorus containing films on aluminum metal. The valence band XPS spectra are shown in Figure 4.8 for PVA coated on abraded aluminum metal treated using $H_4P_2O_7$ (a), H_3PO_3 (b), and H_3PO_2 (c). The spectra involve a combination of the PVA and the phosphate spectra. A peak centered between 17 eV and 17.6 eV appears at a lower binding energy than the O 2s peak. The outer valence band

region between 0 eV and 20 eV is shown in Figure 4.9 with the nonlinear background removed. There are significant differences between these spectra, with the main differences observed in the three higher binding energy peaks. The spectrum of the PVA coated on the $P_2O_7^{4-}$ film on aluminum metal, figure 4.9 (a), has a less intense and more rounded peak at 17 eV compared to the spectra of the PVA coated on the HPO_3^{2-}, Figure 4.9 (b), and $H_2PO_2^-$, Figure 4.9 (c), films. Further discussion of these spectra is in the following section.

4.3.6. Interaction of the phosphorus containing films with PVA. Spectra generated using band structure or Xα cluster calculations can be used to predict the valence band structure of the experimental data when it is in as-received form or containing one film. When multiple coatings are present, the valence band region can become more complicated and the multiple molecules present more difficult to calculate, so a different means of evaluating the data becomes necessary. Addition and subtraction spectra can be used in this case to evaluate the bonding in the buried interface region between the coatings. This technique has been discussed previously[2,16] and in section 1.4.2. This has been performed for the PVA coated on the $P_2O_7^{4-}$, HPO_3^{2-}, and $H_2PO_2^-$ films.

The spectra of the PVA coated on the $P_2O_7^{4-}$ film are shown in Figure 4.10. The $P_2O_7^{4-}$ film on abraded aluminum metal is shown in Figure 4.10 (a) and the spectrum for PVA is shown in Figure 4.10 (b) reprinted from Figure 4.2 (b) and Figure 4.6 (b). The two spectra were added and the resultant spectrum is shown in Figure 4.10 (c) and compared to the experimental spectrum of the PVA coated on the $P_2O_7^{4-}$ film from Figure 4.8 (a) shown again in Figure 4.10 (d) for comparison. The addition spectrum retains the PVA characteristic peak at 18 eV^2 and the pyrophosphate peaks at 13.3 eV and 10 eV. In the experimental spectrum of the PVA coated on the $P_2O_7^{4-}$ film, Figure 4.10 (d), the peak for PVA is shifted from 18 eV to 17 eV and the pyrophosphate peaks are at 12.5 eV and 9.5 eV. The difference between the addition spectrum, Figure 4.10 (c), and the experimental spectrum, Figure 4.10 (d), is determined by subtracting the addition spectrum from the experimental spectrum. The resultant spectrum is shown in Figure 4.10 (e). If the spectrum had been a flat line the experimental spectrum would have been an addition of the PVA and $P_2O_7^{4-}$ indicating no interaction in the buried interface. This was not the case and several peaks are observed in the difference spectrum showing that the chemical environment changes at the buried interface. The shift of the PVA peak can be seen in the difference spectrum by the positive peak at 18 eV and the negative peak at 17 eV. This was

repeated for PVA coated on the HPO_3^{2-} film, Figure 4.12, and $H_2PO_2^-$ film, Figure 4.14, and similar results to the PVA coated on the $P_2O_7^{4-}$ film were shown.

The addition and difference spectra were height normalized to 10000 counts and allied by calibrating the hydrocarbon peak in the C 1s to 284.6 eV. The chi squared value was obtained by following the procedure described in Chapter 1.4.2. The chi squared values where graphed versus the % contribution of PVA, which is shown in Figures 4.11 for $P_2O_7^{4-}$, Figure 4.13 for $H_2PO_2^-$, and Figure 4.15 for HPO_3^{2-} films on aluminum metal.

4.4. CONCLUSION

Novel phosphorus containing films can be formed on abraded aluminum metal using 5 M solutions of $H_4P_2O_7$ and $H_4P_4O_{12}$. This can be seen by comparison to the film formed by using H_3PO_4 and the spectra generated from band structure and Xα cluster calculations. The $P_2O_7^{4-}$, $H_2PO_2^-$, HPO_3^{2-} films were shown to have good adhesive properties by forming bonds between both the metal and the PVA coatings affectively attaching the PVA to the aluminum metal which would not have been possible without the use of the phosphorus containing compounds.

4.5. ACKNOWLEDGEMENTS

This material is based upon work supported by the National Science Foundation under Grant No. CHE-0137502. The U.S. Government has certain rights to this material. I would like to thank LaShonda McIntyre for her help in the collection and analysis of the data and Dr. P. M. A. Sherwood for helping on the band structure calculations and providing the Xα cluster calculations.

4.6. REFERENCES (see Reference chapter)

4.7. TABLES

Table 4-1 Parameters and features of the Xα calculations.

Table 4.1. Parameters and features of the Xα calculations.

Cluster	PO_4^{3-}	$P_2O_7^{4-}$
symmetry	T_d	C_{2v}
P-O bond lengths	1.56Å	1.513 Å – PO (2) 1.513 Å –PO (1) 1.637 Å –POP (1)
Xα parameters:		
outer α value	0.74082	0.74041
intersphere α value	0.74082	0.74041
Phosphorus sphere radius	0.991 Å	0.958 Å
Oxygen sphere radius	0.959 Å	0.893 Å – PO (2) 0.885 Å –PO (1) 1.020 Å –PO (1)
watson sphere radius	1.560 Å	3.443 Å
outer sphere radius	2.519 Å	3.443 Å
virial ratio	1.001 856 8	1.005 559 04

Note: Convergence: When the difference in potentials at the beginning and the end of the iteration were less than 10-5 of the potential at the start of theiteration. This gives the energy levels that differed by less than 10-6 RY between the last two iterations. Core electrons: "Thawed" so that they retain atomic character while being fully included in the iterative process. P(1s), P(2s), P(2p), C(1s), and O(1s) electrons were treated as core electrons. α values:phosphorus, 0.72620; oxygen, 0.74447; hydrogen, 0.77654. Maximum l values: Outer 4; phosphorus 4; oxygen 1; hydrogen 0.

4.8 FIGURES

Figure 4-1 The core level XPS spectra of Al 2p, column I, P 2p, column II, and O 1s, column III, for abraded aluminum metal treated with H_3PO_4 (a), $H_4P_2O_7$ (b), $H_4P_4O_{12}$ (c), H_3PO_3 (d), and H_3PO_2 (e).

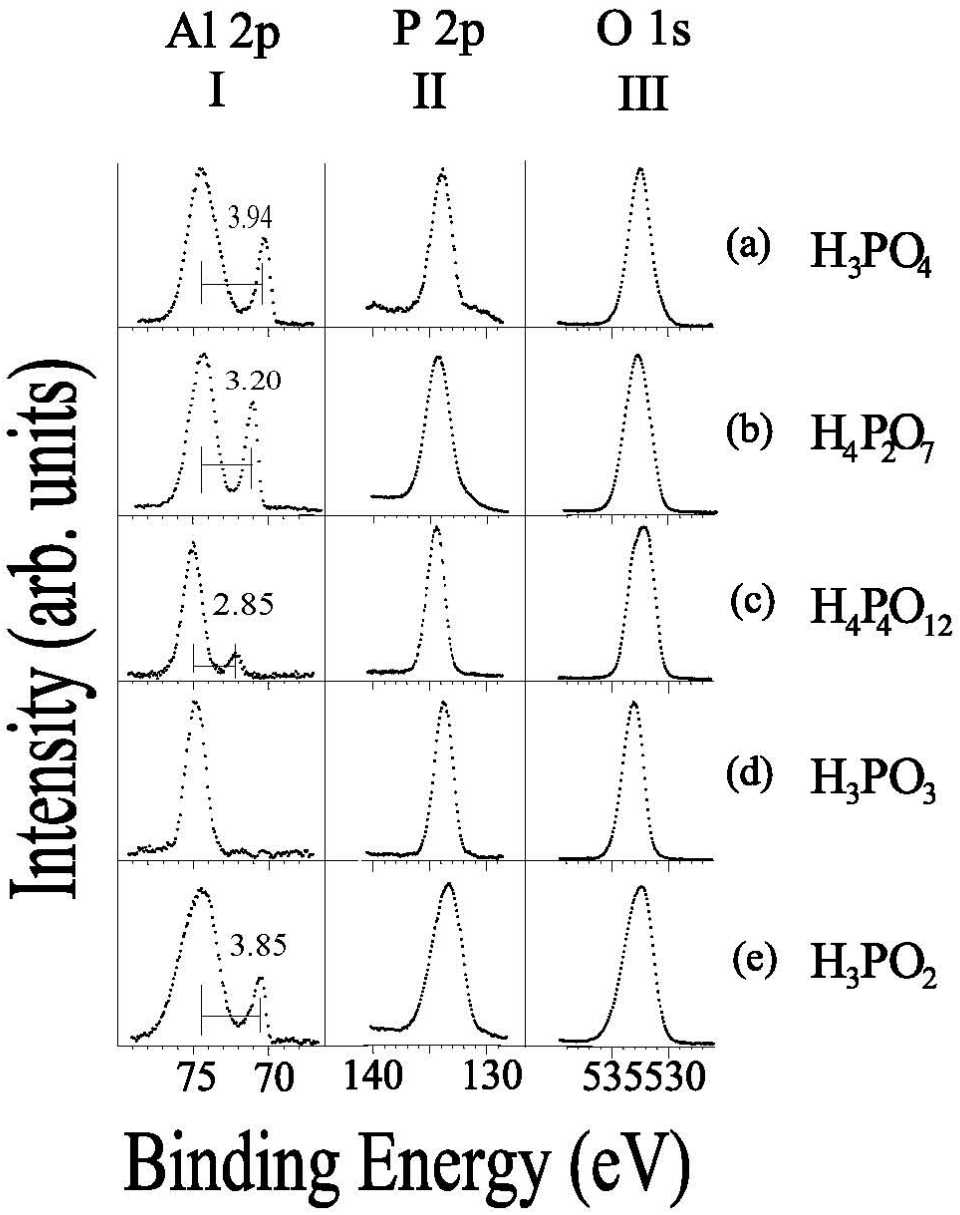

Figure 4-2 The valence band XPS spectra for abraded aluminum metal treated with H_3PO_4 (a), $H_4P_2O_7$ (b), $H_4P_4O_{12}$ (c), H_3PO_3 (d), and H_3PO_2 (e).

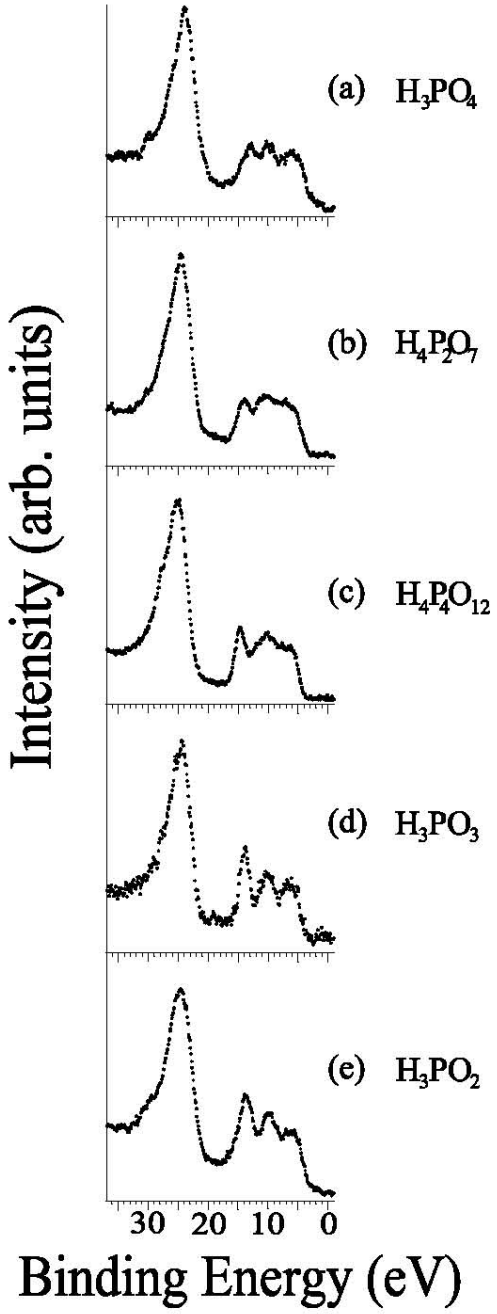

Figure 4-3 The structure of the tetrahedral phosphate, PO_4^{3-}, the linear phosphate, $P_2O_7^{4-}$ and the cyclic phosphate, $P_4O_{12}^{4-}$.

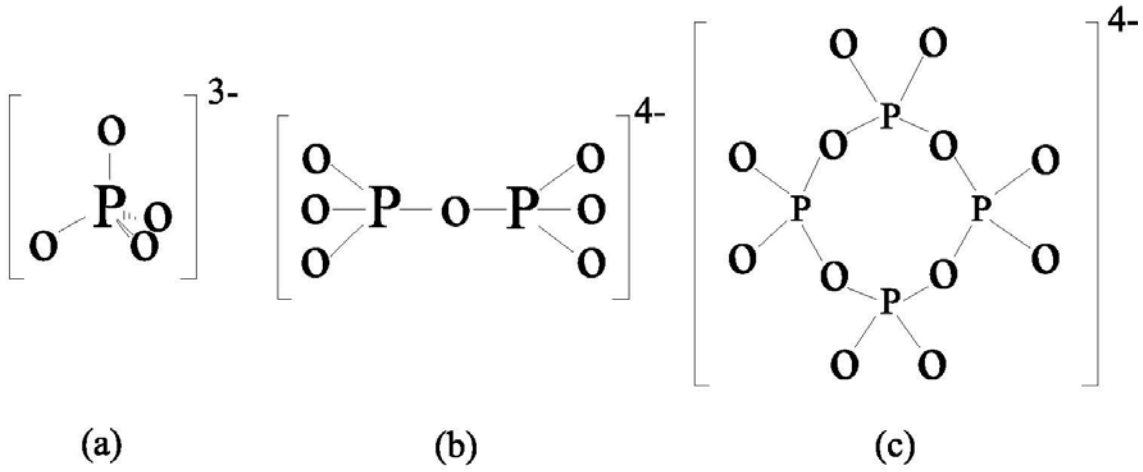

Figure 4-4 The outer valence band XPS spectra of abraded aluminum metal treated with H_3PO_4, column I, and $H_4P_2O_7$, column II. The experimental spectra (a), spectra generated from band structure calculations (b), and Xα cluster calculations (c).

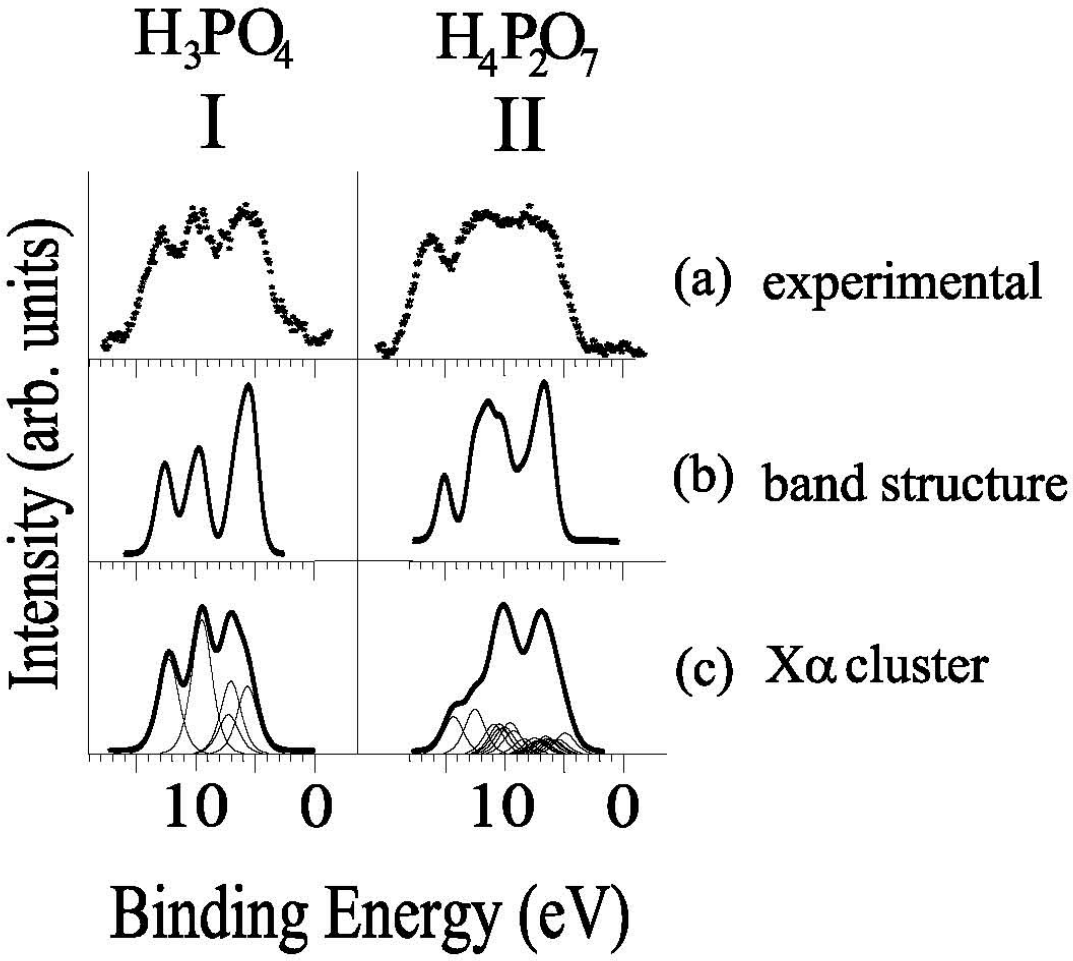

Figure 4-5 The outer valence band XPS spectra of abraded aluminum metal treated with $H_4P_4O_{12}$ (a) and the spectrum generated from band structure calculations of $Na_4P_4O_{12}$ (b).

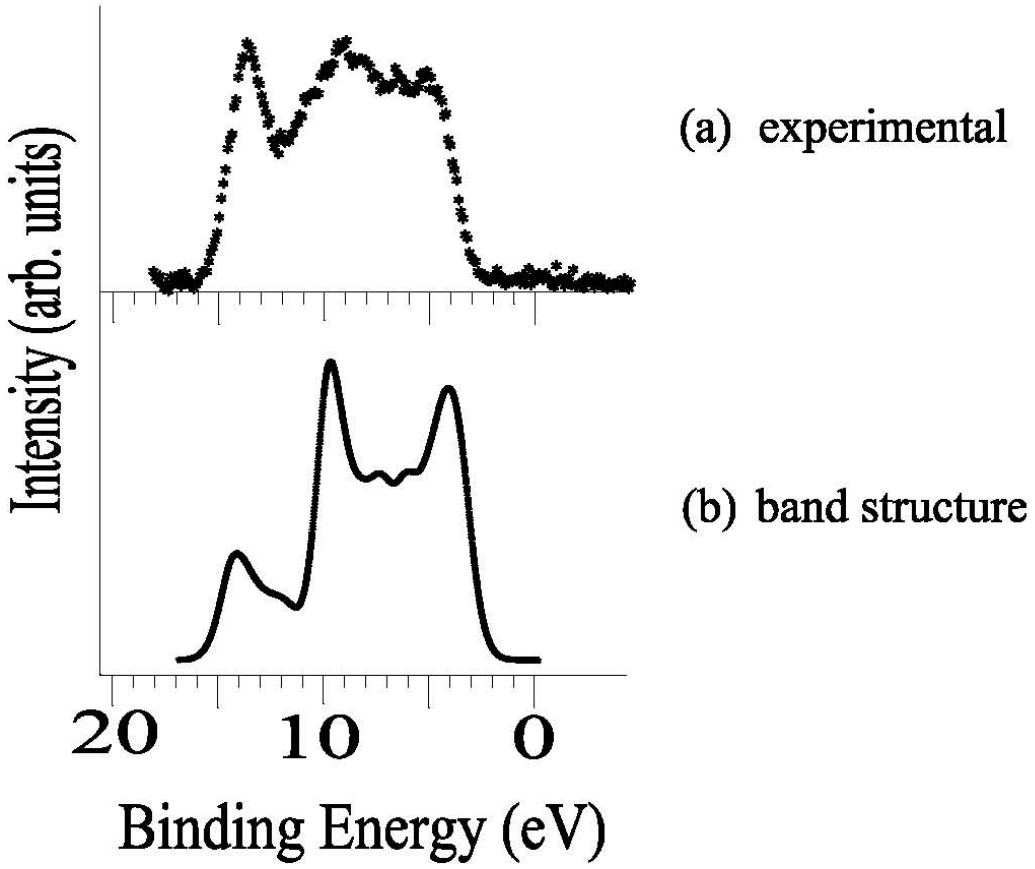

Figure 4-6 The O 1s XPS spectrum (a), the valence band XPS spectrum (b), and the repeat unit of PVA (c). The XPS spectra were collected by forming a thick film of PVA on a copper plate. Reprinted from Y.Wang and P. M. A. Sherwood.[2]

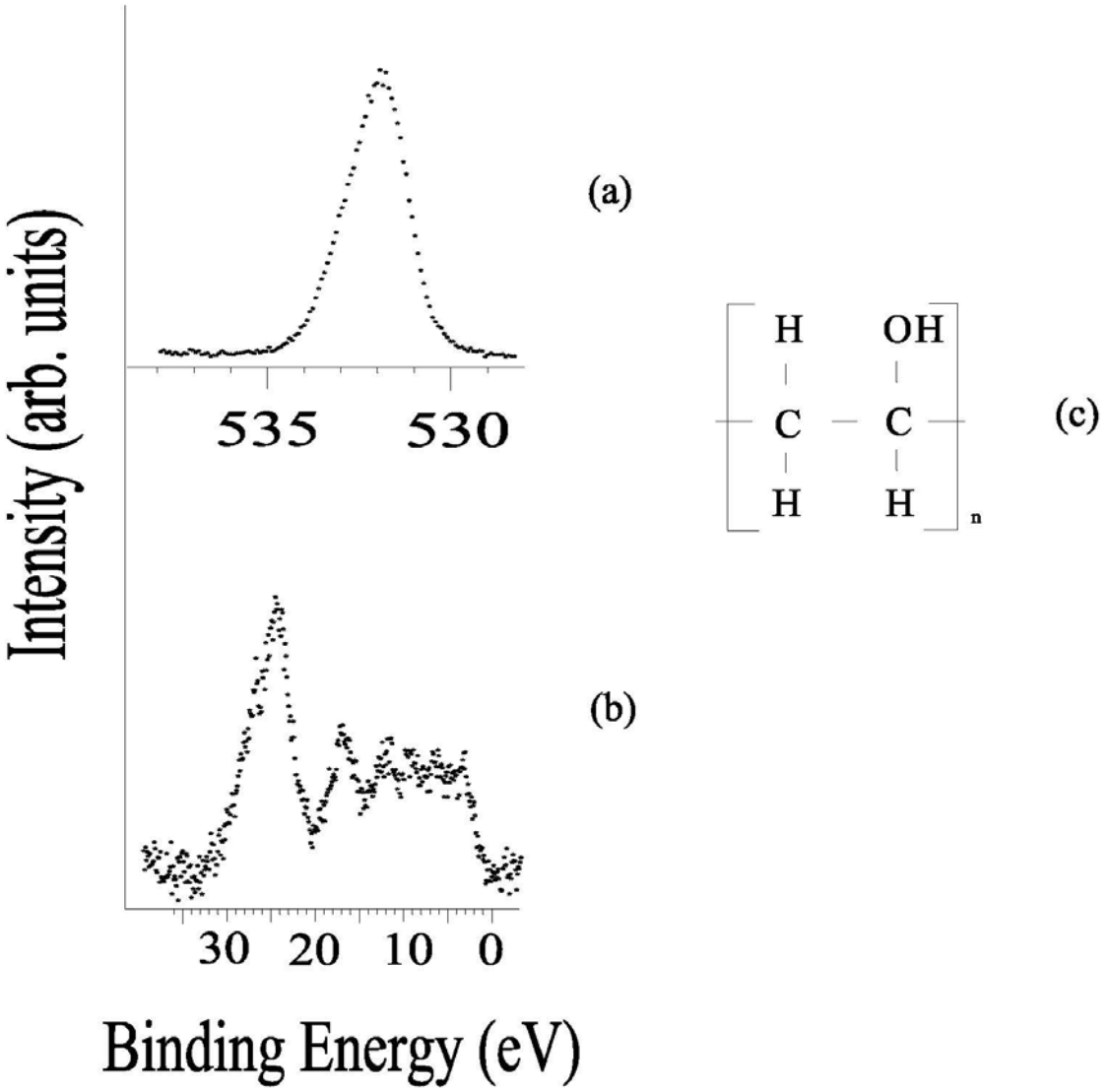

Figure 4-7 The core level XPS spectra of O 1s, column I, C 1s, column II, P 2p, column III, and Al 2p, column IV, for PVA coated on abraded aluminum metal treated with $H_4P_2O_7$ (a), H_3PO_3 (b), and H_3PO_2 (c).

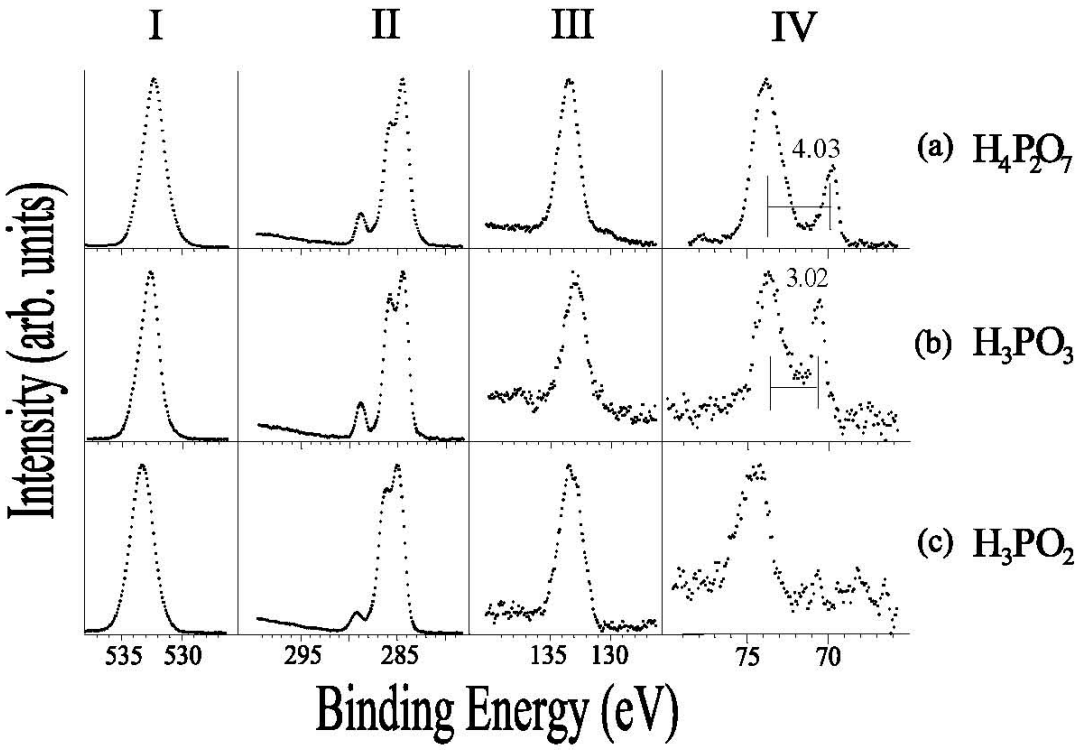

Figure 4-8 The valence band XPS spectra for PVA coated on abraded aluminum metal treated with $H_4P_2O_7$ (a), H_3PO_3 (b), and H_3PO_2 (c).

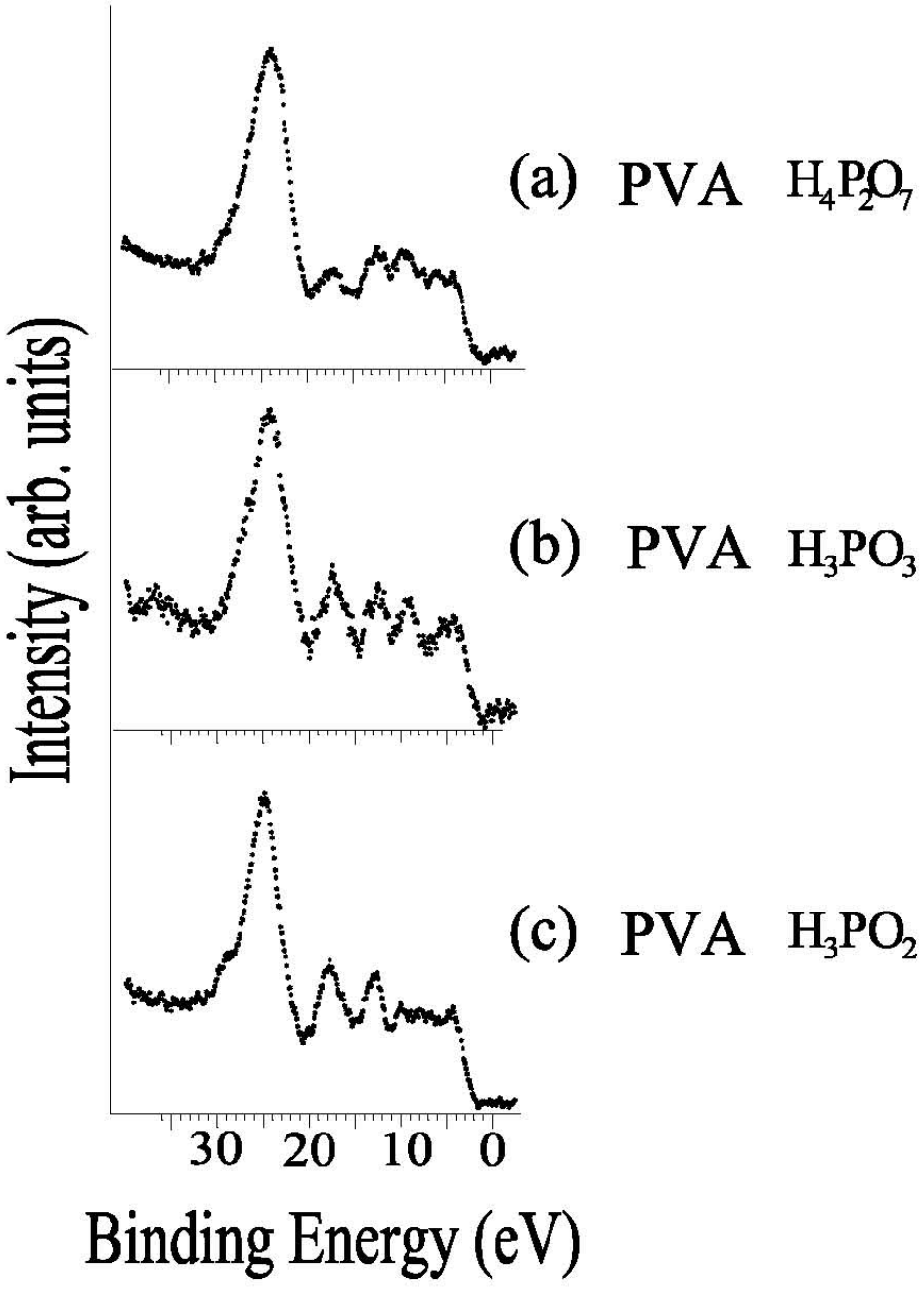

Figure 4-9 The outer valence band XPS spectra for PVA coated on abraded aluminum metal treated with $H_4P_2O_7$ (a), H_3PO_3 (b), and H_3PO_2 (c).

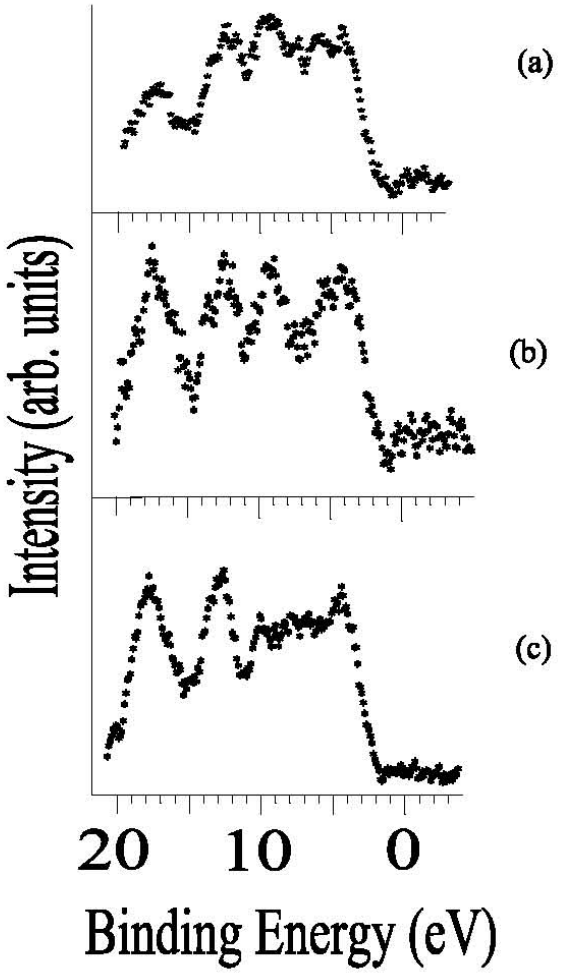

Figure 4-10 Valence band spectra of (a) abraded aluminum metal treated with $H_4P_2O_7$, (b) PVA, (c) sum spectrum of (a) and (b) [= (b) + (a)], (d) PVA coated on abraded aluminum metal treated with $H_4P_2O_7$, (e) difference spectrum of (d) and (c) [= (d) – (c)].

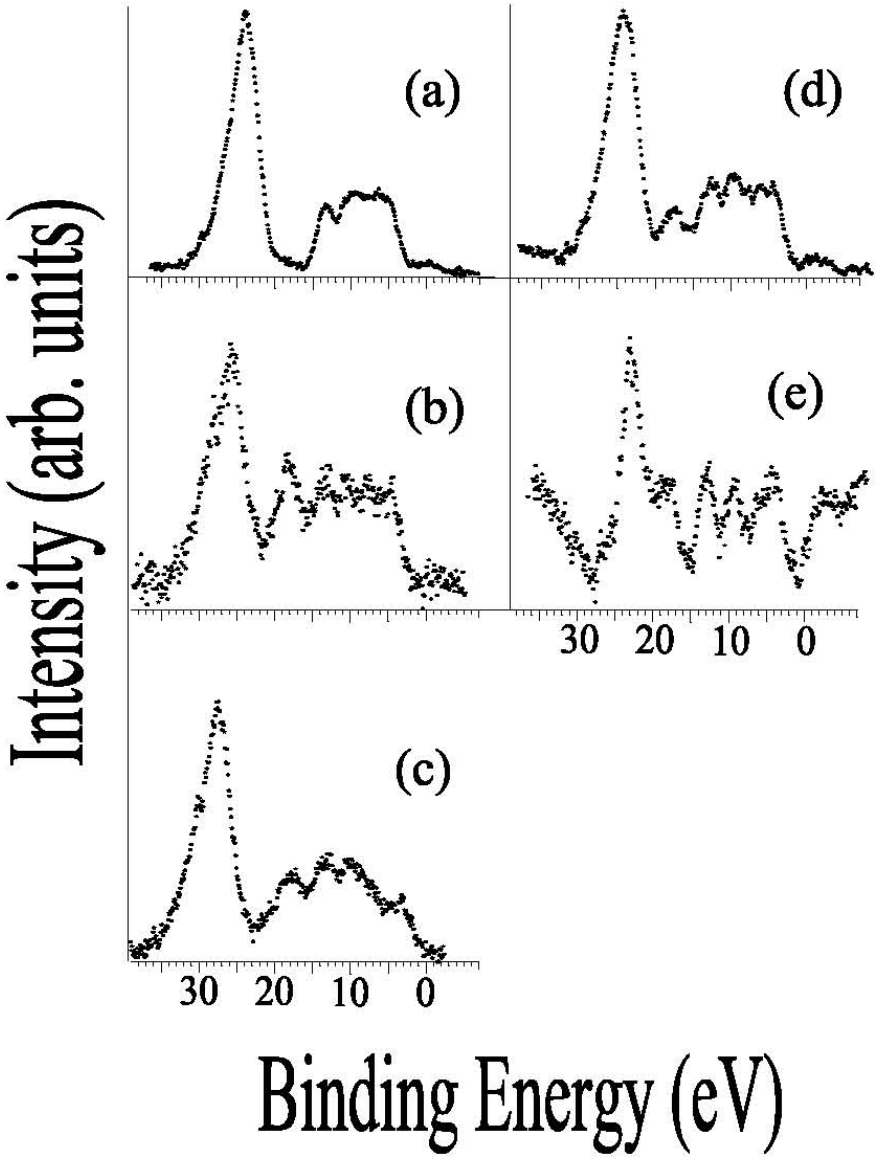

Figure 4-11 Chi squared versus % contribution of PVA for the PVA coated on pyrophosphate film on aluminum metal. The lowest point on the graph at 30% PVA is the value used for creating the addition and difference spectra in Figure 4.10.

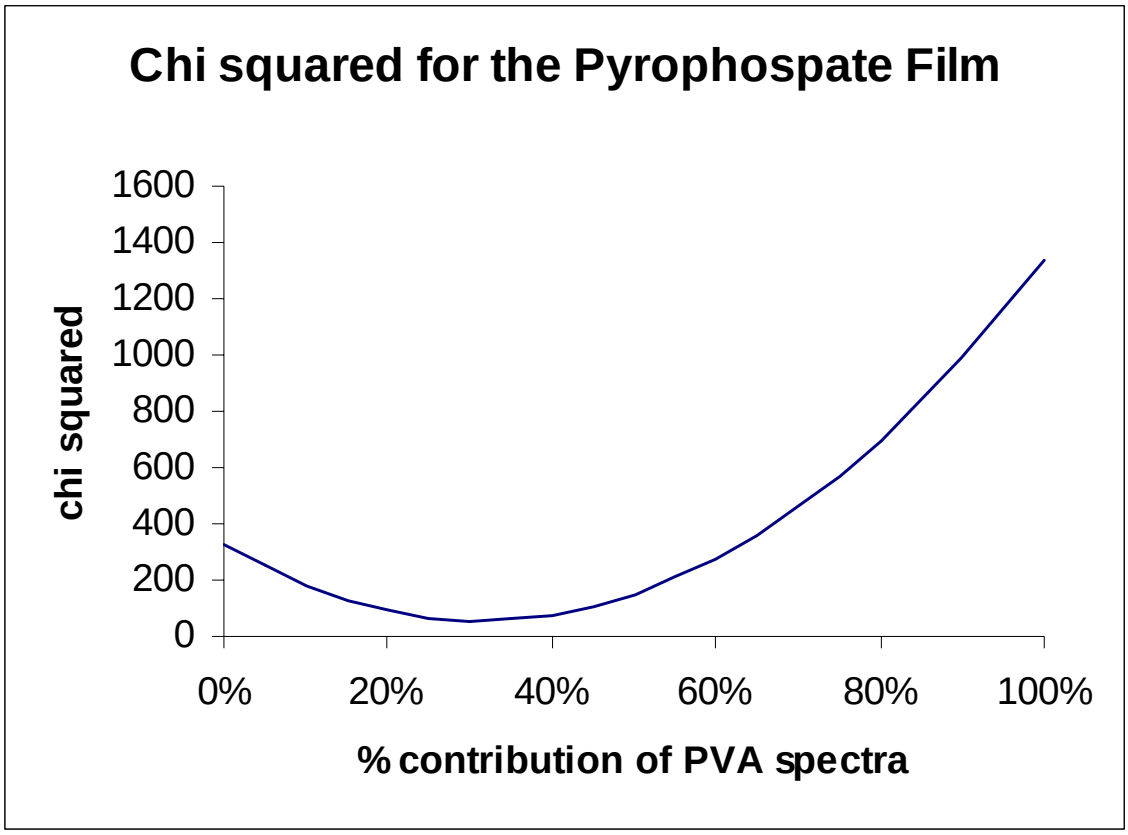

Figure 4-12 Valence band spectra of (a) abraded aluminum metal treated with H_3PO_3, (b) PVA, (c) sum spectrum of (a) and (b) [= (a) + (b)], (d) PVA coated on abraded aluminum metal treated with H_3PO_3, (e) difference spectrum of (d) and (c) [= (c) – (d)].

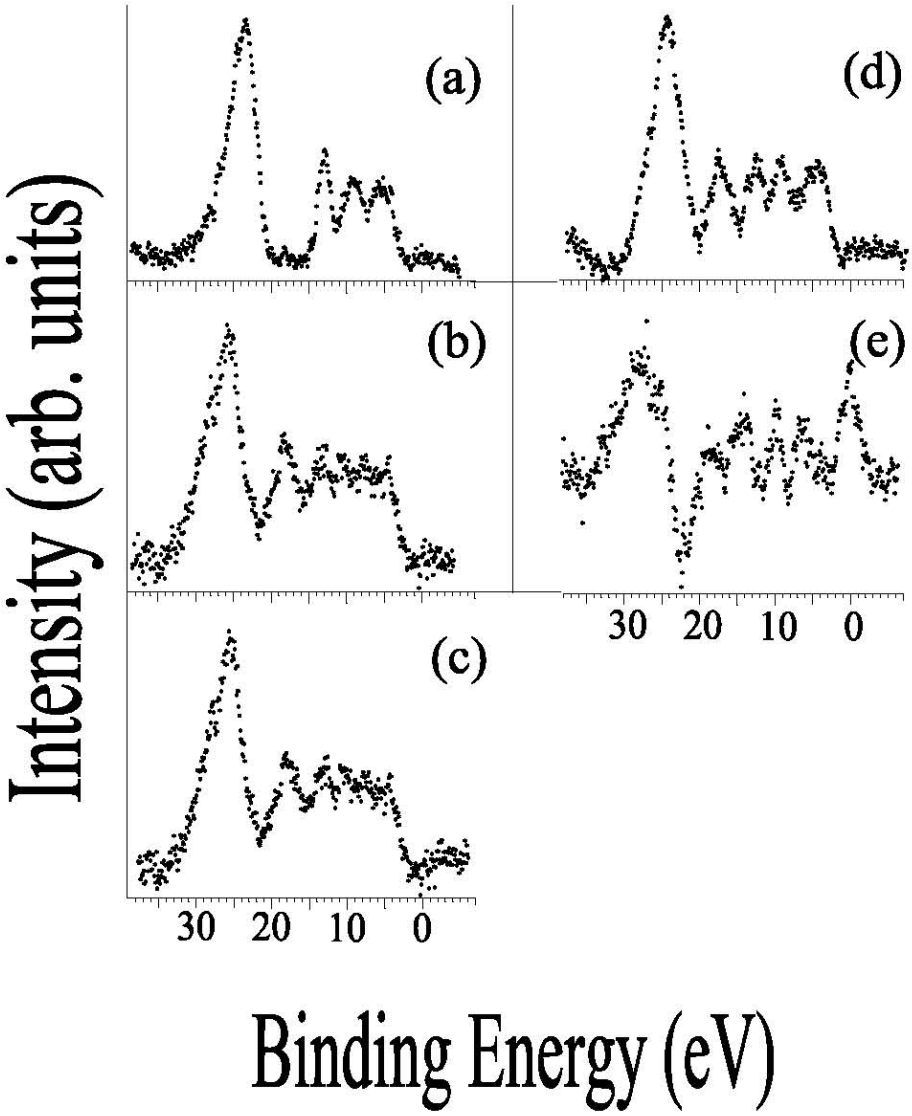

Figure 4-13 Chi squared versus % contribution of PVA for the PVA coated on pyrophosphate film on aluminum metal. The lowest point on the graph at 60% PVA is the value used for creating the addition and difference spectra in Figure 4.12.

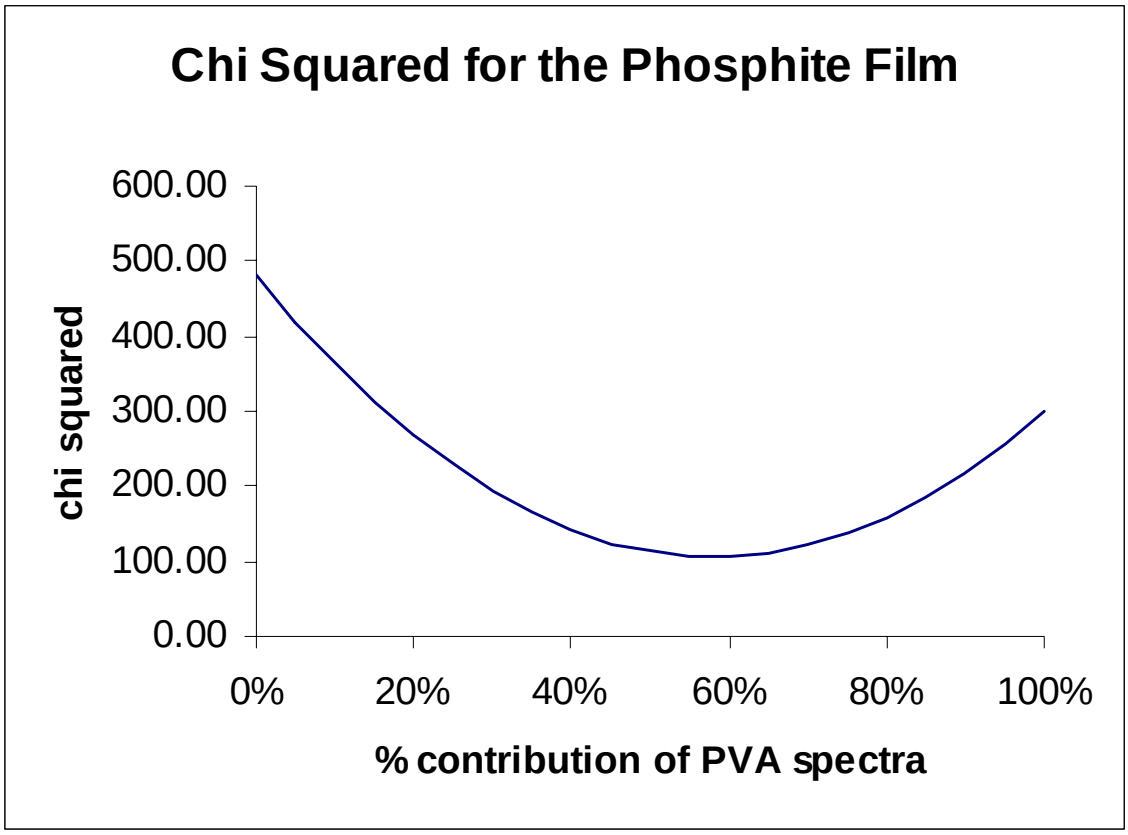

Figure 4-14 Valence band spectra of (a) abraded aluminum metal treated with H_3PO_2, (b) PVA, (c) sum spectrum of (a) and (b) [= (b) + (a)], (d) PVA coated on abraded aluminum metal treated with H_3PO_2, (e) difference spectrum of (d) and (c) [= (d) – (c)].

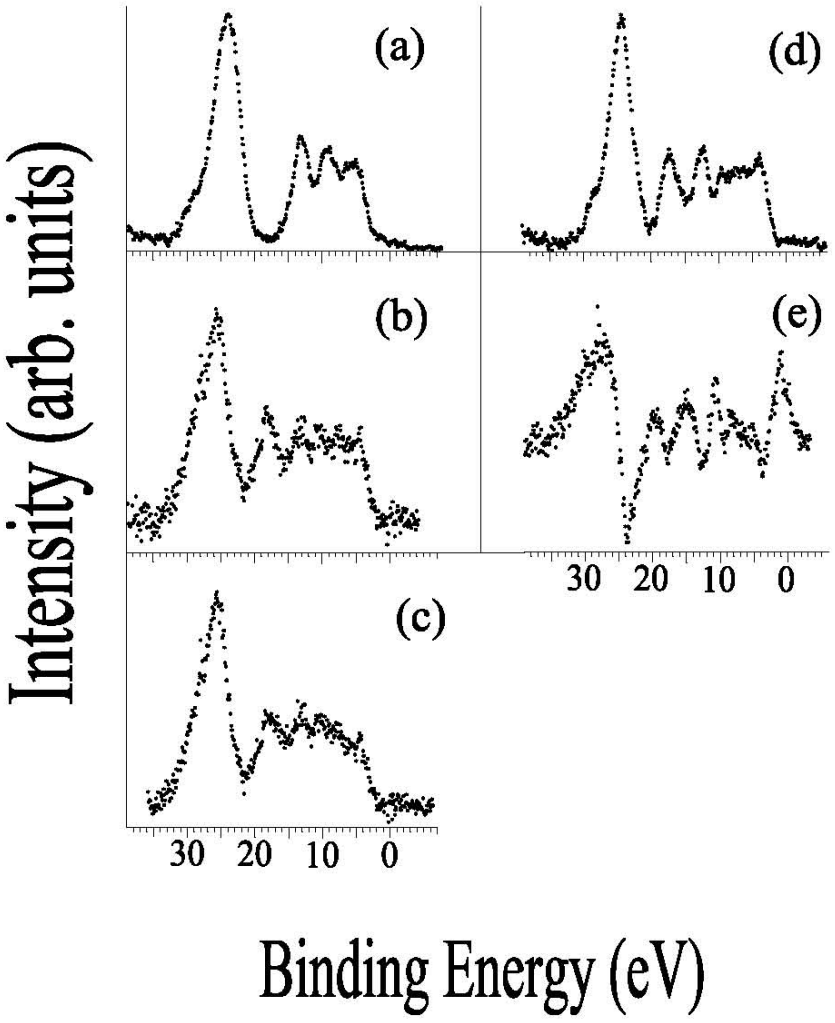

Figure 4-15 Chi squared versus % contribution of PVA for the PVA coated on pyrophosphate film on aluminum metal. The lowest point on the graph at 40% PVA is the value used for creating the addition and difference spectra in Figure 4.14.

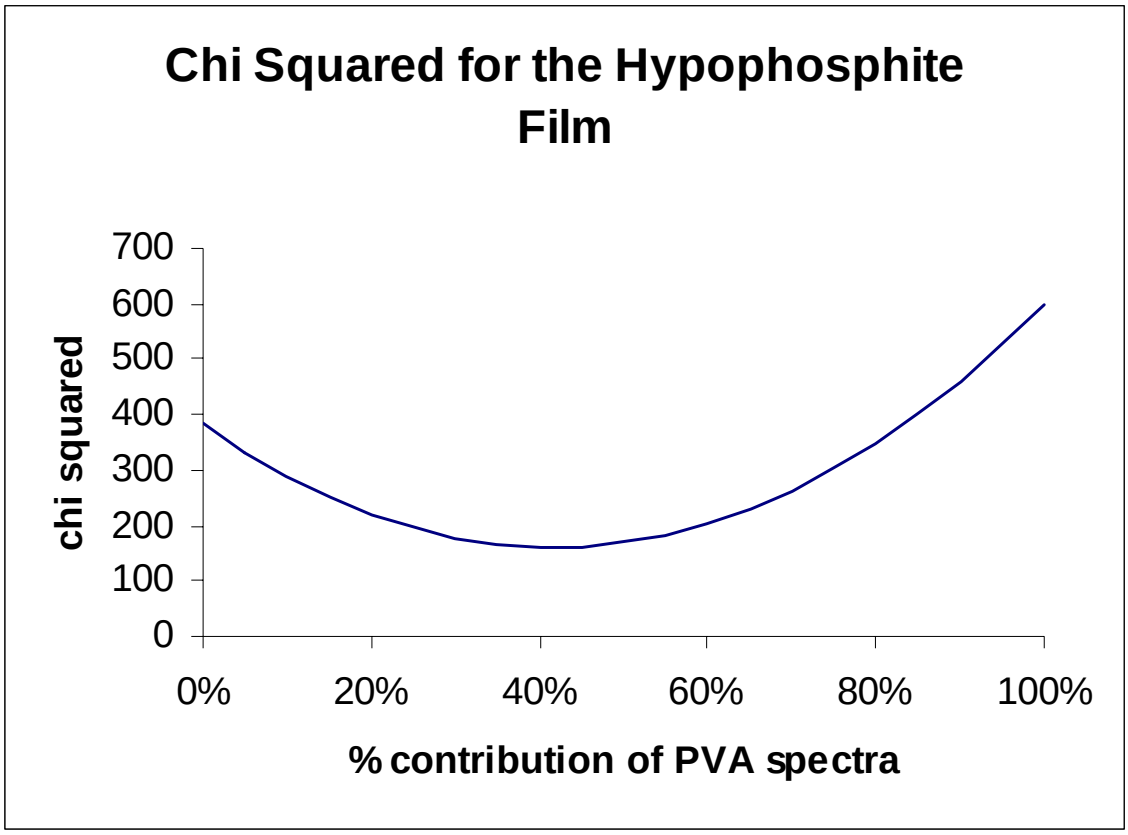

CHAPTER 5 - PEKK Coated on Different Phosphorous containing Films on Aluminum Metal Studied using Core level and Valence Band XPS

5.1. INTRODUCTION

A thin oxide-free phosphate film on aluminum metal has been developed recently in our laboratory with the resultant film being orthophosphate, PO_4^{3-}, and has the advantages of ultra thin films.[1,2] The film has been reproduced on other metals including iron[1,2], copper[3], titanium[4], and vanadium[5]. The film was prepared using two different methods: one method was to prepare the film in an ultra high vacuum chamber in an aerobic cell.[6] The sample was prepare and analyzed without being exposed to atmospheric conditions. The other method was to prepare the films on the bench top and transfer the sample in atmospheric conditions to the vacuum chamber for analysis.[7]

Chapter 4 and an article written by our group[8] discussed the use of different phosphorus containing acids to prepare thin films on aluminum metal with a structure other than orthophosphate. The phosphorus containing acids used were a linear phosphate, pyrophosphoric acid, $H_4P_2O_7$, a cyclic phosphate metaphosphoric acid, $H(PO_3)_n$, and two deprotienated forms of the tetrahedral orthophosphoric acid: phosphorous, H_3PO_3, and hypophosphorous, H_3PO_2, acid. The acids were shown to form thin films of pyrophosphate, $P_2O_7^{4-}$, tetrametaphosphate, $P_4O_{12}^{4-}$, phosphite, HPO_3^{2-}, and hypophosphite, $H_2PO_2^{-}$, respectively. Tetrametaphosphate is the most common structure formed when using $H(PO_3)_n$.[9] The next step was to test the properties of the films. One such test, was to use the chemically bonded phosphorus containing films as adhesives to bond polymers to a metal substrate that may not have otherwise formed bonds with the metal surface.

The adhesion ability of orthophosphate, pyrophosphate, phosphite and hypophosphite for aluminum metal and the water soluble polymer polyvinyl alcohol, PVA, was studied using core

level and valence band XPS. The valence band XPS region showed a shift in the polymer peak between the PVA spectra and the PVA coated on phosphorus containing films on aluminum metal. Addition and difference spectra were used to show other differences in the chemical environment found in the buried interface before and after PVA coating.

In this chapter, the adhesion ability of various phosphorus containing films is studied using core level and valence band XPS. The water insoluble polymer poly(ether ketone ketone), PEKK, will be used to form a coating on the ionic phosphorus containing films on abraded aluminum metal. This semicrystalline polymer was developed by Dupont for use as a thermoplastic resin to be incorporated in composite matrices for aerospace applications. The properties of PEKK and it performance versus other thermoplastic resins has been well documented.[10-15] The buried interface between PEKK and carbon fibers in a separate study was investigated in our laboratory using core level and valence band XPS, along with the effect of exposure to saline solution over varied time intervals.[16] In this study, the core level and valence band XPS for the samples will be used to explore the chemical environment at the buries interface and determine whether there is bonding in that region between the PEKK and phosphorus containing films.

5.2. EXPERIMENTAL

5.2.1. Materials and sample preparation.

5.2.1.1. Materials. Aluminum foil (99.00%) was purchased from Goodfellow Cambridge Limited, England (LS178013 B G) with a thickness of 0.125 mm and degreased with acetone prior to use. Silicon carbide 600 sandpaper was purchased from Carborundum Abrasives. 85% orthophosphoric acid was purchased from Fisher Scientific. 99% phosphorous acid was purchased from Aldrich. 50% hypophosphorous acid was purchased from Sigma-Aldrich. The PEKK resin used in this study was provided by Dupont (P11923-15501). The resin is additives-free with a number average molecular weight of 8220 (GPC) and a weight average molecular weight of 28 500 (GPC). The glass transition temperature is 156 $^{\circ}$C (DSC) and the melting temperature is 305 $^{\circ}$C (DSC).

5.2.1.2. Preparation of the phosphorus containing films on abraded aluminum metal. The phosphorus containing acids were diluted with quadruplely distilled (4-D) water to make 5 M

solutions. The solutions were then deoxygenated for 2 hours using Nitrogen. The aluminum metal was abraded with sandpaper for 5 minutes while in solution and left to stand for an additional 10 minutes in solution. The films were then dried overnight in atmospheric conditions.

5.2.1.3. PEKK film preparation. The as-received PEKK resin was in the form of pellets: two solutions of PEKK were prepared by heating a 1:1 mixture of phenol and 1,2,4-trichlorobenzene to between 100 °C and 120 °C and dissolving enough PEKK resin to form 0.25% and 1% solutions. The concentration of PEKK dissolved in solution can be used to control the thickness of the coating formed. The 1% solution was coated on abraded aluminum metal treated with H_3PO_4 to form a very thick coating. The 0.25 % solution was used to coat the phosphorus containing films formed on abraded aluminum metal used for the adhesion tests. The coatings were dried in a vacuum oven at 90 °C for 48 hours.

5.2.2. Surface analysis. All spectra were collected with a VSW HA150 spectrometer (150mm hemispherical analyzer) operated in the fixed analyzer transmission mode with a pass energy of 20 eV, also equipped with a 16-plate microchannel detection system. The Al Kα X radiation (240 Watts) generated from a 35 quartz crystal monochromator provides a linewidth of better than 0.2 eV. The base pressure of the instrument was 10^{-9} Torr or better. All spectra were referenced against the C1s peak at 284.6 eV.

5.2.3. Data interpretation. The curve fitting of the XPS spectra was carried out using a nonlinear-least-squares curve-fitting program with a Gaussian/Lorentzian product function.[17,18] The Gaussian/Lorentzian mixture was taken as 0.5. The C – C type C 1s peak was fixed with a binding energy of 284.6 eV for calibration. The Proctor-Sherwood non-linear background shape used in the curve fitting have been reported previously.[19.20] Ab initio Hartree- Fock calculations were preformed to obtain the XPS valence band spectra. The calculations used a modified version of the program HONDO (copyright IBM) with an STO-3G minimal basis set.[21]

5.3. RESULTS AND DISCUSSION

The chemical composition of the films formed on aluminum metals after exposure of the abraded metal to different phosphorus containing acid solutions was discussed in detail in Chapter 4. These films were determined to be similar in chemical composition to the acid

solutions used. Their adhesive properties were tested using the polymer poly(vinyl alcohol), PVA, to form a second film over the phosphorus containing films and the results showed evidence that the films adhere well to both aluminum metal and PVA. In this chapter, the films' adhesive properties will be tested again between aluminum metal and the polymer Poly(ether ketone ketone), PEKK. The chemistry at the interface between the phosphorus containing films and PEKK will be discussed.

5.3.1. PEKK surface chemistry and XPS spectra. The spectra of PEKK has been published elsewhere.[15,16] In order to compare the spectra obtained in this chapter with PEKK spectra, we examined a thick film of PEKK.* Figure 5.1 shows the core level and valence band XPS spectra for PEKK along with a spectrum generated using ab-initio Hartree-Fock calculation and the repeat unit for PEKK. The repeat unit for PEKK is shown in Figure 5.1 (a) and consists of three types of aromatic rings: phenyl ether, terephthalaldehyde, and isophthalaldehyde. Assuming that the surface and bulk of the PEKK have the same chemical structure, there are four types of carbon and two types of oxygen that can be expected in the core level XPS spectra. Figure 5.1 (a) is labeled to show the carbons and oxygen, the carbons are (C-H and C-C) type 1, (C-C=O) type 2, (C-O) type 3 and (C=O) as type 4. The two oxygen are (C=O) type 5 and (C-O) as type 6.

The core level XPS spectra for the O 1s and C 1s region are shown in Figure 5.1 (b) and (c), respectively. The spectra have been curve fitted to accentuate the contributions to the peaks with the PEKK repeat unit in mind. The curve fit results are shown in Table 5.1. The C 1s level XPS spectrum was fitted to five peaks of type1, type 2, type 3, type 4 and a $\pi \rightarrow \pi^*$ shakeup. The area ratio of the peaks in the form type 1: type 2: type 3: type 4: $\pi \rightarrow \pi^*$ is 5.98: 3.59: 0.85: 0.85: 0.85 and is similar to the PEKK repeat unit stoichiometric ratio that predicted 6: 2: 1: 1. The O 1s level XPS spectrum was fitted to two peaks with an area ratio of type 5: type 6 1.5: 1, which is comparable to the PEKK stoichiometric ratio of 2: 1.

Figure 5.1 (d) shows the nonlinear background subtracted valence band XPS spectrum for PEKK. The O 2s region located between 22 eV and 30 eV has been shown in both metallic and nonmetallic systems[22] to be more sensitive to the chemical environment of the

* This thick film was actually obtained as a coating on an abraded aluminum metal treated with H_3PO_4. The thick film was produced as the solution was concentration was adjusted to give a thin enough film to see the interface region.

surface than the O 1s core region. The O 2s region would be expected to have two overlapping peaks, one, at the highest binding energy, corresponding to the (C-O) type 6 oxygen, and the other, at the lower binding energy, corresponding to the (C=O) type 5 oxygen. These two features can be seen in the calculated spectrum in Figure 5.1 (e). A triplet peak structure is also present between 10 eV and 22 eV that has been discussed previously and confirmed for other aromatic systems.[15,22]

5.3.2. Core level XPS for PEKK coated on phosphorus containing films formed on aluminum metal. The Al 2p, P 2p, C 1s, and O1s core level XPS spectra were recorded and shown in Figure 5.2 through 5.4. The C 1s and O 1s spectra were curve fitted using the repeat unit for PEKK, Figure 5.1 (a). They are displayed in different figures to better show the resulting spectra of the curve fit.

5.3.2.1. Al 2p and P 2p core level XPS. The XPS spectra for the Al 2p region was discussed in chapter 4 for different phosphorus containing films formed on aluminum metal. The Al 2p was used to compare the thickness of the films formed on aluminum metal by using the peak for aluminum metal which is located between 69 eV and 72 eV. The peak is more intense the thinner the film is because the signal from the underlying metal is stronger for thinner films. A shift between the metal peak and the oxygen component peak between 72 eV and 77 eV was also observed and it was noted that the thinner the film the larger the separation between these peaks.

Figure 5.2 I shows the Al 2p core level XPS spectra for PEKK coated on PO_4^{3-} (a), HPO_3^{2-} (b), and $H_2PO_2^-$ (c) formed on abraded aluminum metal. The aluminum metal peak is the most intense peak in Figure 5.2 I (a) and the intensities, therefore the thicknesses, are similar in Figure 5.2 I (b) and (c). The separation between the metal and oxygen peak for the PO_4^{3-} and $H_2PO_2^-$ films are 3.1 eV and HPO_3^{2-} is 3.5 eV, which does not follow the trend of the thickness versus shift noted before the PEKK film was applied, section 4.3.1. The separation before PEKK of the PO_4^{3-} and $H_2PO_2^-$ film were both 3.9 eV and after the separation were both 3.1 eV.

Recently, two review papers were written on the effects of conducting polymer coatings on metal and semiconductor substrates.[23,24] An energy shift, ΔE, was observed between the Fermi level of the substrate and the valence band edge of the polymer. In one of the studies, Indium tin oxide, ITO, spin-caste coated using poly(*p*-phenylenevinylene), PPV, was studied and ΔE determined.[25] PPV was then coated on a doped conducting polymer poly(3,4-ethylenedioxythiophene) doped with poly(4-styrenesulfonate), PEDOT-PSS coated on ITO. The

addition of the conducting polymer caused the affect of the ITO on the PPV to decrease and since the PEDOT-PSS has a higher work function, Φ, than ITO the ΔE decreased. This shifting could help account for the shifts observed in the Al 2p region since the underlying metal and the oxygen content are in different layers of the surface.

The spectra for the P 2p region is shown in Figure 5.2 II for PEKK coated on PO_4^{3-} (a), HPO_3^{2-} (b), and $H_2PO_2^-$ (c) films on abraded aluminum metal. The P 2p is centered between 133 eV and 134 eV and confirms the presence of the phosphorus containing film after the PEKK coating.

5.3.2.2 C 1s and O 1s core level XPS. The C 1s and O 1s were curve fitted using the components of the repeat unit of PEKK in Figure 5.1 (a). The C 1s core level XPS spectra are shown in Figure 5.3 for PEKK coated on PO_4^{3-} (a), HPO_3^{2-} (b), and $H_2PO_2^-$ (c) films on abraded aluminum metal. The curve fit parameters are listing in Table 5.2 for C 1s and O 1s with the peak types the same as the PEKK repeat unit. The shift of the peaks, in eV, from the lowest binding energy peak, type 1, set at zero in the form type 2, type 3, type 4 is 0.5, 1.56, and 2.21 for PO_4^{3-}, 0.37, 1.65, and 2.39 for HPO_3^{2-}, and 0.37, 1.29, and 2.21 for $H_2PO_2^-$. These values are similar to those reported in Table 5.1 for PEKK.

The area ratio of the four fitted peaks in the C 1s spectra, in the form type 1: type 2: type 3: type 4, are 6: 1.5: 0.5: 0.5 for PO_4^{3-}, 5.75: 1.5: 1.25: 0.5 for HPO_3^{2-}, and 5: 2: 0.75: 0.5 for $H_2PO_2^-$. These compare well to the atomic ratio for the model structure of PEKK of 6: 2: 1: 1, with a slight increase in intensity of the type 3 and decrease in intensity of the type 4 peaks for the PEKK coated phosphorus containing films. The increase in the type 3 peak, which corresponds to the C-O bond, and the decrease in the type 4 bond, corresponding to the C=O bond, would be expected if the C=O bond in PEKK was to react with the Al^{3+} cation at the buried interface and form C-O bonds.

Figure 5.4 shows the curve fit data results for the O 1s XPS spectra for PEKK coated on PO_4^{3-} (a), HPO_3^{2-} (b), and $H_2PO_2^-$ films. The shift of the type 6, C-O, peak at higher binding energy from the type 5, C=0, at lower binding energy is 1.01 eV for PO_4^{3-}, 0.55 eV for HPO_3^{2-}, and 1.01 for $H_2PO_2^-$, which are 1 eV to 1.5 eV smaller than PEKK, Table 5.1. The area ratios type 6: type 5 are 2: 1, 2: 1.2, and 2: 1 for PEKK coated on PO_4^{3-}, HPO_3^{2-}, and $H_2PO_2^-$ films, respectively. The atomic ratio of model PEKK is predicted to be, type 6: type 5, 1: 2, which is opposite to what the experimental data shows. This would be expected if the oxygen in C=O

type 5 bond reacted with Al^{3+} cation to form a C-O type 6 bond at the buried interface, effectively switching their intensities.

5.3.3. Valence band XPS for PEKK coated on phosphorus containing films formed on aluminum metal. The valence band XPS spectra are shown in Figure 5.5 for PEKK coated on PO_4^{3-} (a), HPO_3^{2-} (b), and $H_2PO_2^-$ (c) film on abraded aluminum metal. The spectra, when compared to the spectra without PEKK shown in Chapter 4 Figure 4.2 (b, d, e), still retain the three peak structure representative of phosphorus containing compounds. A peak centered between 18 eV and 19 eV appears next to the O 2s peak in the PEKK coated phosphorus containing films.

The XPS spectra of the outer valence band region of the phosphorus containing films before and after PEKK coating between 0 eV and 20 eV is shown in Figure 5.6 with the nonlinear background removed. The main differences between the six spectra are shown in the two higher binding energy peaks before PEKK coating and the three higher binding energy peaks after. The three spectra of the PEKK coated on the PO_4^{3-}, column I, HPO_3^{2-}, column II, and $H_2PO_2^-$, column III, in figure 5.6 (b) have less intense peaks at 13 eV than the respective spectra recorded before PEKK coating Figure 5.6 (a). There is also an additional peak at 18.8 eV for the PO_4^{3-} film, I (b), 18.9 eV for the HPO_3^{2-} film, II (b), and 18 eV for the $H_2PO_2^-$ film, III (b), corresponding to the triplet peak structure of PEKK at 17 eV.

The peaks in the XPS spectra for the PO_4^{3-} film shift from 13 eV and 10 eV with a separation of 3 eV before PEKK coating, Figure 5.6 I (a), to 12.8 eV and 9.2 eV with a separation of 3.6 eV after PEKK coating, Figure 5.6 I (b). The peaks in the XPS spectra for the HPO_3^{2-} film shift from 13.1 eV to 9.2 eV with a separation of 3.9 eV before PEKK coating to 13 eV and 9.3 eV with a separation of 3.7 eV after PEKK coating. The peaks in the XPS spectra for the $H_2PO_2^-$ film shift from 13 eV and 9 eV with a separation of 4 before to 13 eV and 8 eV with a separation of 5 eV after PEKK coating.

5.3.4 Interaction between PEKK and the phosphorus containing films. Spectra generated using band structure or Xα cluster calculations can be used to predict the valence band structure of the experimental data when it is in as-received form or containing one film. When multiple coatings are present, the valence band region can become more complicated and the multiple molecules present more difficult to calculate, so a different means of evaluating the data becomes necessary. Addition and subtraction spectra can be used in this case to evaluate the

bonding in the buried interface region between the coatings. This technique has been discussed previously[7,8] and in section 1.4.2. This has been performed for the PEKK coated on the PO_4^{3-}, HPO_3^{2-}, and $H_2PO_2^-$ films.

The analysis of PEKK coated on PO_4^{3-} film formed on abraded aluminum metal is shown in Figure 5.7. The valence band XPS spectrum for the PO_4^{3-} film on abraded aluminum metal is shown in Figure 5.7 (a) and the spectrum for PEKK is shown in Figure 5.1 (d) and again in Figure 5.7 (b), for comparison. The PEKK spectrum was added to the spectrum of the PO_4^{3-} film on abraded aluminum metal and the resultant spectrum is shown in Figure 5.7 (c). The addition spectrum was compared to the experimental spectrum of PEKK coated on the PO_4^{3-} film in Figure 5.5 shown again in Figure 5.7 (d), for comparison. The addition spectrum retains the PEKK triplet peak structure[15] at 17 eV and the peaks at 26 eV, 13 eV, and 9 eV and the shoulder at 3.5 eV. The orthophosphate peak is combined with the PEKK peak resulting in an intense peak at 13 eV in the addition spectrum compared to the less intense peak found at 12.8 eV in the experimental spectra in Figure 5.7 (d). The orthophosphate peaks at 10 eV and 6 eV are also seen in the addition spectrum.

In the experimental spectrum of PEKK coated on the PO_4^{3-} film, Figure 5.7 (d), the triplet peak structure for the PEKK is less intense and shifted to 18.8 eV and the orthophosphate peaks are at 12.8 eV and 9.2 eV. The difference spectrum is then made by subtracting the added spectrum in Figure 5.7 (c) from the experimental spectrum in Figure 5.7 (d). If the spectrum had been a flat line the spectra would have been the same spectra and there would not have been any bonding. This was not the case and several peaks can be seen when the chemical environment changes at the buried interface. The shift of the PEKK peak can be seen in the difference spectrum by the positive peak at 18.8 eV and the negative peak at 17 eV. This was repeated for PEKK coated on the HPO_3^{2-} film, Figure 5.9, and $H_2PO_2^-$ film, Figure 5.11, and shows similar results to PEKK coated on the PO_4^{3-} film. The PEKK triplet structure shifted from 17 eV to 18.9 and 17 eV to 18 eV in the PEKK coated on the HPO_3^{2-} and $H_2PO_2^-$ films, respectively.

The addition and difference spectra were height normalized to 10000 counts and allied by calibrating the hydrocarbon peak in the C 1s to 284.6 eV. The chi squared value was obtained by following the procedure described in Chapter 1.4.2. The chi squared values where graphed versus the % contribution of PVA, which is shown in Figures 5.8 for PO_4^{3-}, Figure 1.10 for $H_2PO_2^-$, and Figure 1.12 for HPO_3^{2-} films on aluminum metal.

5.4. CONCLUSION

PEKK has been shown to react at the buried interface to form bonding between the phosphorus containing films and the PEKK film. This can be seen in the shifting of the binding energy of the peaks and intensity of the peaks in both core level and valence band XPS spectra. This further confirms the ability of phosphorus containing films to be used as adhesive material between metals and polymers that had little to no interaction without the phosphorus films. Valence band XPS can be used to study the buried interface between films and distinguish subtle chemical differences in the environment in this interface.

5.5. ACKNOWLEDGEMENTS

This material is based upon work supported by the National Science Foundation under Grant No. CHE-0137502. The U.S. Government has certain rights to this material. I would like to thank Dr. Yuqing Wang and Dr. P. M. A. Sherwood for providing the ab initio Hartree-Fock calculations.

5.6. REFERENCES (see Reference chapter)

5.7 TABLES

Table 5-1 Nonlinear Least-Squared Curve-fitting Results for PEKK

Table 5.1. Nonlinear Least-Squares Curve-fitting results for PEKK.

sample	peak type	assignment	chemical shift from main peak (eV)	rel. peak area	rel. peak area (%)
		C 1s Region			
PEKK	1	C–H, C–C	0	5.98	49.34%
	2	C–C=O	0.74	3.59	29.63%
	3	C–O	1.84	0.85	7.01%
	4	C=O	2.76	0.85	7.01%
			7.18	0.85	7.01%
		O 1s region			
PEKK	5	C=O	0	1.5	60.00%
	6	C–O	2.02	1	40.00%

Table 5-2 Nonlinear Least-Squares Curve-fitting Results for PEKK Coated on Phosphorus Containing Films on Abraded Aluminum Metal.

Table 5.2. Nonlinear Least-Squares Curve-fitting results for PEKK coated on phosphorus containing films on abraded aluminum metal

C 1s Region					
sample	peak type	assignment	chemical shift from main peak (eV)	rel. peak area	rel. peak area (%)
PEKK on PO_4^{3-}	1	C–H, C–C	0	6	70.59%
film [a] (a)	2	C–C=O	0.55	1.5	17.65%
	3	C–O	1.56	0.5	5.88%
	4	C=O	2.21	0.5	5.88%
PEKK on HPO_3^{2-}	1	C–H, C–C	0	5.75	63.89%
film [a] (b)	2	C–C=O	0.37	1.5	16.67%
	3	C–O	1.65	1.25	13.88%
	4	C=O	2.39	0.5	5.56%
PEKK on $H_2PO_2^-$	1	C–H, C–C	0	5	60.61%
film [a] (c)	2	C–C=O	0.37	2	24.24%
	3	C–O	1.29	0.75	9.09%
	4	C=O	2.21	0.5	6.06%
O 1s region					
PEKK on PO_4^{3-} film [b] (a)	5	C=O	0	1	33.33%
	6	C–O	1.01	2	66.67%
PEKK on HPO_3^{2-} film [b] (b)	5	C=O	0	1.2	37.50%
	6	C–O	0.55	2	62.50%
PEKK on $H_2PO_2^-$ film [b] (c)	5	C=O	0	1	33.33%
	6	C–O	1.10	2	66.67%

a Most intense peak is no. 1. b Most intense peak in no. 6.

5.8 Figures

Figure 5-1 XPS spectra of a thick film of poly(ether ketone ketone) on abraded aluminum and repeat unit of PEKK. (a) repeat unit of PEKK, (b) O 1s, (c) C 1s, (d) valence band, (e) valence band calculated from a molecular orbital calculation using the polymer repeat unit.

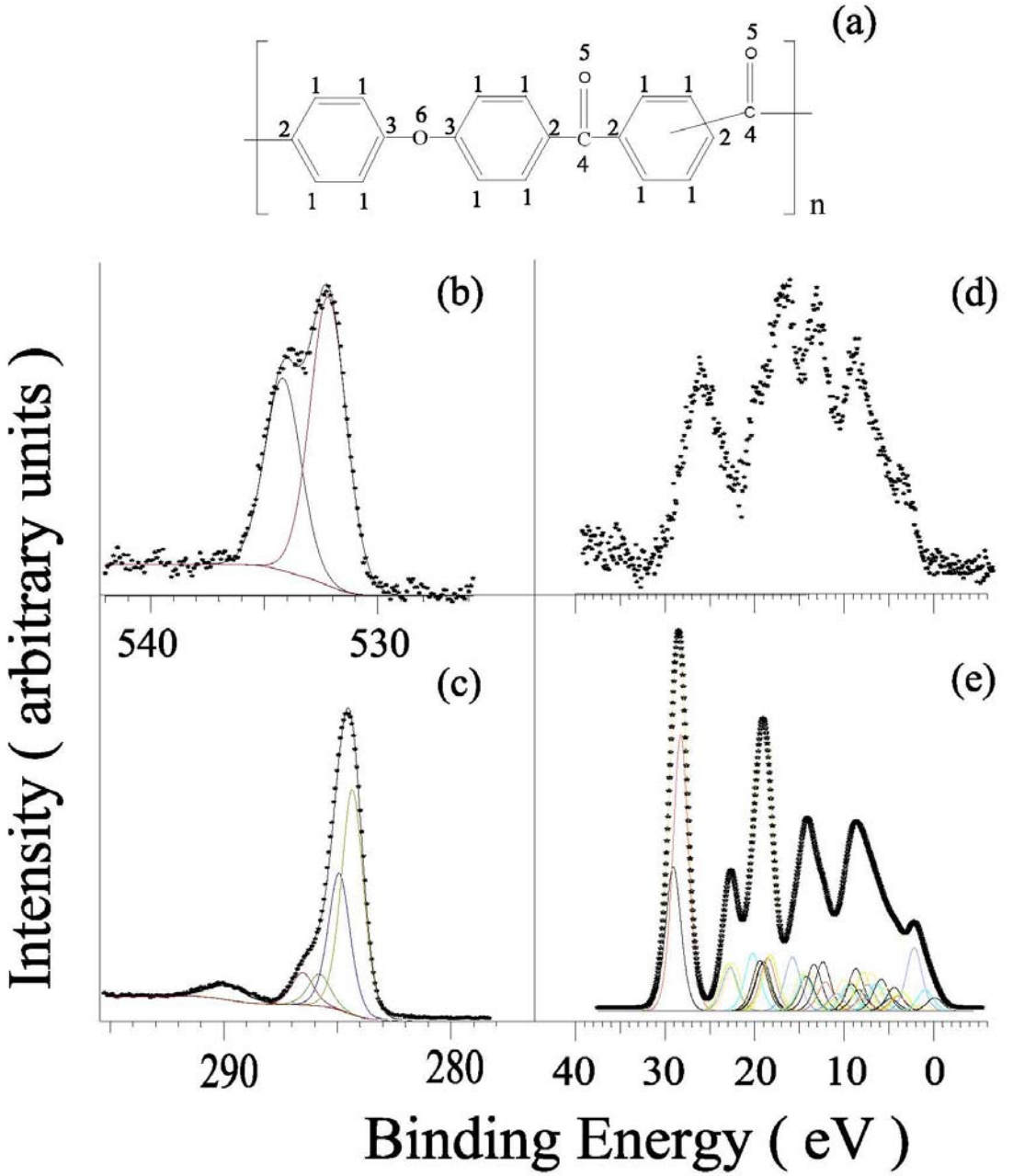

Figure 5-2 Al 2p and P 2p core level XPS spectra for poly(ether ketone ketone) coated on ionic films of PO_4^{3-}, HPO_3^{2-} and $H_2PO_2^-$ on abraded aluminum metal. Column I is Al 2p, II is P 2p for (a) PO_4^{3-}, (b) HPO_3^{2-}, and (c) $H_2PO_2^-$.

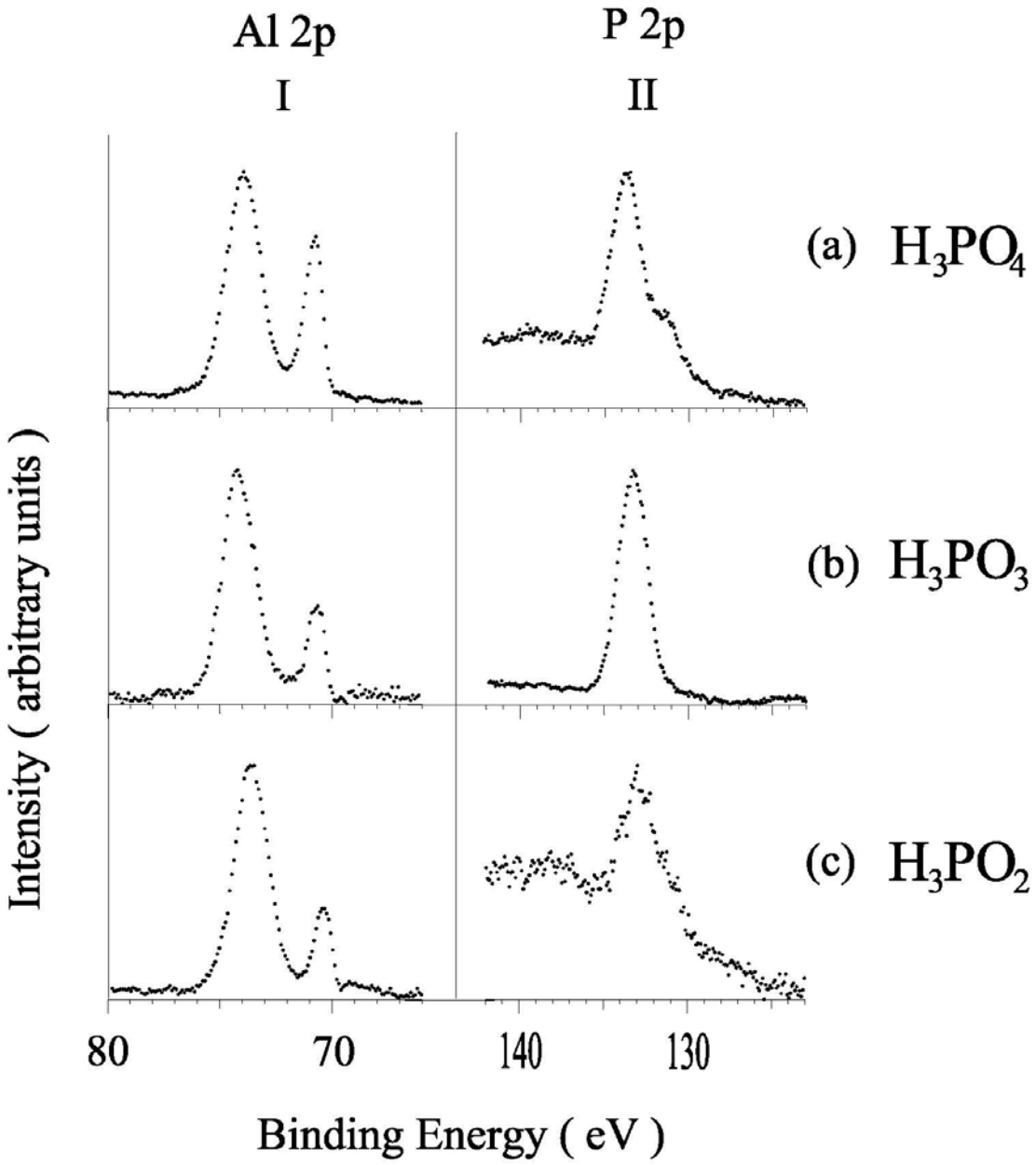

Figure 5-3 C 1s core level XPS spectra for poly(ether ketone ketone) coated on ionic films of PO_4^{3-}, HPO_3^{2-} and $H_2PO_2^-$ on abraded aluminum metal: (a) PEKK from Figure 5.1, (b) PO_4^{3-}; (c) HPO_3^{2-}; and (d) $H_2PO_2^-$.

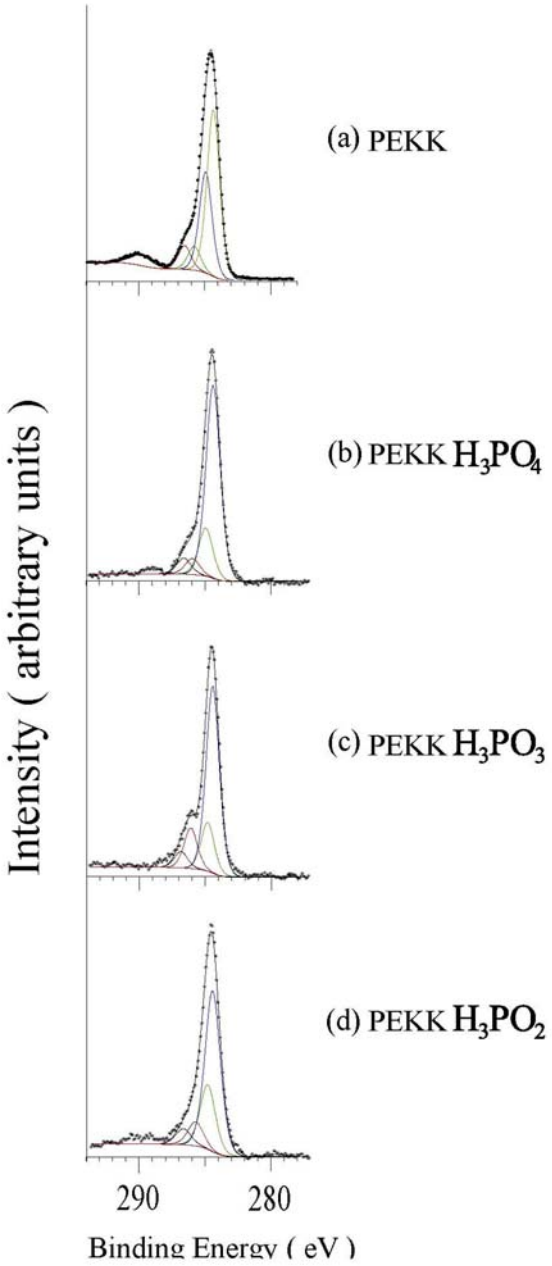

Figure 5-4 O 1s core level XPS spectra for poly(ether ketone ketone) coated on ionic films of PO_4^{3-}, HPO_3^{2-} and $H_2PO_2^-$ on abraded aluminum metal: (a) PEKK from Figure 5.1, (b) PO_4^{3-}; (c) HPO_3^{2-}; and (d) $H_2PO_2^-$.

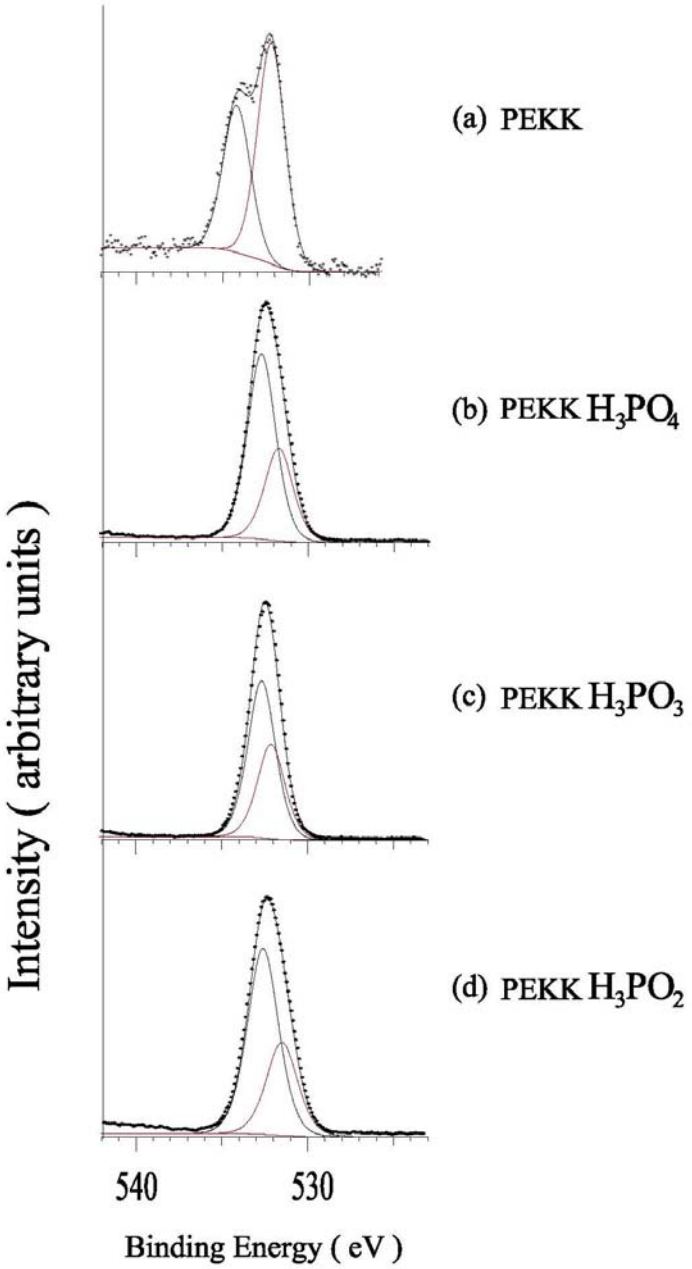

Figure 5-5 The valence band XPS spectra for poly(ether ketone ketone) coated on ionic films of PO_4^{3-}, HPO_3^{2-} and $H_2PO_2^-$ on abraded aluminum metal: (a) PO_4^{3-}; (b) HPO_3^{2-}; and (c) $H_2PO_2^-$.

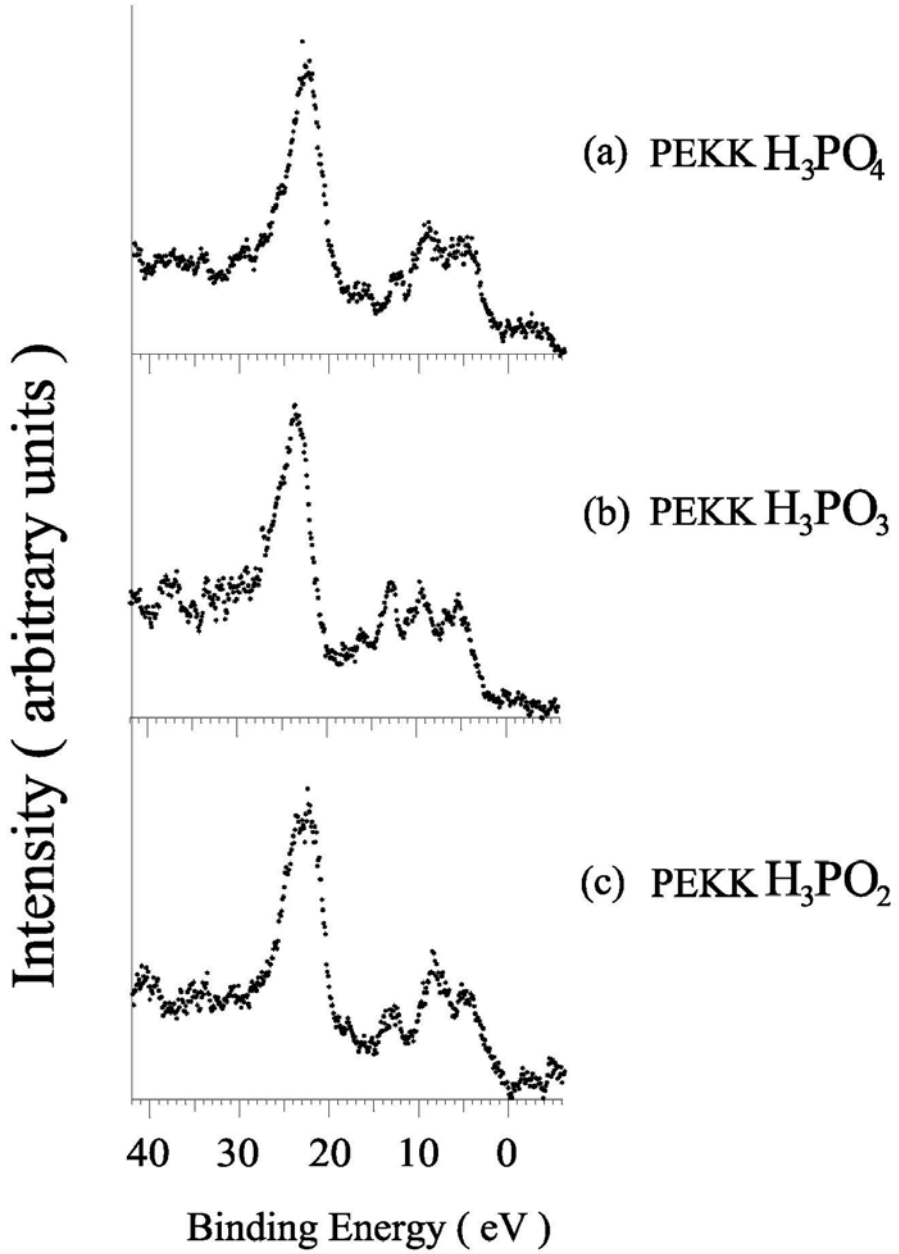

Figure 5-6 Background-subtracted valence band XPS spectra showing only the lower valence band region between 0 eV and 20 eV for the ionic films of PO_4^{3-}, HPO_3^{2-} and $H_2PO_2^-$ on abraded aluminum metal before and after poly(ether ketone ketone) coating. Column I is PO_4^{3-}; II is HPO_3^{2-}; and III is $H_2PO_2^-$, and (a) is before poly(ether ketone ketone) coating and (b) after poly(ether ketone ketone) coating.

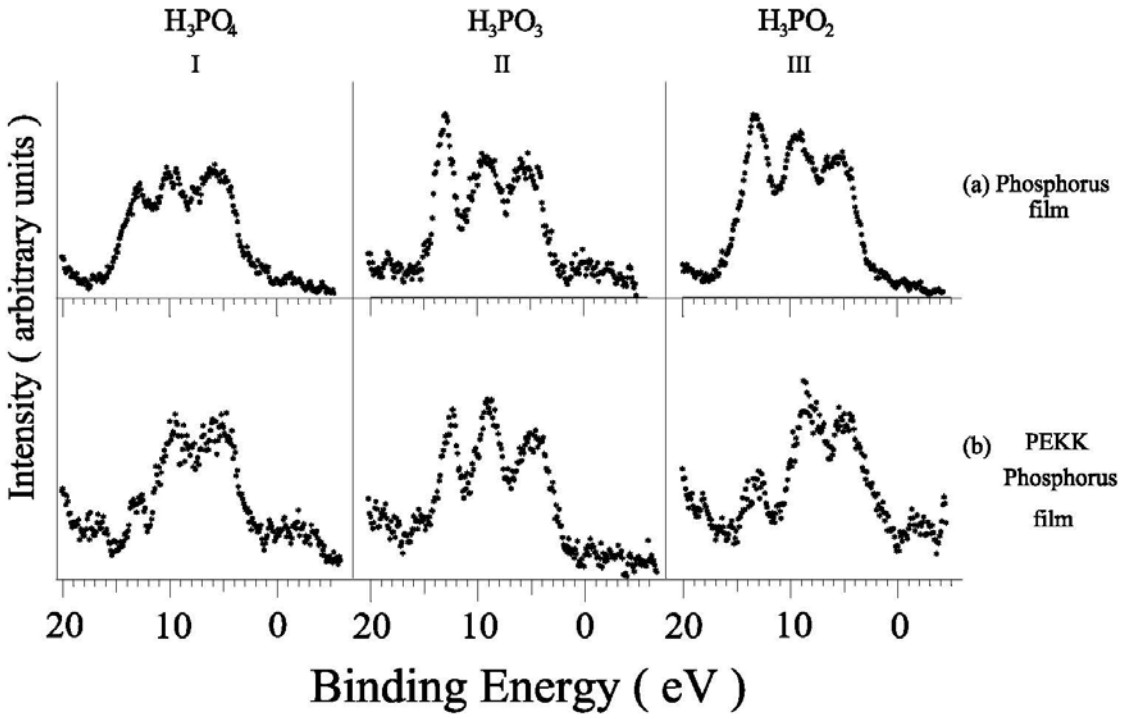

Figure 5-7 Valence band XPS spectra of (a) abraded aluminum metal treated with H_3PO_4, (b) poly(ether ketone ketone), (c) sum spectrum of (a) and (b) [= (a) + (b)], (d) poly(ether ketone ketone) coated on abraded aluminum metal treated with H_3PO_4, (e) difference spectrum of (d) and (c) [= (d) – (c)].

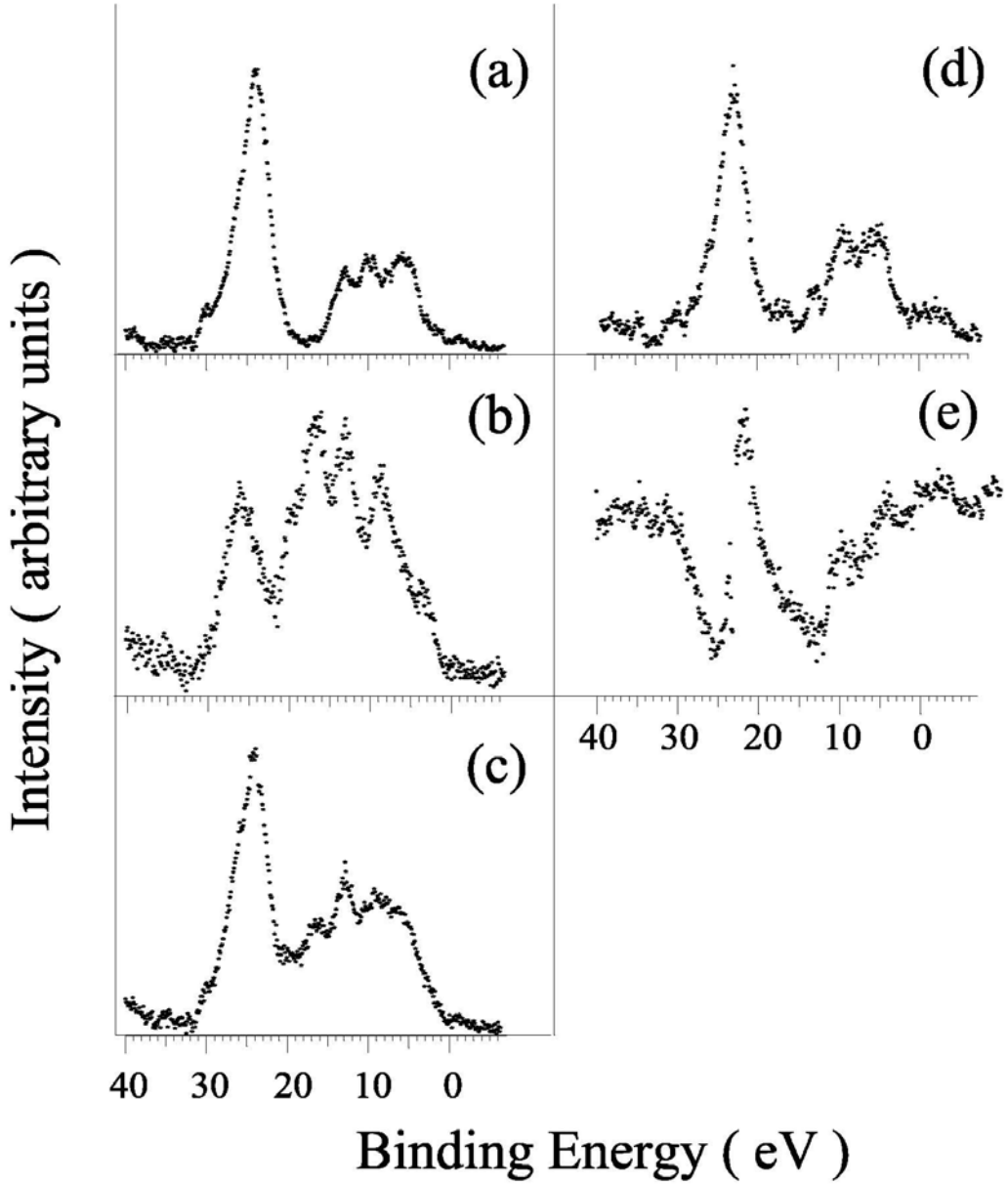

Figure 5-8 Chi squared versus % contribution of PEKK for the PEKK coated on pyrophosphate film on aluminum metal. The lowest point on the graph at 10% PEKK is the value used for creating the addition and difference spectra in Figure 5.7.

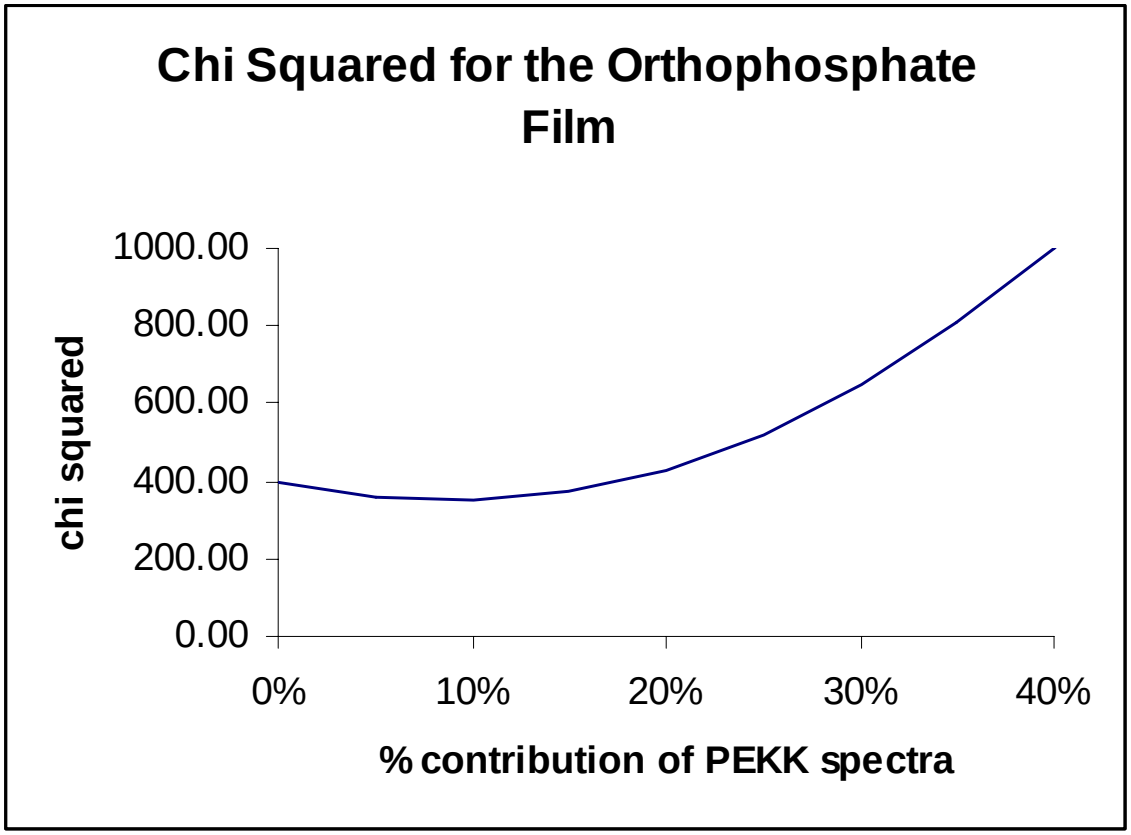

Figure 5-9 Valence band XPS spectra of (a) abraded aluminum metal treated with H_3PO_3, (b) poly(ether ketone ketone), (c) sum spectrum of (a) and (b) [= (a) + (b)], (d) poly(ether ketone ketone) coated on abraded aluminum metal treated with H_3PO_3, (e) difference spectrum of (d) and (c) [= (c) – (d)].

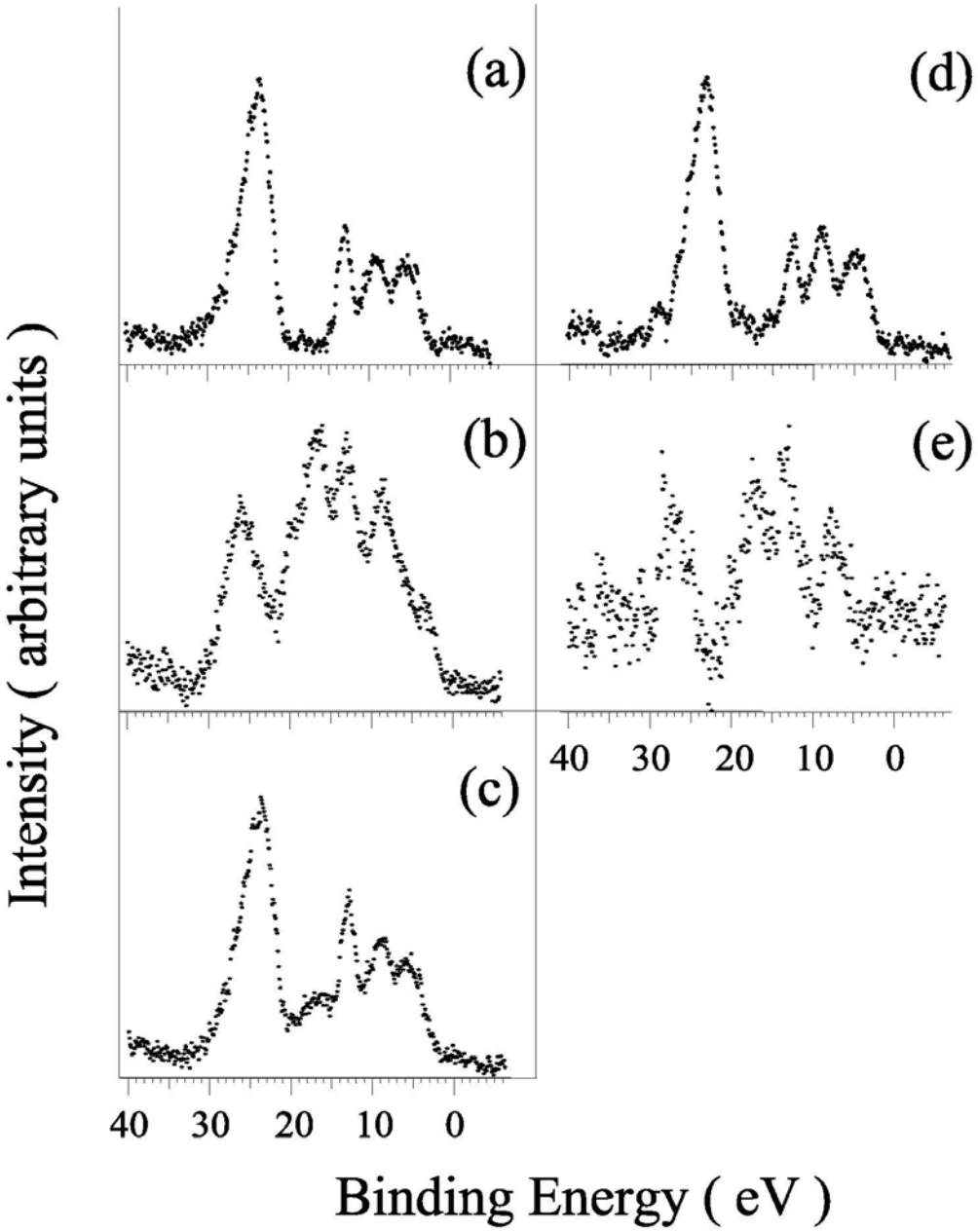

Figure 5-10 Chi squared versus % contribution of PEKK for the PEKK coated on pyrophosphate film on aluminum metal. The lowest point on the graph at 5% PEKK is the value used for creating the addition and difference spectra in Figure 5.7.

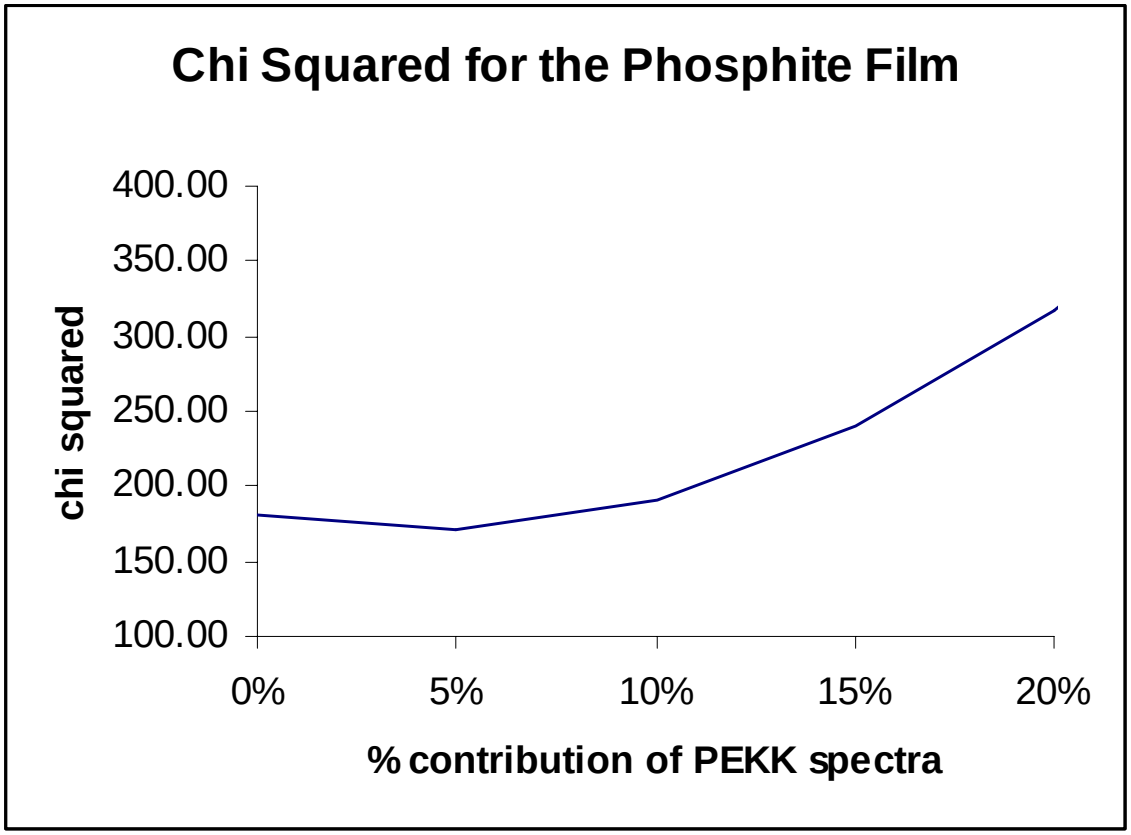

Figure 5-11 Valence band XPS spectra of (a) abraded aluminum metal treated with H_3PO_2, (b) poly(ether ketone ketone), (c) sum spectrum of (a) and (b) [= (a) + (b)], (d) poly(ether ketone ketone) coated on abraded aluminum metal treated with H_3PO_2, (e) difference spectrum of (d) and (c) [= (d) – (c)].

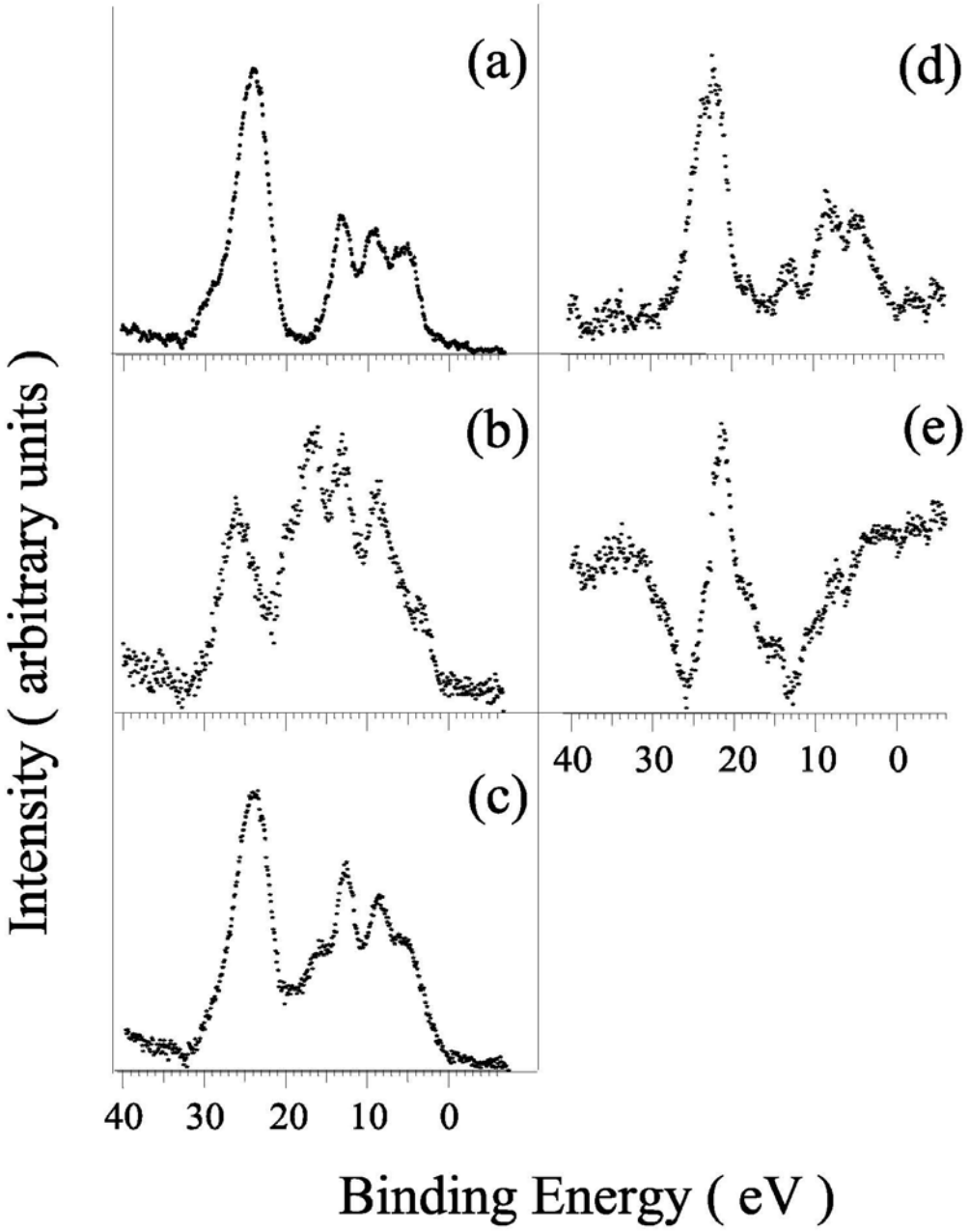

Figure 5-12 Chi squared versus % contribution of PEKK for the PEKK coated on pyrophosphate film on aluminum metal. The thin film shows the lowest point between 0 and 1% on the graph at so 1% contribution for the PEKK spectra is the value used for creating the addition and difference spectra in Figure 5.9.

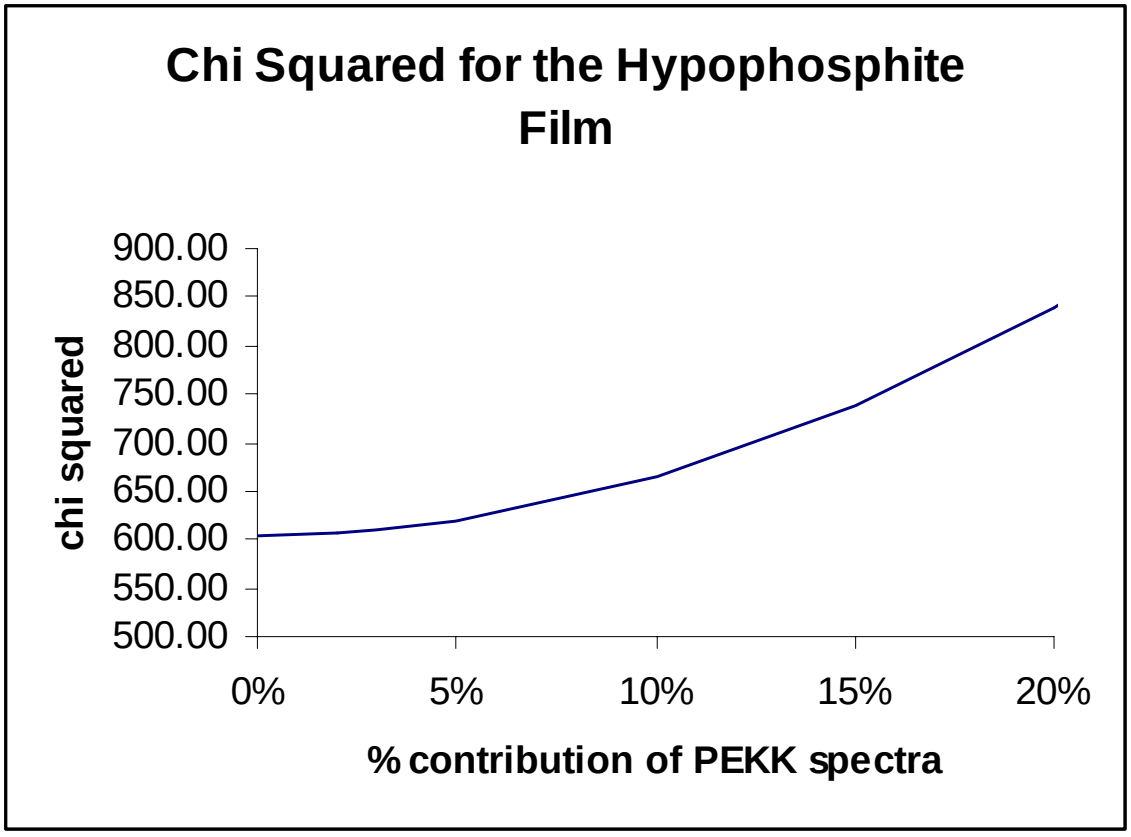

CHAPTER 6 - Corrosion Studies of As-received Mild Steel and Mild Steel Coated with Different Phosphorus Containing Acids and PEKK Characterized Using Core Level and Valence Band XPS

6.1. INTRODUCTION

Chapter 4 and 5 dealt with films formed on the surface of metallic aluminum. When the native oxide is removed from the aluminum metal surface it is very reactive with the oxygen in the air and forms an aluminum oxide layer. This new oxide layer serves to protect the surface from further reaction with the air.[1] Metallic iron has a different reaction when the native oxide is removed and it is exposed to atmospheric conditions.

The surface reacts slowly with oxygen in the air to form iron oxide on the surface commonly known as rust. Rust is brittle and flaky and is easily removed from the surface exposing additional surface iron metal to react with oxygen, therefore creating a cycle in which the surface iron is slowly eaten away. This is an issue today in industrial countries because iron's strength is important in the construction of buildings, bridges and many other structures. Many methods have been proposed to counteract this form of corrosion and protect the integrity of the iron, iron alloy, and other metals used for construction.[1-8]

Our group has been researching new methods of phosphatizing metals to protect against corrosion of construction metals. Metals such as aluminum[1,9], iron[1,9], copper[10], titanium[11], and vanadium[12] have been studied.

This chapter is a continuation of the study to understand corrosion and methods to best protect against it. Mild steel will be coated with a thin film of orthophosphate using orthophosphoric acid, H_3PO_4. The polymer, poly(ether ketone ketone) or PEKK will be used to form a second, separate film on the phosphate film. The as- received mild steel, phosphate coated mild steel and PEKK/phosphate coated mild steel will be subjected to corrosion tests in quadruplely distilled water and sodium chloride solutions in order to test their protection of mild

steel. Core level and valence band XPS spectra will be used to evaluate the resultant surfaces of the metal alloy and films before and after corrosion testing.

6.2. EXPERIMENTAL

6.2.1. Materials and sample preparation.

6.2.1.1. Materials. The mild steel was a commercial alloy containing carbon and iron. The mild steel was cut into 0.5 cm by 1.5 cm rectangles to ensure uniform surface area. Silicon carbide 600 sandpaper was purchased from Carborundum Abrasives. 85% orthophosphoric acid was purchased from Fisher Scientific. The PEKK resin used in this study was provided by Dupont (P11923-15501). The resin is additives-free with a number average molecular weight of 8220 (GPC) and a weight average molecular weight of 28 500 (GPC). The glass transition temperature is 156 $^{\circ}$C (DSC) and the melting temperature is 305 $^{\circ}$C (DSC).

6.2.1.2. Preparation of the phosphate film on abraded mild steel. The 85% orthophosphoric acid was diluted with quadruplely distilled (4-D) water to make a 5 M solution. The solution was then deoxygenated for 2 hours using nitrogen. Three different coating times were used for the mild steel. The same preparation method was used for the three coating times. The mild steel surface was abraded with sandpaper to remove the native oxide and then placed in the deoxygenated orthophosphoric acid solution. The mild steel was abraded for an additional 5 minutes while submersed in solution and then left to stand for 10 minutes in solution. Three methods were used to create three coatings dependent on the time exposed to the orthophosphoric acid after removal of the mild steel from solution.

Method 1: The sample was removed from solution and immediately rinsed with 4-D distilled water. The sample was left to dry overnight in atmospheric conditions.

Method 2: The sample was removed from solution and allowed to sit without rinsing for 20 minutes. The sample was then rinsed with 4-D distilled water and left to dry overnight in atmospheric conditions.

Method 3: The sample was removed from solution and allowed to sit without rinsing for 720 minutes. The sample was then rinsed with 4-D distilled water and left to dry overnight in atmospheric conditions.

6.2.1.3. PEKK film preparation. The as-received PEKK resin was in the form of pellets. The PEKK solution was prepared by heating a 1:1 mixture of phenol and 1,2,4-trichlorobenzene to between 100 °C and 120 °C and dissolving enough PEKK resin to form a 1% solution. The 1 % solution was used to coat the orthophosphate films formed on abraded mild steel used for the corrosion tests. The coatings were dried in a vacuum oven at 90 °C for 48 hours.

6.2.1.4. Corrosion tests. The as-received, orthophosphate coated, and PEKK/ orthophosphate coated mild steel was subjected to two solutions representing two different environments in which corrosion occurs. The first solution was 4-D water solution to represent a moisture rich environment and the second was 1M sodium chloride solution to represent a salt water environment. Each sample was placed in solution for 2 hours. The corrosion tests were preformed in ambient conditions without oxygenating or deoxygenating the solutions.

6.2.2. Surface analysis. The spectra were collected with a VSW HA150 spectrometer unless otherwise stated. The VSW HA150 has a 150mm hemispherical analyzer operated in the fixed analyzer transmission mode with a pass energy of 20 eV and is also equipped with a 16-plate microchannel detection system. The Al Kα X radiation (240 Watts) generated from a 35 quartz crystal monochromator provides a linewidth of better than 0.2 eV. The base pressure of the instrument was 10^{-9} Torr or better.

The spectra in Figure 6.11, used to verify the corrosion tests on the PEKK coating, were collected with a SPECS Sage 100 spectrometer. The SPECS Sage 100 has a 95 mm hemispherical analyzer operated in the fixed analyzer transmission mode with a pass energy of 15 eV. The x-ray gun used produced achromatic Mg Kα (1253.6 eV) radiation at 240W and was equipped with a water-cooled x-ray gun cap. The water-cooled cap is used to reduce the chance of sample decomposition and carbon contamination.[13] The base pressure of the instrument was 2 x 10^{-8} torr or better. All spectra were referenced against the C1s peak at 284.6 eV.

6.2.3. Calculations. Both band-structure and Xα cluster calculations were used to interpret the experimental valence band XPS spectra. The band structure calculations were carried out using an extended version of the program CRYSTAL.[14,15] This program performs *ab initio* calculations of the ground state energy, electronic wave function and properties of periodic systems. One electron eigenfunctions of the Fock Hamiltonian are represented by linear combinations of Bloch functions, which are also a linear combination of atomic orbitals. A Mulliken analysis is used to obtain orbital, atomic and total densities of states. The separate densities of states for each type

of orbital for each atom in the compound were evaluated. This set of atomic orbital densities of states was adjusted by their atomic photoelectron cross-sections using values determined by Scofield.[16] The cross-section-adjusted total density of states were then convoluted with a Gaussian /Lorentzian product function. All of the calculations employed the STO-3G basis set. Calculations were performed for the cubic (Fm3m) NaCl structure of FeO and Cmcm structure of γ-FeOOH.

The metallic iron valence band XPS spectrum was generated using band structure calculations run on a substantially modified version of the program BNDPKG2 (part of the MOTECC90 suite of programs, copyright IBM).[17,18] The Parameters used in the calculation were previously published by J. Callaway and C. S. Wang.[19] The density of states was adjusted by the Scofield cross-section values and convoluted with a 50 % Gaussian/Lorentzian product function with a FWHM of 0.5 eV.[20]

Since the energies in the band structure calculations do not vary much for the different directions of the crystal, the bands are very flat. This allows the spectra to be interpreted by both band-structure and cluster calculations. Cluster calculations[21] were carried out using multiple scattered-wave Xα calculations based on a finite model approximated using a "Watson sphere" to neutralize the charge of the ions PO_4^{3-} used in the calculation.

6.3. RESULTS AND DISCUSSION

The results before and after the corrosion tests on as-received mild steel, an orthophosphate film on mild steel, and PEKK/ orthophosphate films on mild steel were analysed using core level and valence band XPS spectra and are discussed here.

6.3.1. corrosion studies on as-received mild steel using 4-D water and sodium chloride (Samples EI, EII, and EIII). A list of the samples studied in this chapter is shown in Table 6.1. Sample EI is the as-received mild steel that was abraded and placed in the XPS instrument for analysis. The as-received mild steel was then corrosion tested in the 4-D water and NaCl solutions to obtain the samples EII and EIII. The resultant core level and valence band XPS spectra are discussed here.

6.3.1.1. core level XPS. Abraded as-received mild steel was exposed to 4-D water and NaCl solutions for two hours. The core level XPS spectra for C 1s, column I, O 1s, column II, and Fe

2p, column III, for as-received mild steel (a) and the two corrosion studies: 4-D water (b) and sodium chloride (c) solutions are shown in Figure 6.1. As-received iron metal and mild steel have been previously discussed.[1,5,22] The core level and valence band XPS spectra for mild steel are shown here for comparison purposes.

The C 1s spectra, column I, have a peak calibrated at 284.6 eV for the hydrocarbon adsorbed to the sample surface and two peaks shifted to 286.3 eV and 288 eV for the carbon component in the mild steel reacting in air after abrasion to form C-O type and C=O type bonds. The peak at 286.3 eV for the C-O type bond increases in intensity in the two corrosion tests, Figure 6.1 (b) and (c).

The O 1s core level spectra, column II, have a peak between 530 eV and 530.5 eV for FeO and two shifted peaks: one between 531 eV and 532 eV after for FeOOH, and one at 533 eV for Fe_2O_3. The O 1s XPS spectrum for the corrosion test in 4-D water, Figure 6.1 II (b), shows an increase in intensity of the Fe_2O_3 peak at 533 eV compared to the as-received mild steel before testing. The O 1s spectrum for the sodium chloride corrosion test, Figure 6.1 II (c), shows an increase of intensity in the FeOOH peak at 531 eV when compared to the as-received mild steel. When the abraded mild steel surface was exposed to 4-D water there was an increase in the Fe_2O_3 film formed and when exposed to the NaCl solution there was an increase in the FeOOH film formed.

For the as-received and two corrosion tests, the Fe 2p XPS spectra show two features: Fe $2p_{3/2}$ and Fe $2p_{1/2}$. There are two peaks in the Fe $2p_{3/2}$, one between 706 eV and 707 eV for iron metal and a broader peak at 711 eV for iron oxide. The two peaks on the Fe $2p_{1/2}$ are between 719 eV and 720 eV for the iron metal and 724 eV for iron oxide. Super Coster-Kronig broadening, which causes the iron oxide peak in Fe $2p_{1/2}$ at 724.4 eV to be less intense and broader than Fe $2p_{3/2}$, is observed here.[23]

Since the iron metal peaks can be seen the iron oxide film thickness is <100 Å. The iron metal peaks decrease in Fe 2p XPS spectrum for the 4-D water corrosion test and more so in the spectrum for the NaCl corrosion test showing that exposure of the mild steel surface to 4-D water and NaCl solutions are causing an increase of the thickness of the iron oxide film.

6.3.1.2. valence band XPS. The valence band XPS spectrum for the as-received mild steel, Figure 6.2 (a), has two peaks in the outer valence band region between 0 eV and 20 eV. The peak for the iron metal is the narrow, sharp peak at 1 eV and the iron oxide peak is the broader,

less intense peak at 3.5 eV with two shoulders at 6 eV and 7.9 eV. The iron metal peak appears to be more intense in the valence band region seeming to contradict to the intensity ratio seen in the Fe 2p region XPS spectrum, Figure 6.1 III (a). This is not the case in that the intensity is higher in the valence band spectrum simply because they are higher kinetic energy electrons. This compares well to previously published data on iron metal.[22]

The as-received mild steel was tested in 4-D water for 2 hours and the resultant spectrum is shown in Figure 6.2 (b). The iron oxide intensity has increased compared to the as-received mild steel. The abraded mild steel surface, when exposed to the 4-D water, formed an iron oxide film that was thicker than the iron oxide film formed when exposed to atmospheric conditions.

The valence band XPS spectrum for the mild steel corrosion test in NaCl solution is shown in Figure 6.2 (c). The iron oxide peak at 3.8 eV has increased in intensity again showing that an even thicker iron oxide has formed when exposed to the NaCl solution. The O 2s peak at 22 eV has a smaller FWHM compared to the O 2s peak in the as-received mild steel spectrum and the spectrum of as- received mild steel exposed to 4-D water. This same trend was observed for the O 1s spectra in Figure 6.1 column II.

The outer valence band region XPS spectra with the nonlinear background removed are shown in Figure 6.3 I for the as-received mild steel (a) and the two corrosion tests: in 4-D water (b) and NaCl (c) solutions. The increase in the intensity of the iron oxide peak is also seen here. The valence band XPS spectra compare well to spectra generated by band structure calculations of metallic iron in Figure 6.3 II (a) compared to the XPS spectrum of the as-received mild steel and FeO, shown in Figure 6.3 II (b), compared to the XPS spectra for both corrosion tests.

6.3.2. corrosion studies on orthophosphate film on mild steel using 4-D water and sodium chloride (Samples EIV, EV, EVI, EVII, and EVIII). The low reactivity of the mild steel led to the use of varied exposure times to orthophosphoric acid to form the orthophosphate film on the surface of the mild steel. These experiments are marked as sample EIV, EV, and EVI in Table 6.1 for exposure times of 0, 20, and 720, respectively. The three films formed using different exposure times and the corrosion tests in 4-D water, sample EVII, and NaCl, sample EVIII, solutions conducted on the film formed after an exposure time of 720 minutes were studied using core level and valence band XPS.

6.3.2.1. the PO43- film preparation. Previously[5], an orthophosphate coating was applied to mild steel using etidronic acid ($C_2P_2O_7H_8$) with varied exposure times. The reaction was proposed to be[5]:

$$3H_2O + C_2P_2O_7H_8 \leftrightarrow 2PO_4^{3-} + CH_3CO_3H + 8H^+ + 6e^-$$
$$Fe^{3+} + e^- \leftrightarrow Fe^{2+}$$

In the technique discussed in this chapter, the abraded mild steel surface reacts directly with orthophosphoric acid to form an orthophosphate film using varied times exposed to the acid. The orthophosphate film was applied using three different reaction times before rinsing the orthophosphoric acid from the surface. The reaction time after the initial coating process in the 5 M solution of orthophosphoric acid with the mild steel was increased from 0 to 20 minutes to 720 minutes.

The valence band XPS spectra, Figure 6.4, show a decrease in the iron oxide and iron metal peak from the spectrum of mild steel exposed to the orthophosphoric acid for 0 minutes, Figure 6.4 (a), where the peaks are the dominate features of the outer valence band region between 0 eV and 20 eV, to the spectrum of mild steel exposed for 720 minutes, Figure 6.4 (c), where the features are replaced by the orthophosphate peaks. The valence band XPS spectrum in Figure 6.4 (a) shows two peaks: one lower binding energy peak at 0.5 eV for the iron metal and a broader peak at 4.5 eV for the iron oxide. In Figure 6.4 (b), two low intensity peaks are shown at 9.9 eV and 12.3 eV, with iron oxide still present at 4.5 eV. There is also a peak at 34.9 eV in both Figure 6.4 (a) and (b) that is present in a region where a few metals such as sodium that has occupied levels at that energy. This is difficult to identify since iron, carbon and phosphate do not have peaks in that energy range.

The valence band XPS spectrum of the mild steel with an exposure time of 720 minutes to the phosphoric acid, Figure 6.4 (c), is similar to valence band XPS spectra previously reported for aluminum and iron phosphate.[1] The two peaks for phosphate have shifted from 9.9 eV and 12.3 eV in Figure 6.4 (b) to 8.8 eV and 11.50 eV with a separation of 2.7 eV.

The outer valence band region XPS spectrum of the mild steel exposed to orthophosphoric acid for 720 minutes, with the non linear background removed, is shown in Figue 6.5. This is compared to a spectrum generated using Xα calculations of the PO_4^{3-} ion

shown in Figure 4.3, reprinted here for comparison in Figure 6.5 (b). For the remainder of the chapter, the orthophosphate film formed on mild steel and used in further coatings and corrosion tests will refer to the phosphate film formed using mild steel exposed to orthophosphoric acid for 720 minutes, Figure 6.4 (c).

6.3.2.2. core level XPS. The core level XPS spectra for C 1s, column I, O 1s, column II, P 2p, column III, and Fe 2p, column IV, for the orthophosphate film on mild steel (a) and the two corrosion tests in: 4-D water (b) and NaCl (c) solutions are shown in Figure 6.6. The C 1s spectrum has a peak calibrated at 284.6 eV for the hydrocarbon adsorbed to the sample surface and two less intense peaks at 286 eV for the C-O type bond and 288.5 eV for the C=O type bond from the carbon component in the mild steel as seen in the as-received mild steel, Figure 6.1 I.

The O1s has a peak at 532 eV for $FePO_4$ for the orthophosphate film on mild steel in Figure 6.6 II (a), which is shifted 2 eV from the FeO peak in as-received mild steel between 530 eV to 530.5 eV. The PO_4^{3-} peak is at the same energy as the FeOOH peak between 531 eV and 532 eV in as-received mild steel. The O 1s XPS spectra for the two corrosion tests, Figure 6.6 II (b) and (c), have a peak at 532 eV for $FePO_4$ also, but have an added peak shifted to 530.5, seen in the as-received mild steel, for FeO. The appearance of the FeO peak in the O 1s XPS spectrum shows that when the mild steel is exposed to the 4-D water and NaCl solutions an FeO film is formed. The peak at 532 eV is due to both $FePO_4$ and FeOOH intensity so the O 1s region can not be used to confirm changes, if any, in the $FePO_4$ film.

There are two peaks in the Fe 2p region XPS spectrum for the orthophosphate film on mild steel, Figure 6.6 IV (a): one at 712.8 for iron oxide in Fe $2p_{3/2}$ and one at 726.8 eV for iron oxide in Fe $2p_{1/2}$. This shows that the orthophosphate film initially formed on the mild steel is sufficiently thick to not show the underlying iron. There are four peaks in the Fe 2p XPS spectrum of the orthophosphate film on mild steel after the two corrosion studies, Figure 6.6 IV (b) and (c): two peaks corresponding to the iron metal peak at 707.5 eV in Fe $2p_{3/2}$ and 720 eV in Fe $2p_{1/2}$. This shows that the orthophosphate film thickness has decreased when the samples were exposed to the 4-D water and NaCl solutions. This observation is confirmed by the appearance of an iron oxide film in the O 1s region, along with a decrease in the intensity of the phosphorus peak in the P 2p XPS spectra, shown in Figure 6.6 column III, from (a) to (c).

6.3.2.3. valence band XPS. The valence band XPSspectra also show a decrease in the PO_4^{3-} film on mild steel. The valence band XPS spectra for the orthophosphate film on mild steel (a) and

the two corrosion tests in: 4-D water (b) and NaCl (c) solutions are shown in Figure 6.7. The two phosphate peaks at 8.8 eV and 11.5 eV in Figure 6.7 (a) are not seen in the two corrosion tests.

The outer valence band region of the XPS spectra is shown in Figure 6.8 column I with the non-linear background removed. The spectra show more clearly the decrease of the phosphate peaks from before to after both corrosion tests were conducted. The spectrum for the corrosion test in 4-D water shows a sloping tail in the oxide peak from 6.5 eV to 10 eV that is not present in the spectrum for the corrosion test in the NaCl solution. This corresponds to the sloping tail found in the FeOOH valence band spectrum reported by W. Temesghen and P. M. A. Sherwood [22] This compared well to the spectrum generated using band structure calculations for FeOOH, Figure 6.8 II (b). The XPS spectrum for the corrosion test in the NaCl solution is predicted well by the XPS spectrum calculated using band structure calculations for FeO, Figure 6.8 II (c). The band structure calculations were also reported by W. Temesghen and P. M. A. Sherwood and are reprinted here for comparison.

Another study was conducted in the group, unpublished, on an orthophosphate coating on mild steel. This phosphate film was prepared using the same method described here and corrosion tested by submersion in aerated 4-D water for two hours. The outer valence band region XPS spectra are shown in Figure 6.8 III, where Figure 6.8 (a) is the XPS spectrum of initial orthophosphate film on mild steel and (b) is the XPS spectrum of the orthophosphate on mild steel after a two hour exposure in aerated 4-D water. The after spectrum shows no change compared to the initial film. This information states that the phosphate film was able to provide protection to the mild steel when exposed to 4-D water saturated with oxygen, but only provided limited protection in the 4-D water without any prior treatment. This is in contrast to what would be expected in the oxygen rich solution.

6.3.3. corrosion studies on PEKK coated on orthophosphate film on mild steel using 4-D water and sodium chloride (Samples EIX, EX, and EXI). The mild steel coated with an orthophosphate film was further coated to create a second, separate film of PEKK contiguous the orthophosphate film (Samples EIX, EX, and EXI). The core level and valence band XPS spectra are discussed in the following sections.

6.3.3.1. core level XPS. The core level XPS spectra for C 1s, column I, O 1s, column II, P 2p, column III, and Fe 2p column IV, for PEKK coated on an orthophosphate film on mild steel (b),

and the two corrosion tests in: 4-D water (c) and NaCl (d) solutions are shown in Figure 6.9. The presence of the PEKK on the surface creates a more complex C 1s XPS spectrum for PEKK than the previously mentioned C 1s XPS spectra in this chapter because of the carbon features due to the PEKK repeat unit. The repeat unit for the polymer, PEKK, is shown in Figure 6.9 (a) with the different types of bonds numerically labeled. The C 1s spectra in Figure 6.9 have the peak calibrated at 284.6 eV for the hydrocarbon adsorbed to the sample surface, which is at the same energy as the C-C type bonds for the PEKK, labeled 1 in Figure 6.9 (a). There are three other features in the C 1s spectra due to PEKK: one at 285 eV for C-C=0 type bonds, labeled 2, one at 286 eV for C-O type bonds, labeled 3, and one at 287 eV for C=O type bonding, labeled 4.

The O1s XPS spectrum for the PEKK coated on the orthophosphate film on mild steel has two peaks at 531.9 eV for C=O type bonding, labeled 5 and 533.6 eV for C-O type bonding, labeled 6. The PEKK for the coating was a 1 % wt solution compared to the 0.25% wt solution used to make the PEKK coatings in chapter 5. The concentration of PEKK in solution determines the thickness of the film formed so the PEKK film is thicker and the spectra look closer to pure PEKK shown in Figure 5.1, previously described.[24]

The O 1s region XPS spectra for the two corrosion tests have two peaks also at 531.6 eV for the C=O and 533.5 eV for C-O and a shoulder for the corrosion test in 4-D water solution and a peak for the corrosion test in the NaCl solution appears at 530 eV for FeO. The presence of the FeO peak shows that an iron oxide film is formed when the sample is exposed to the NaCl solution for two hours. A small amount of iron oxide is also detected when the sample is exposed to the 4-D water solution. The peak intensity for the C-O type bond for the PEKK decreases after both corrosion tests showing that either the PEKK film thickness is decreasing or that the peak intensity at 531 eV is increasing due to an increase of FeOOH present on the surface.

The P 2p XPS spectra have one peak at 133 eV that decreases from the PEKK coated on the orthophosphate film on mild steel before the corrosion tests to having no intensity after the sample is exposed to the NaCl solution. There are two peaks in the Fe 2p XPS spectrum; one peak in the Fe $2p_{3/2}$ at 711.5 eV to 712 eV and one peak in the Fe $2p_{1/2}$ at 725 eV to 726 eV for iron oxide. The films are sufficiently thick to not show the underlying mild steel.

6.3.3.2. valence band XPS. The PEKK coated on orthophosphate film on mild steel valence band XPS spectra has a triple peak structure seen previously in PEKK at 17 eV discussed in

chapter 5. Figure 6.10 shows the valence band XPS of PEKK coated on the orthophosphate film on mild steel (a) and the two corrosion tests in: 4-D water (b) and NaCl (c) solutions. The valence band XPS spectra show no differences between the XPS spectrum of the initial PEKK coated on orthophosphate film on mild steel and the XPS spectrum of the corrosion test in 4-D water solution, but significant differences between the initial sample and the corrosion test in the NaCl solution. In Figure 6.10 (c), the PEKK decomposes to form another species. This is seen in the shifting of the O 2s peak to make two separate peaks at 22 eV and 25 eV. This was reported in an earlier publication where a corrosion test was conducted on a thick PEKK film on copper submersed in a NaCl solution at 92 °C for 10 days, reprinted here for comparison in Figure 6.11 IV (c).[24] The samples were not rinsed after the corrosion tests were conducted and left some of the decomposed PEKK to dry on the sample surface.

The corrosion tests were conducted on fresh samples and rinsed immediately after. The XPS spectra were run on a SPECS Sage 100 with achromatic radiation and single channel (channeltron) detector and the resultant XPS spectra are shown in Figure 6.12 for the core levels P 2p, column I, and Fe 2p, column II, and the valence band, column III and background subtracted outer valence band region, column IV. The core level XPS spectra of P 2p and Fe 2p show the same trend as the first set of tests with decreasing P 2p intensity and decreasing film thickness. The difference is shown in the valence band region. The PEKK peaks were still present after the corrosion test in the 4-D water solution, but were not after the corrosion test in the NaCl solution. An iron oxide peak is observed in the valence band XPS after exposure of the sample to the NaCl solution. The PEKK film provided protection to the mild steel surface in 4-D water, but was only mildly successful in the NaCl solution.

6.4. CONCLUSION

Orthophosphate was coated on the surface of mild steel by exposing the mild steel to orthophosphoric acid for 720 minutes. This coating and a second, separate coating of PEKK were tested for their protection of mild steel against corrosion. The orthophosphate film showed protection abilities when exposed to aerated 4-D water. The PEKK coating on the orthophosphate film was able to protect the mild steel when exposed to 4-D water at atmospheric conditions, but decomposed in the NaCl solution to form a new species. Valence band spectra

generated by band structure and Xα cluster calculations predicted the changes in the experimental XPS spectra.

6.5. ACKNOWLEDGEMENTS

This material is based upon work supported by the National Science Foundation under Grant No. CHE-0137502. The U.S. Government has certain rights to this material. I would like thank Dr. Yuqing Wang and Rachael Smith for there contributions to this work and Dean P.M.A. Sherwood for the Xα cluster and band structure calculations.

6.6 REFERENCES (see Reference chapter)

6.7 Tables

Table 6-1 Description of Sample Studied

Table 6.1: Description of Samples Studied

Designation	Description of treatment
EI	as-received mild steel (polished in air by fine sandpaper)
EII	as-received mild steel tested in 4-D water
EIII	as-received mild steel tested in sodium chloride
EIV	PO_4^{3-} coated on mild steel rinsed immediately
EV	PO_4^{3-} coated on mild steel for 20 minutes
EVI	PO_4^{3-} coated on mild steel for 720 minutes
EVII	PO_4^{3-} coated on mild steel tested in 4-D water
EVIII	PO_4^{3-} coated on mild steel tested in sodium chloride
EIX	PEKK coated on PO_4^{3-} film on mild steel
EX	PEKK coated on PO_4^{3-}/mild steel tested in 4-D water
EXI	PEKK coated on PO_4^{3-}/mild steel tested in sodium chloride

6.8. FIGURES

Figure 6-1 Core level XPS spectra, C 1s column I , O 1s column II, and Fe 2p column III, for as-received mild steel (a) and the corrosion tests on as-received mild steel in 4-D water (b) and sodium chloride (c) solutions for two hours.

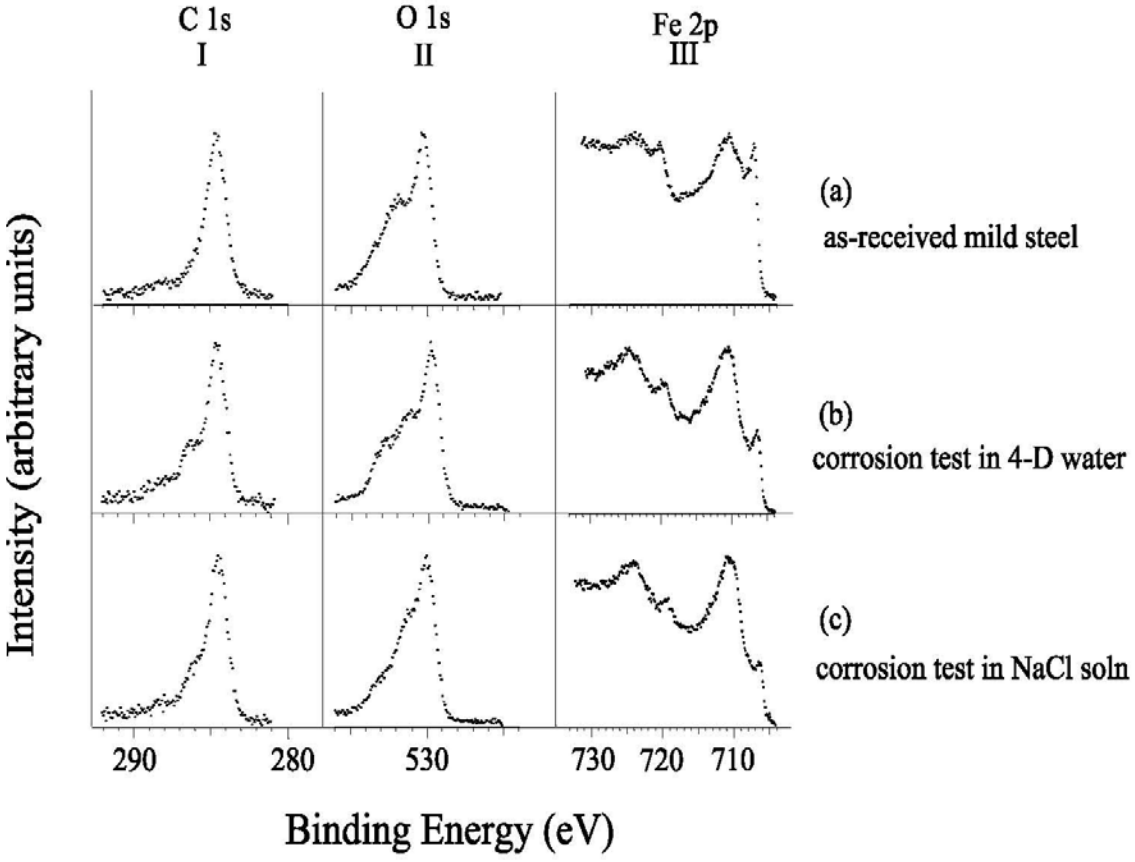

Figure 6-2 Valence band XPS spectra of the as-received mild steel (a) and the corrosion tests on as-received mild steel in 4-D water (b) and sodium chloride (c) solutions for two hours.

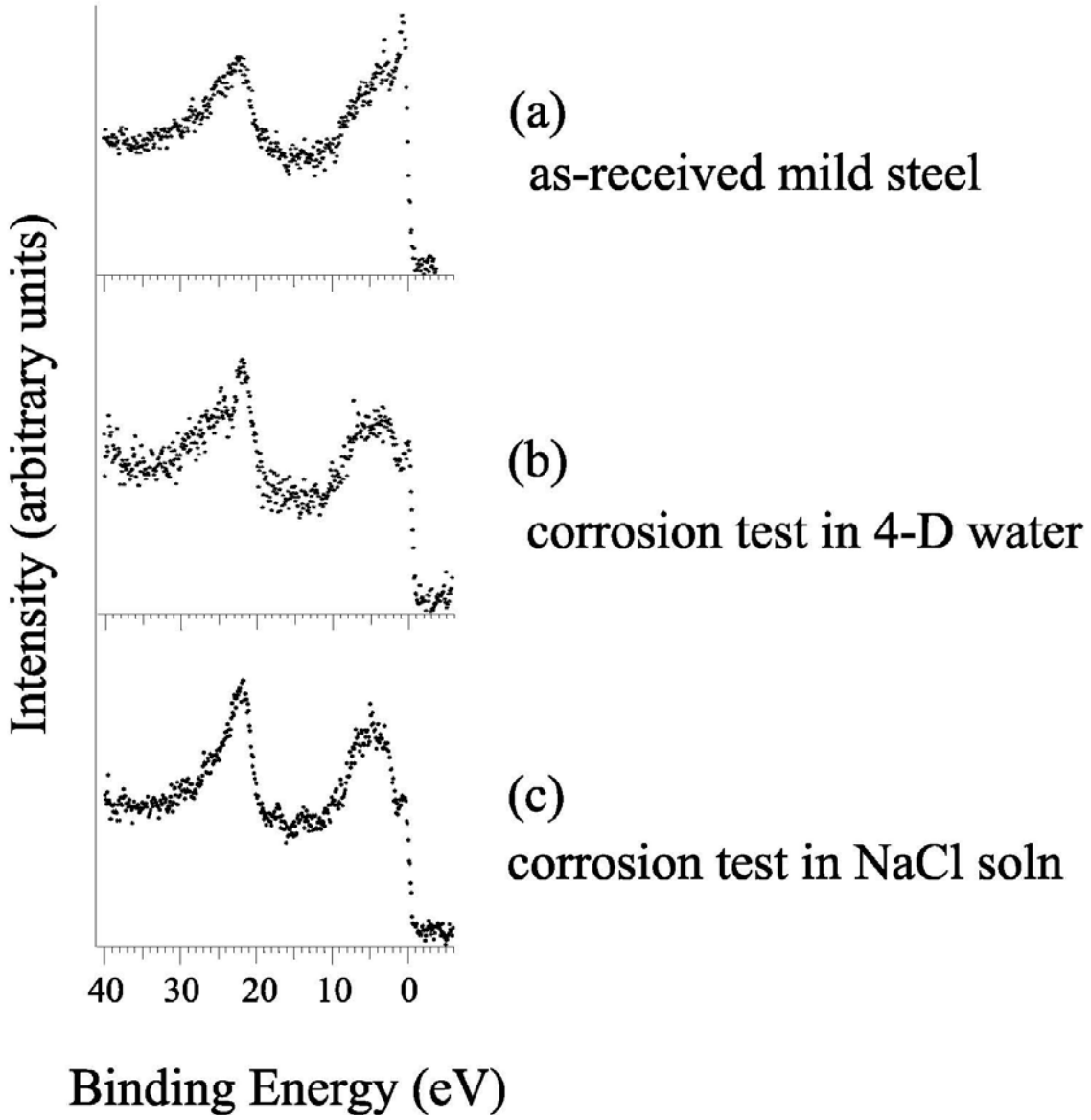

Figure 6-3 Background subtracted outer valence band XPS spectra of the as-received mild steel (a) and the corrosion tests on as-received mild steel in 4-D water (b) and sodium chloride (c) solutions. Spectra generated by band structure calculations of metallic iron (a) and FeO (b).

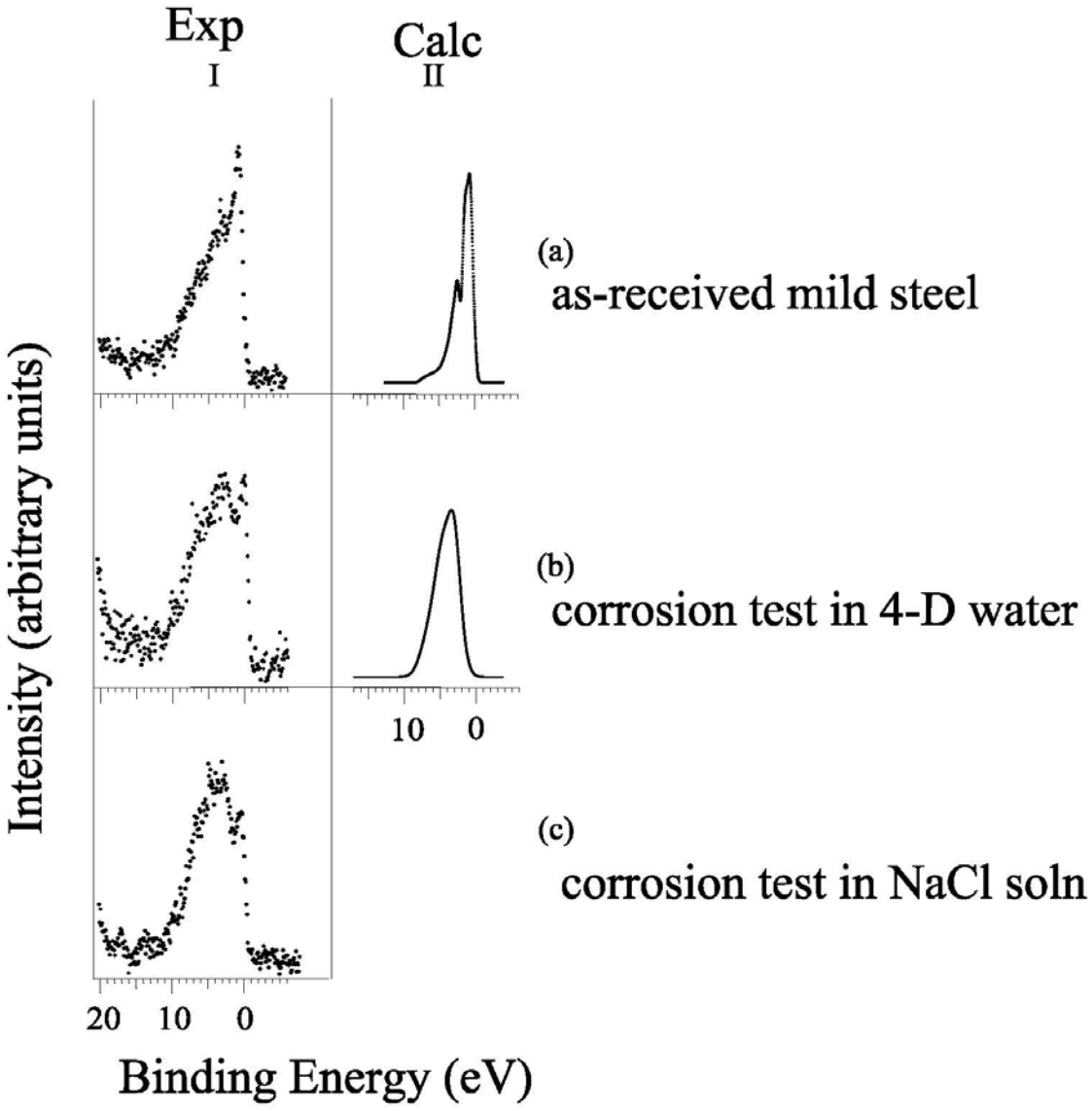

Figure 6-4 Valence band XPS spectra of mild steel exposed to H_3PO_4 for 0 minutes (a), 20 minutes (b), and 720 minutes (c) after the initial reaction in solution.

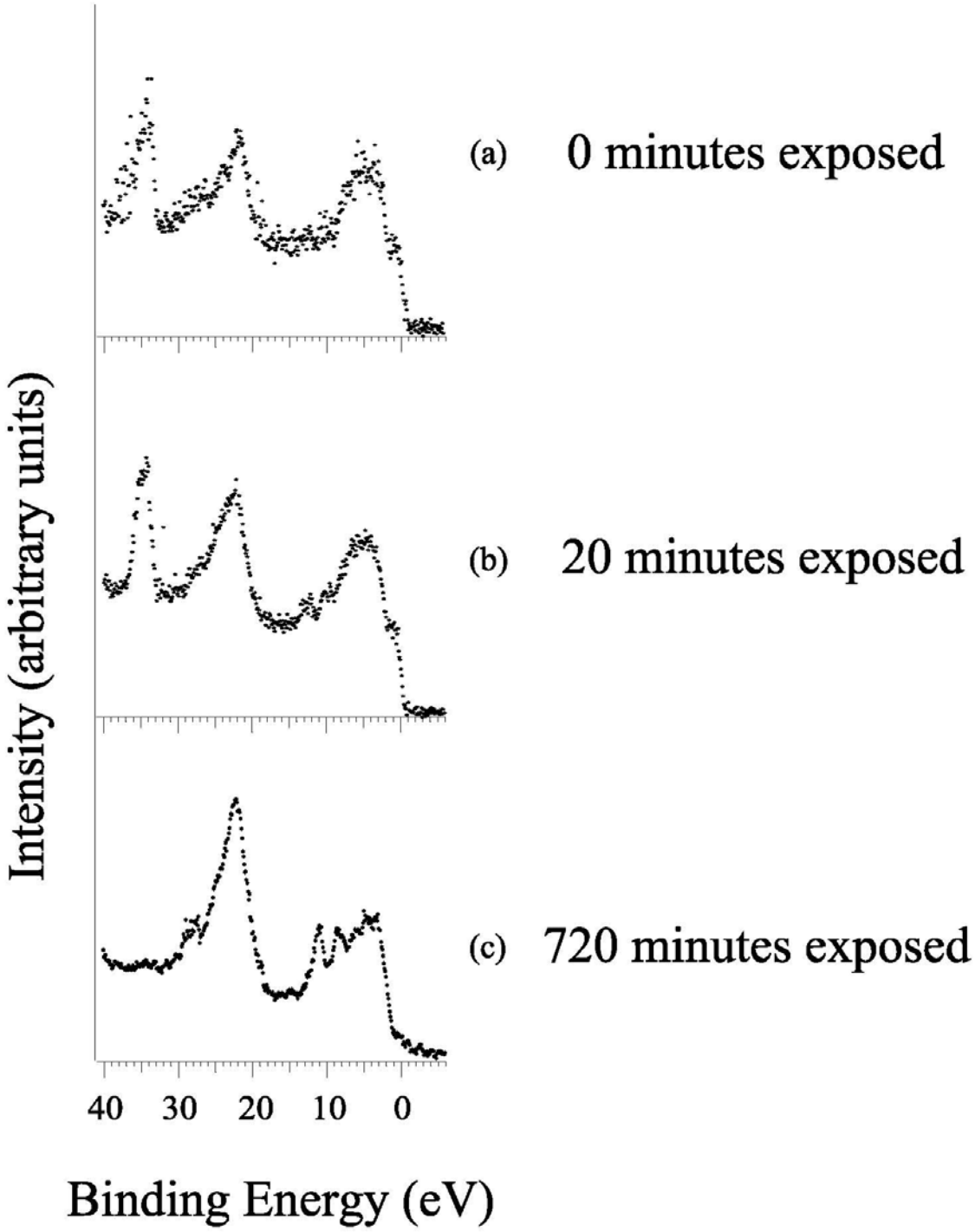

Figure 6-5 The background subtracted outer valence band XPS spectrum of the mild steel exposed to H_3PO_4 for 720 minutes (a) compared to a spectrum generated using band structure calculations of $FePO_4$ (b).

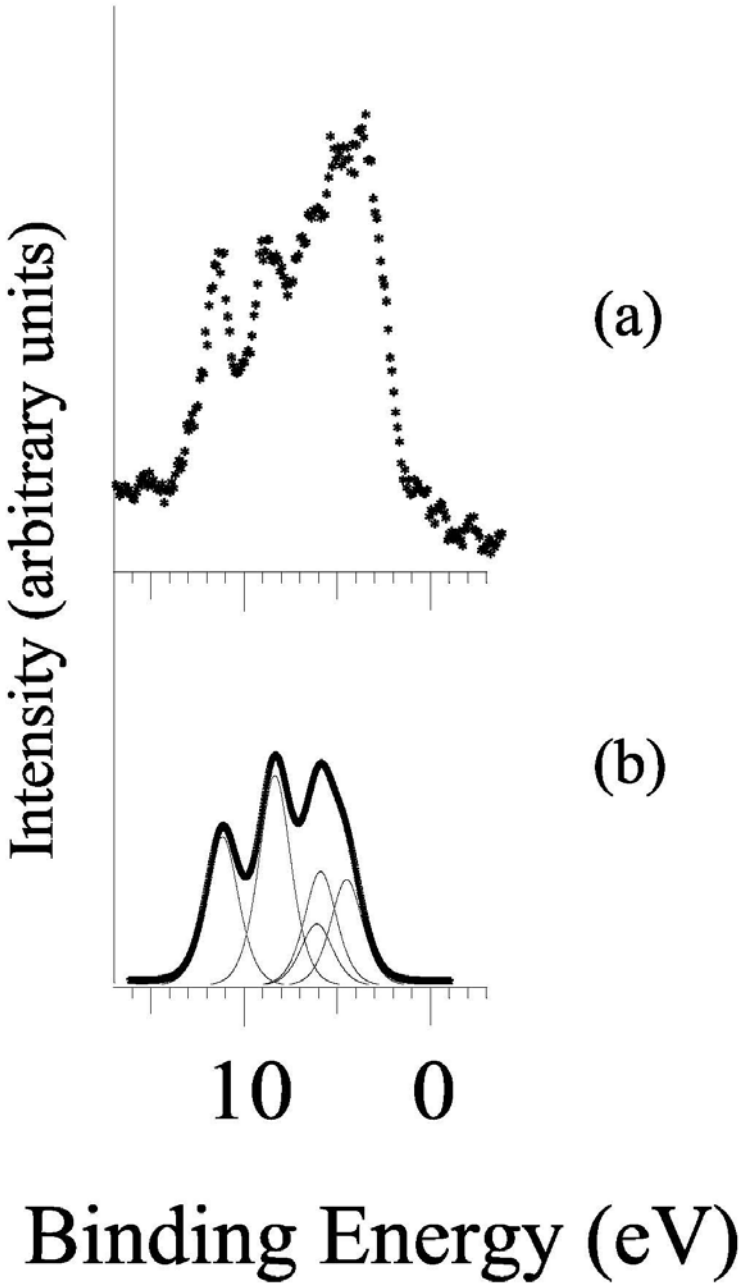

Figure 6-6 Core level XPS spectra, C 1s column I , O 1s column II, P 2p column III, and Fe 2p column IV, for mild steel treated with H_3PO_4 for 720 minutes (a) and the corrosion tests in 4-D water (b) and sodium chloride (c) solutions for two hours.

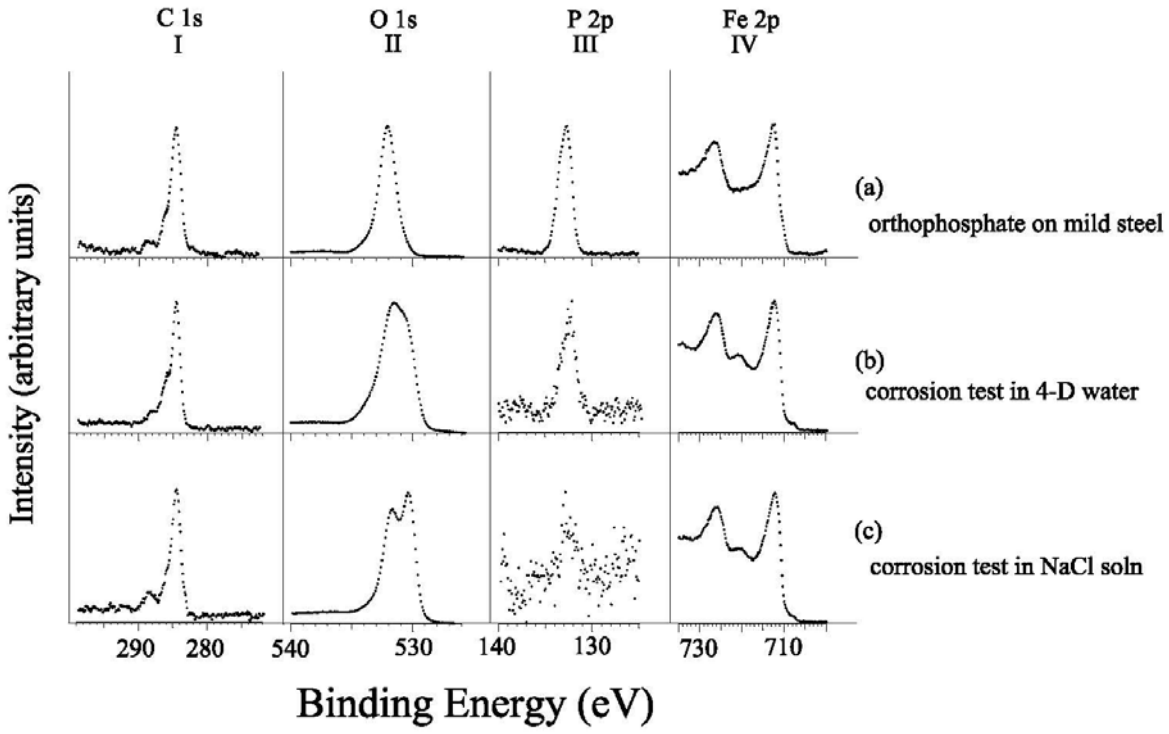

Figure 6-7 Valence band XPS spectra of mild steel treated with H_3PO_4 for 720 minutes (a) and the corrosion tests in 4-D water (b) and sodium chloride (c) solutions.

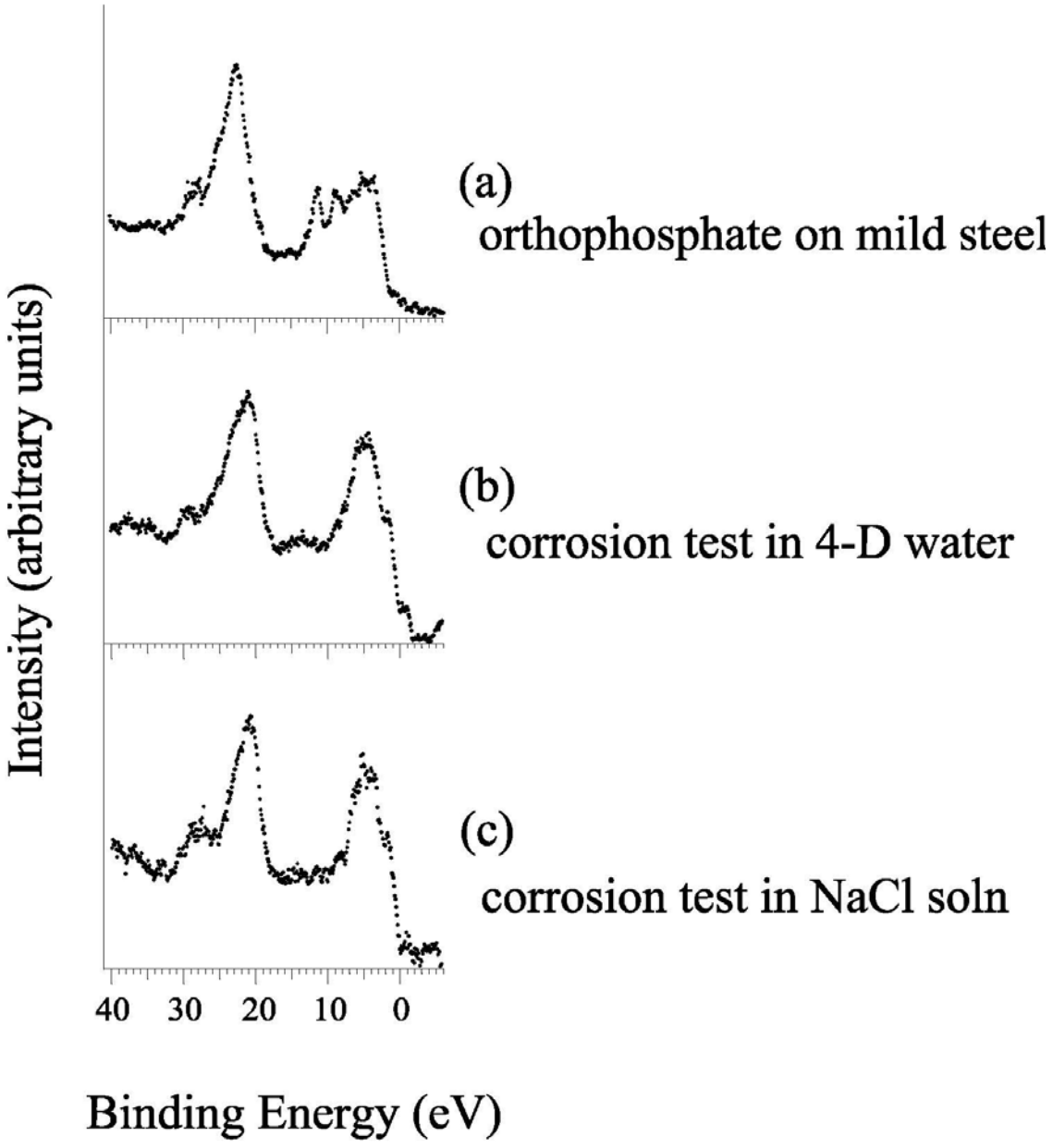

Figure 6-8 Background subtracted outer valence band XPS spectra, column I, of mild steel treated with H_3PO_4 for 720 minutes (a) and the corrosion tests in 4-D water (b) and sodium chloride (c) solutions. Spectra generated by band structure calculations, column II, of FeOOH (b) and FeO (c). A separate study, column III, conducted on an orthophosphate film on mild steel (a) after a two hour exposure time to Aerated 4-D water.

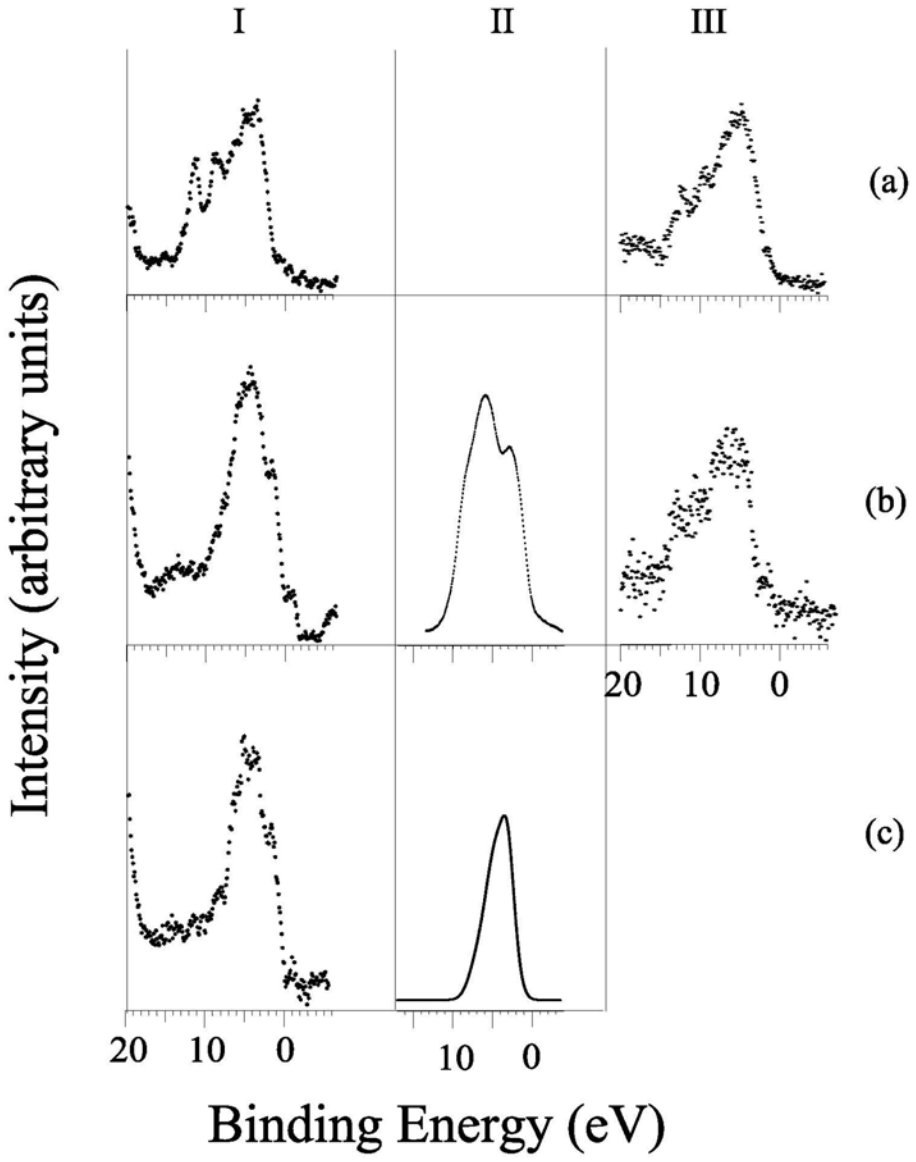

Figure 6-9 The core level XPS spectra, C 1s, column I, O 1s, column II, P 2p, column III, and Fe 2p column IV, for mild steel treated with H_3PO_4 for 720 minutes and PEKK (a) and the two corrosion test in: 4-D water (b) and NaCl (c) solutions.

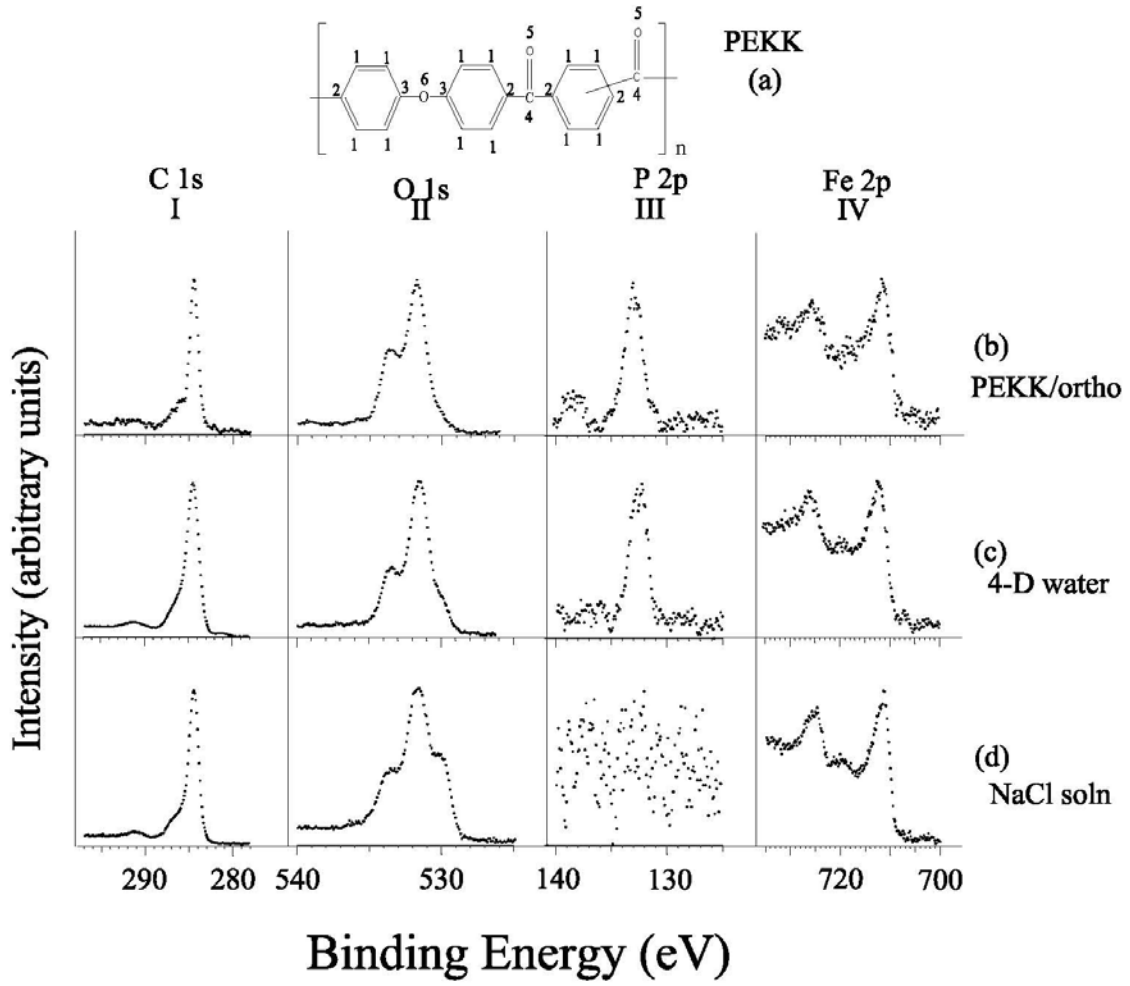

Figure 6-10 The valence band region XPS spectra for mild steel treated with H_3PO_4 for 720 minutes and PEKK(a) and the two corrosion tests in: 4-D water (b) and NaCl (c) solutions.

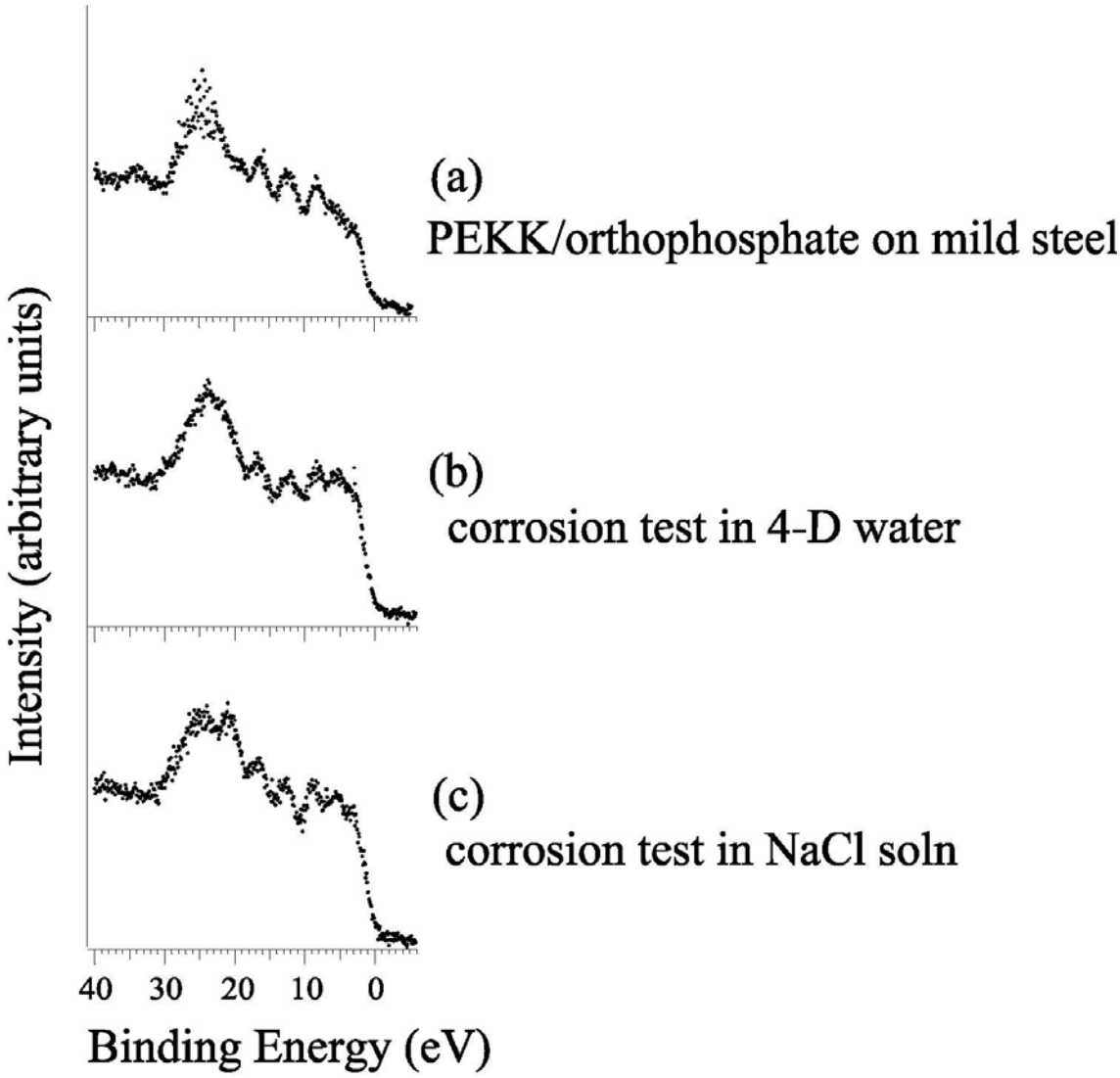

Figure 6-11 The XPS spectra of the overall (I), core level C 1s (II) and O 1s (III), and the valence band (IV). The PEKK coating on copper (a) and tested in NaCl solution at 92 °C for 5 days (b) and 10 days (c). Reprinted from Dr. Sherwood's publication.[24]

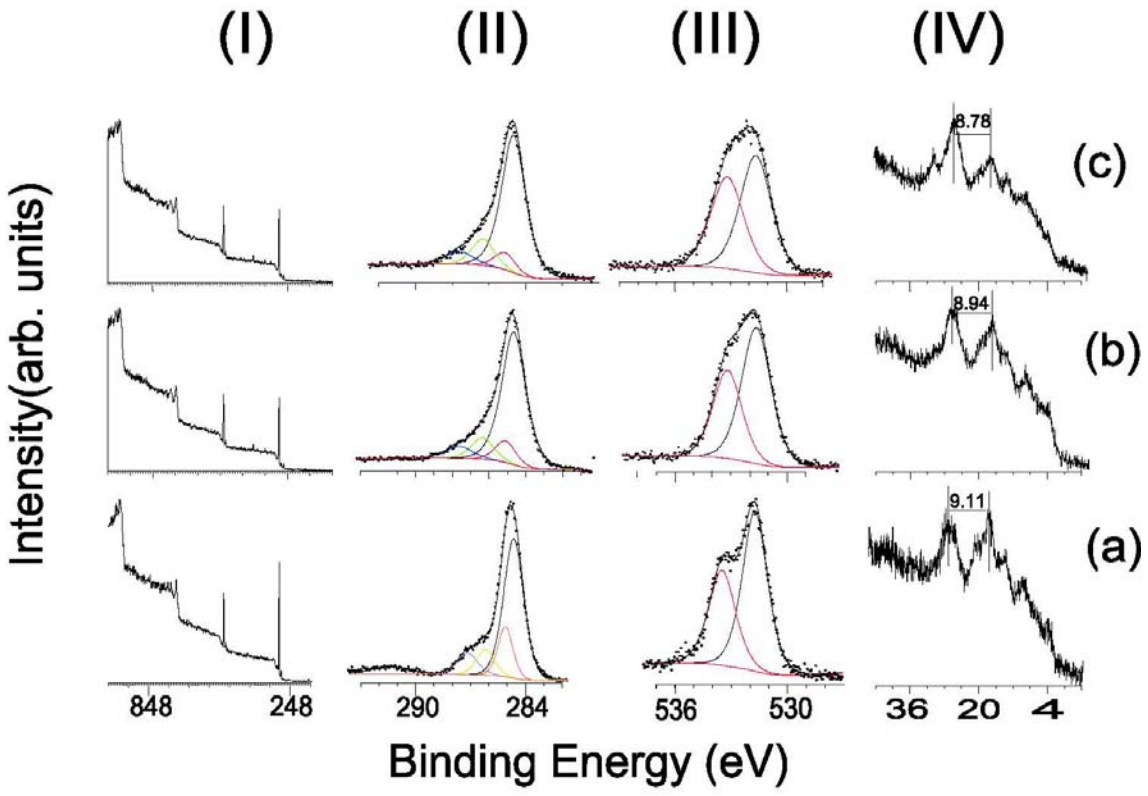

Figure 6-12 The XPS spectra reran on the Sage 100 data for the corrosion tests on PEKK coated on a PO_4^{3-} film on mild steel. The core level XPS spectra, P 2p, column I, Fe 2p, column II, and the valence band, column III, and background subtracted outer valence band, column IV. XPS spectra are shown for the PEKK coated on PO_4^{3-} film on mild steel (a) and the two corrosion tests in: 4-D water (b) and NaCl (c) solutions.

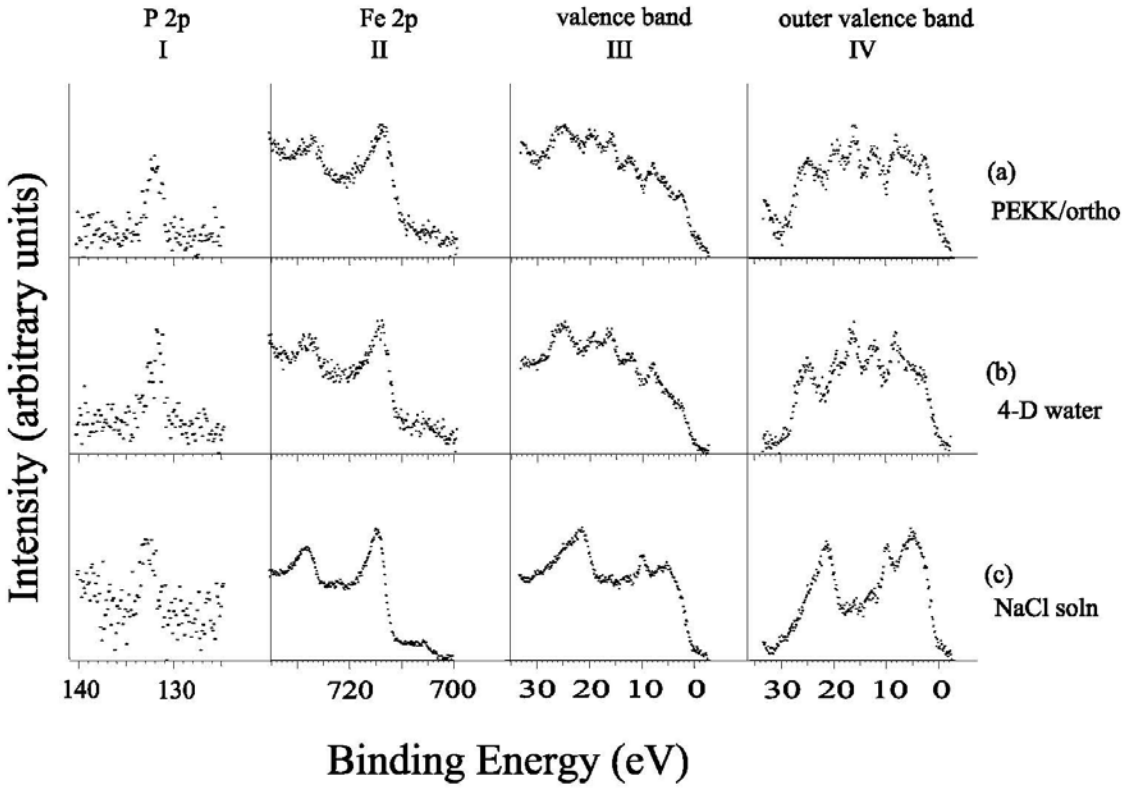

CHAPTER 7 - CONCLUSION

Phosphates and other phosphorus-oxygen containing compounds have been used in a variety of applications including: corrosion inhibition films, adhesion promoters for coatings which otherwise would not attach to the surface and in biocompatible materials that use phosphate compounds that mimic the body's natural phosphates. In my work, I addressed the first two capabilities by looking at a variety of different phosphorus containing films other than orthophosphate that could be formed on a metal surface and then using those films as adhesion promoters to attach a polymer film to the surface.

The initial step was to investigate the formation of novel phosphorus containing films that can be formed on abraded aluminum metal. In previous studies 5 M orthophosphoric acid was used to form both orthophosphate and tetrametaphosphate film on aluminum metal and orthophosphate on iron metal in the anaerobic cell on the HA150. 5 M solutions of pyrophosphoric acid and metaphosphoric acid were used to form novel films on the surface of aluminum metal. Valence band XPS was proven useful by providing a way of distinguishing between the subtle differences in the surface chemistry of these films, which are well resolved in this region. The valence band spectra for the pyrophosphate and metaphosphate films formed were predicted using spectra generated by band structure and scattered wave Xα cluster calculations. The less symmetric pyrophosphate and metaphosphate films showed a replacement of some of the triplets and doublets with singlets that covered a larger energy range causing the peaks to broaden, this was seen in both the calculated and experimental spectra.

The second step was to test the adhesive abilities of these novel surface films. Pyrophosphate, phosphate and hypophosphite films were shown to have good adhesive properties by forming bonds between both the metal and a polyvinyl alcohol coating affectively attaching the PVA to aluminum metal which would not have been possible without the use of the phosphorus containing compounds. A buried interface technique was used to determine of there was bonding in the interface between the PVA and phosphorus containing films. Addition and difference spectra were created by first determining the chi squared value by varying the %

contribution between a spectrum of PVA alone and a spectrum of the phosphorus containing film on aluminum metal. The resultant difference spectra showed shifts in the peaks due to the chemical environment in the interface.

PEKK was then used to replace the PVA film and was shown to also react at the buried interface to form bonding between the phosphorus containing films and the PEKK film. The buried interface technique was repeated for PEKK and similar results were observed. The % contribution of the PEKK spectra was less than the % contribution of the PVA spectra for the PVA film due to the intense peaks and thinner PEKK film produced in the PEKK spectra. This further confirms the ability of phosphorus containing films to be used as adhesive material between metals and polymers that had little to no interaction without the phosphorus containing films.

The final step was to test the corrosion behavior of mild steel with an orthophosphate and PEKK /orthophosphate film. The orthophosphate film showed protection abilities when exposed to aerated 4-D water. The PEKK coating on the orthophosphate film was able to protect the mild steel when exposed to 4-D water at atmospheric conditions, but decomposed in the NaCl solution to form a new species.

References

Chapter 1:

1. D. Briggs, M. P. Seah, Practical Surface Analysis Vol. 1: Auger and X-ray Photoelectron Spectroscopy, 2nd ed.; Wiley and Sons, inc.: New York, (1983).
2. K. Siegbahn, C. N. Nordling, A. Fahlman, R. Nordberg, K. Hamrin, J. Hedman, G. Johansson, T. Bermark, S. E. Karlsson, I. Lindgren, and B. Lindberg, ESCA: Atomic, Molecular and Solid State Structure Studied by Means of Electron Spectroscopy, Almqvist and Wiksells, Uppsala (1967).
3. W. E. Spicer, Phys. Rev. 112, 114 (1958).
4. C. N. Berglund and W. E. Spicer, Phys. Rev. 136, A1030 (1964).
5. A. Joblonski and C. J. Powell, Surf. Interface Anal. 20, 771 (1993).
6. D. Briggs, Surface Analysis of Polymers by XPS and Static SIMS, Cambridge University Press: Cambridge (1998), Section 2.2.
7. C. Pissani, R. Dovesi, and C. Roetti, Hartree-Fock Ab Initio Treatment of Crystalline Systems, Lecture Notes in Chemistry, Vol. 48. Springer, Berlin (1988) and QCPE 577.
8. V. R. Saunders, R. Dovsi, C. Roetti, M. Causa, N. M. Harrison, R. Orlando, and C. M. Zicovidh-Wilson, Crystal 98 User's Manual, University of Torino, Torino (1998).
9. D. T Clark, J. Electron Spectrosc. Relat. Phenom. 10, 455 (1977).
10. P. M. A. Sherwood, J. Chemical Society, Faraday Transactions II. 72, 1791 (1976).
11. P. M. A. Sherwood, Surface Analysis if Advanced Polymers. L. Sabbatini and P. G. Zambonin (ed.) VCH Press: Weinheim, (1993). Chapter 7.
12. J. H. Scofield, J. Electron Spectrosc. Relat. Phenom. 8, 129 (1976).
13. P. M. A. Sherwood, Proceedings of the Electrochemical Society. PV 2001- 2005, 46- 65 (2001).
14. A. A. Audi and P. M. A. Sherwood, Surf. Interface anal. 29, 265 (2000).
15. Y. Q. Wang and P. M. A Sherwood, J. Vac. Sci. Technol. A 21, 1120 (2003).
16. K. Siegbahn, Science. 176, 245 (1972).

Chapter 2:

1. J. R. Van Wazer. Phosphorus and Its Compound vol. I. Interscience Publishers: New York. (1958).

2. T. P. Whaley. Sodium, Potassium, Rubidium, Cesium, and Francium, Comprehensive Inorganic Chemistry, vol. 1. Pergamon Press: Oxford. (1973).

3. A. D. F. Toy. Phosphorus, Comprehensive Inorganic Chemistry, vol. 2. Pergamon Press: Oxford. (1973).

4.A. Le Beuze, R. Lissillour, A. Quemerais, D. Agliz, R. Marchand, and H. Chermette, Phys. Rev. B 39, 11055 (1998).

5. S. J. Sferco, G. Allan, I. Lefebvre, M. Lannoo, E. Bergignat, and G. Hollinger, Phys. Rev. B 42,11232 (1990).

6. G. Hollinger, and E. Bergignat, J. Vac. Technol. A 3, 2082 (1985).

7. A. L. A. Asunskis, K. Gaskell, D. J. A. Asunskis, and P. M. A. Sherwood, J. Vac. Sci. Technol. A 21, 1126 (2003).

8. Chemische Fabbrik Griesheim Elektron, Ger. Pat. 271, 381 (1912).

9. Consortium Für Elektrochemische Industrie G. m. b. H. Ger. Pat. 483, 780 (1924)

10. Consortium Für Elektrochemische Industrie G. m. b. H. Ger. Pat. 485, 271 (1927)

11. H. Winkler and K. Toyoshima, Polyvinyl Alcohol. C. A. Finch (ed.) John Wiley and Sons, inc.: London, (1973). Chapters 1 and 2.

12. Y. Q. Wang and P. M. A Sherwood, J. Vac. Sci. Technol. A 21, 1120 (2003).

13. Y. Chang, Sampe Q. 19, 29 (1988).

14. Y. Z. Ke, Z. W. Wu, J. Appl. Polym. Sci. 67, 659 (1998).

15. H. R. Lin, S. J. Advani, Polym. Compos. 18, 405 (1997).

16. I. Y. Chang, B. S. Hsiao, 36th Int. Sampe Symp. 1587 (1991).

17. H. H. Kausch, Advanced Thermoplastic Composites Characterization and processing; Hauser and Mücher: Germany (1992).

18. Y. Q. Wang, F. Q. Zhang, and P. M. A. Sherwood, Chem. Mater. 13, 832 (2001).

19. Y. Xie and P. M. A. Sherwood, Chem. Mater. 3, 164 (1991).

Chapter 3:

1. J. A. Rotole and P. M. A. Sherwood, Chem. Mater. 13, 3933 (2001).
2. J. E. Castle, Surf. Sci. 68, 583 (1977).
3. D. T. Larson, Corros. Sci. 19, 657 (1979).
4. A. Joshi, Rev. Coat. Corros. 3, 51 (1979).
5. P. M. A. Sherwood, Chem. Soc. Rev. 14, 1 (1985).
6. I. D. Welsh, Chem. Mater. 4, 133 (1992).
7. P. M. A. Sherwood, J. Vac. Sci. Technol. A 9, 1493 (1991).
8. M. A. Stranick, Corrosion, 40, 296 (1984).
9. U. R. Evans, The Corrosion Handbook. H. H. Uhlig (ed.) sponsored by The Electrochemical society. John Wiley and Sons, inc.: London (1948) pg 3.
10. J. A. Rotole and P. M. A Sherwood, U.S. Patent No. 6,066,403 "Metals having Phosphate Protective Films"-23 May 2000.
11. Y. Q. Wang and P. M. A Sherwood, J. Vac. Sci. Technol. A 21, 1120 (2003).
12. J. A. Rotole and P. M. A. Sherwood, J. Vac. Sci. Technol. A 18, 1066 (2000).
13. J. A. Rotole, K. Gaskell, A. Comte, and P. M. A. Sherwood, J. Vac. Sci. Technol. A 19, 1176 (2000).
14. D. J. A. Asunskis and P. M. A. Sherwood, J. Vac. Sci. Technol. A 21, 1133 (2003).
15. P. M. A. Sherwood, J. Vac. Sci. Technol. A 11, 2280, (1993).
16. P. M. A. Sherwood, Anal. Chim. Acta. 283, 52 (1993).
17. A. D. F. Toy and E. N. Walsh. Phosphorus Chemistry in Everyday Living. American Chemical Society: Washington DC. (1987).
18. J. R. Van Wazer. Phosphorus and Its Compounds vol. II. Interscience Publishers: New York. (1961).
19. G. D. Davis, T. S. Sun, J. S. Ahearn, and J. D. Venables, J. Mater. Sci. 17, 1807 (1982).
20. Y. Liang, D. Paul, Y. Xie, and P. M. A. Sherwood, Anal. Chem. 65, 2276 (1993).

Chapter 4:

1. J. A. Rotole and P. M. A Sherwood, U.S. Patent No. 6,066,403 “Metals having Phosphate Protective Films”-23 May 2000.
2. Y. Q. Wang and P. M. A Sherwood, J. Vac. Sci. Technol. A 21, 1120 (2003).
3. J. A. Rotole and P. M. A. Sherwood, Chem. Mater. 13, 3933 (2001).
4. J. A. Rotole and P. M. A. Sherwood, J. Vac. Sci. Technol. A 18, 1066 (2000).
5. J. A. Rotole, K. Gaskell, A. Comte, and P. M. A. Sherwood, J. Vac. Sci. Technol. A 19, 1176 (2000).
6. D. J. A. Asunskis and P. M. A. Sherwood, J. Vac. Sci. Technol. A 21, 1133 (2003).
7. A. L. A. Asunskis, K. Gaskell, D. J. A. Asunskis, P. M. A. Sherwood, J. Vac. Sci. Technol. A 21, 1126 (2003).
8. C. Pissani, R. Dovesi, and C. Roetti, Hartree-Fock Ab Initio Treatment of Crystalline Systems, Lecture Notes in Chemistry, Vol. 48. Springer, Berlin (1988) and QCPE 577.
9. V. R. Saunders, R. Dovsi, C. Roetti, M. Causa, N. M. Harrison, R. Orlando, and C. M. Zicovidh-Wilson, Crystal 98 User’s Manual, University of Torino, Torino (1998).
10. J. H. Scofield, J. Electron Spectrosc. Relat. Phenom. 8, 129 (1976).
11. Wyckoff, R. W.G., Crystal Structures, 2nd ed.; Wiley: New York, 1965; Vol. 3.
12. K. Y. Leung and C. Calvo, Can. J. Chem. 50, 2519 (1972).
13. A. Immirzi and W. Porozio, Acta. Crystallogr., Sect. B: Struct. Crystallogr. Cryst. Chem. 38. 2788 (1982).
14. D. A. Case, Annu. Rep. Phys. Chem. 33, 151 (1982).
15. Y. Q. Wang, F. Q. Zhang, and P. M. A. Sherwood, Chem. Mater. 11, 2573 (1999).
16. K. J. Gaskell, M. M. Smith, and P. M. A. Sherwood, J. Vac. Sci. Technol. A22, 1331 (2004).

Chapter 5:

1. J. A. Rotole and P. M. A. Sherwood, Chem. Mater. 13, 3933 (2001)
2. J. A. Rotole and P. M. A Sherwood, U.S. Patent No. 6,066,403 “Metals having Phosphate Protective Films”-23 May 2000.
3. J. A. Rotole and P. M. A. Sherwood, J. Vac. Sci. Technol. A 18, 1066 (2000).
4. J. A. Rotole, K. Gaskell, A. Comte, and P. M. A. Sherwood, J. Vac. Sci. Technol. A 19, 1176 (2000).
5. D. J. A. Asunskis and P. M. A. Sherwood, J. Vac. Sci. Technol. A 21, 1133 (2003).
6. Y. Liang, D. Paul, Y. Xie, and P. M. A. Sherwood, Anal. Chem. 65, 2276 (1993).
7. Y. Q. Wang and P. M. A Sherwood, J. Vac. Sci. Technol. A 21, 1120 (2003).
8. K. J. Gaskell, M. M. Smith, and P. M. A. Sherwood, J. Vac. Sci. Technol. A 22, 1331 (2004).
9. A. L. A. Asunskis, K. Gaskell, D. J. A. Asunskis, P. M. A. Sherwood, J. Vac. Sci. Technol. A 21, 1126 (2003).
10. Y. Chang, Sampe Q. 19, 29 (1988).
11. Y. Z. Ke, Z. W. Wu, J. Appl. Polym. Sci. 67, 659 (1998).
12. H. R. Lin, S. J. Advani, Polym. Compos. 18, 405 (1997).
13. I. Y. Chang, B. S. Hsiao, 36th Int. Sampe Symp. 1587 (1991).
14. H. H. Kausch, Advanced Thermoplastic Composites Characterization and processing; Hauser and Mücher: Germany (1992).
15. T. Wang, X. Yaoming and P. M. A. Sherwood, Chem. Mater. 5, 1007 (1993).
16. Y. Q. Wang, F. Q. Zhang, and P. M. A. Sherwood, Chem. Mater. 13, 832 (2001).

T. Wang, X. Yaoming and P. M. A. Sherwood, Chem. Mater. 5, 1007 (1993).

17. P. M. A. Sherwood, Practical Surface Analysis Vol. 1: Auger and X-ray Photoelectron Spectroscopy, 2nd ed.; D. Briggs, M. P. Seah, eds.; Wiley and Son, inc.: New York (1990); appendix 3.
18. R. O. Ansell, T. Dickinson, A. F. Povery, and P. M. A, Sherwood, Electroanal. Chem. 98, 79. (1979).
19. A. Proctor and P. M. A. Sherwood, Anal. Chem. 52, 2315 (1980).
20. A. Proctor and P. M. A. Sherwood, Anal. Chem. 54, 13 (1982).

21. M. Dupuis, A. Farazdal, S. P. Karna, and S. A. Maluends, Modern Techniques in Computational Chemistry: MOTECC-90; E. Clement, ed.; Escom: Leiden, (1990); Chapter 6, p 277.
22. Y. Xie and P. M. A. Sherwood, Chem. Mater. 3, 164 (1991).
23. M. Fahlman and W. R. Salaneck, Surface Science 500, 904 (2002).
24. W. R. Salaneck, M. Lögdlund, M. Fahlman, G. Greczynski, and Th. Kugler, Mater. Scie. and Eng. R. 34, 121 (2001).
25. T. Kugler, W. R. Salaneck, H. Rost, A. B. Holmes, Chem. Phys. Lett. 310, 391 (1999).

Chapter 6:

1. J. A. Rotole and P. M. A. Sherwood, Chem. Mater. 13, 3933 (2001).
2. J. E. Castle, Surf. Sci. 68, 583 (1977).
3. D. T. Larson, Corros. Sci. 19, 657 (1979).
4. A. Joshi, Rev. Coat. Corros. 3, 51 (1979).
5. P. M. A. Sherwood, Chem. Soc. Rev. 14, 1 (1985).
6. I. D. Welsh, Chem. Mater. 4, 133 (1992).
7. P. M. A. Sherwood, J. Vac. Sci. Technol. A 9, 1493 (1991).
8. M. A. Stranick, Corrosion, 40, 296 (1984).
9. J. A. Rotole and P. M. A Sherwood, U.S. Patent No. 6,066,403 "Metals having Phosphate Protective Films"-23 May 2000.
10. J. A. Rotole and P. M. A. Sherwood, J. Vac. Sci. Technol. A 18, 1066 (2000).
11. J. A. Rotole, K. Gaskell, A. Comte, and P. M. A. Sherwood, J. Vac. Sci. Technol. A 19, 1176 (2000).
12. D. J. A. Asunskis and P. M. A. Sherwood, J. Vac. Sci. Technol. A 21, 1133 (2003).
13. D. T Clark, J. Electron Spectrosc. Relat. Phenom. 10, 455 (1977).
14. C. Pissani, R. Dovesi, and C. Roetti, Hartree-Fock Ab Initio Treatment of Crystalline Systems, Lecture Notes in Chemistry, Vol. 48. Springer, Berlin (1988) and QCPE 577.
15. V. R. Saunders, R. Dovsi, C. Roetti, M. Causa, N. M. Harrison, R. Orlando, and C. M. Zicovidh-Wilson, Crystal 98 User's Manual, University of Torino, Torino (1998).
16. J. H. Scofield, J. Electron Spectrosc. Relat. Phenom. 8, 129 (1976).
17. C. S. Wang and J. Callaway, Comp. Phys. Commun. 14. 327 (1978).
18. N. E. Brener, J. Callaway, J. M. Tyler, Modern techniques in computational chemistry. In: E. Clementi (ed.) MOTECC-90 chapter 16. Escom, Leiden, pp 785-803.
19. J. Callaway and C. S. Wang, Phys. Rev. B. 16, 2095 (1977).
20. R.O Ansell, T. Dickinson, A. F. Povey and P. M. A. Sherwood, J. Electroanal. Chem. 98, 79 (1979).
21. D. A. Case, Annu. Rep. Phys. Chem. 33, 151 (1982).
22. W. Temesghen and P. M. A. Sherwood, Anal. Bioanal. Chem. 373. 601 (2002).

23. D. Briggs, M. P. Seah, Practical Surface Analysis Vol. 1: Auger and X-ray Photoelectron Spectroscopy, 2nd ed.; Wiley: Chichester, (1990); appendix 3.
24. Y. Q. Wang, F. Q. Zhang, and P. M. A. Sherwood, Chem. Mater. 13, 832 (2001).